INTEGRATED HIGH-THROUGHPUT DROPLET MICROFLUIDIC BASED SCREENING SYSTEMS

A Dissertation

by

ADRIAN RYAN GUZMAN

Submitted to the Office of Graduate and Professional Studies of
Texas A&M University
in partial fulfillment of the requirements for the degree of

DOCTOR OF PHILOSOPHY

Chair of Committee,	Arum Han
Co-Chair of Committee,	Paul Defigueiredo
Committee Members,	Arul Jayaraman
	Vladislav V. Yakovlev
Head of Department,	Mark Weichold

December 2019

Major Subject: Interdisciplinary Engineering

ABSTRACT

Considering drug discovery, since the golden era in the mid 1900's there has been a drastic decrease in the number of novel and useful compounds discovered from environmental samples. Furthermore, due to diminishing returns there has been even less success in discovering broad spectrum anti-microbial and anti-fungal compounds of clinical relevance. Although technology advancements in robotics have improved the process for finding novel compounds, financing conventional multi-well plate assays have become economically infeasible. Furthermore, new methods for drug discovery such as rational drug design, investigation of "unculturables", and next generation sequencing have shown promise, but lack the ability for robustly analyzing samples and churning out "hits". With the addition of resistant strains of bacteria/fungi, prevalence of new pathogens, and the natural evolution of these pathogens, we have found ourselves on the losing side of a war against virulent pathogens. In lieu of these facts, it is more pertinent than ever that we revolutionize and advance our methods for discovering and combating select agents before we reach a point of no return.

In our pursuit for developing a large-scale versatile comprehensive fully integrated screening system, we have developed a Microfluidic Based High-throughput Analysis Platform for the Study of Polymicrobial Interactions, termed the Poly-chip. This highly complex fully integrated system is comprised of fundamental functionalities necessary for conducting continuous large volume-based screening assays for the discovery of novel compounds. Utilizing all prior capabilities exhibited in previous works and a novel process for fabrication and realization of an integrated bottom-up 16 to 21-layer Poly-chip screening system, the Poly-chip platform is a pivotal step toward revolutionizing the current state of drug discovery. With the integration of: on-chip droplet generation, large-volume bottom-up first-in first-out culture chambers, on-the-fly generation/synchronization, three-dimensional liquid metal injected electrodes for merging/shielding/sorting, multi-parallel culture chambers, on-the-fly laser based detection, high speed electric-field based sorting, a novel basket trapping structure, automated valve controls, and a comprehensive LabView-based graphical interface, the Poly-chip system is a ground breaking technology for the discovery of novel compounds. The Poly-chip system is not only the first fully integrated droplet microfluidic system, but integrating these functionalities improves the platform stability by eliminating the need for tubing which often leads to issues in droplet merging or splitting at the interface of adjacent devices. In addition, this full integration allows for the use of imbedded valves at each stage of operation, providing precise control of fluidic components and automated control using a graphical user interface (GUI). Considering that current conventional droplet screening assays are conducted on several tethered chips or conducted partially on-chip followed by conventional off-chip fluorescence-activated cell sorting, the Poly-chip is an innovative comprehensive platform with a novel fabrication process that can pave the way for future highly complex multi-layer droplet screening systems for a variety of applications.

DEDICATION

I would like to dedicate this dissertation to all those who have supported me both emotionally and financially through my journey. First and foremost, I would like to thank my mother (Ofelia Galvan) for her consistent support, love, and understanding. Since a young age she has always truly been the rock and motivation that drives me to strive to be the best man that I can be, and without her I could have never come so far. I would like to thank my father (Joe E. Guzman) for teaching me the hard lessons in life that at the time seemed trivial and difficult, but that I have come to understand on a deeper level. Thanks to my loving sister (Serena G. Friedman) who took her time as we were children to teach me Mathematics and English, which helped me develop a love for education. I cannot say how lucky I am to have a sister that showed so much interest in a younger sibling and to this day has been a guide for me in so many ways.

I would also like to give a special dedication to my fiancé (Hoai-Trang Thi Le) for being the most supportive partner I could ask for and always lifting me up when I am down. In addition, I would like to give a special dedication to my children (Abigail Le-Guzman, Abraham Le-Guzman, and Adam Le-Guzman) who I hope can view my accomplishments as a goal to aspire to and surpass.

Also, I would like to dedicate this work to Mr. James K.B. Nelson for being my role model as a child, encouraging me to follow his footsteps in becoming an aggie engineer, and graciously financially supporting me on my journey.

This is for you.

ACKNOWLEDGEMENTS

First and foremost, I would like to thank Dr. Arum Han for his guidance, wisdom, support, mentorship, and funding during my Ph.D. process. He helped me to grow as an individual, researcher, and professional and I hope to continue to take the lessons he has bestowed upon me to further grow as I embark on a new path. Without him none of this would have been possible, and for all that he has done I am grateful.

I would also like to give a special thanks to Hyun Soo Kim for being my mentor during graduate school and teaching me the basics in microfluidic fabrication, proper experimental design, and experimentation. Some of my fondest memories are the countless late nights and sleepless days spent conducting experiments under his supervision and I am so thankful for the time that we spent together.

In addition, I would like to thank Dr. Paul de Figueiredo for his guidance, mentorship, and support as my biological supervisor on many of my projects. He always had an aura about him that made working in an occasionally stressful environment relaxing. I appreciate his biological expertise and thoughtful nature during my graduate education. Furthermore, I would like to thank Dr. Jarayaman, Dr. Yakovlev, and Dr. Lin for being critical committee members and providing insightful views/opinions to problems faced during the Poly-chip development process.

I would also like to thank my past and present group members for their training, support, and help. Having such a knowledgeable group of individuals around you to bounce ideas off helps a tremendous amount in the development process.

Finally, thanks again to my family for their loving support.

CONTRIBUTORS AND FUNDING SOURCES

Contributors

This work was supervised by a dissertation committee consisting of Professor Arum Han (advisor) of the Department of Electrical Engineering, Professor Paul de Figueiredo (co-advisor) of the Department of Microbial Pathogenesis and Immunology, Professor Vladislav V. Yakovlev of the Department of Biomedical Engineering, and Professor Arul Jayaraman of the Department of Chemical Engineering.

The data analyzed for Chapter 2 was partially conducted by Hyun Soo Kim and was published in 2016. The analysis depicted in Chapter 3 was conducted by Dr. Jing Dai and was published in 2016. The microalgae experimentation presented in Chapter 4 was conducted by Hyun Soo Kim and Song I Han and was published in 2017.

All other work conducted for this dissertation was completed by the student independently.

Funding Sources

This work was made possible in part by DTRA under Grant Number HDTRA1-12-1-0028. Its contents are solely the responsibility of the authors and do not necessarily represent the official views of the Department of Threat Reduction Agency.

This work was made possible in part by NSF Emerging Frontiers in Research and Innovation (EFRI) under Grant Number #EFRI-1240478 and #DBI-1353759. Its contents are solely the responsibility of the authors and do not necessarily represent the official views of the National Science Foundation.

NOMENCLATURE

x	by
%	Percent
P	Pressure
t	Time
V	Voltage
A	Amp
Hz	Hertz
s	Second
h	Hour
min	Minute
mol	Mole
g	Gram
L	Liter
m	Meter
Å	Angstrom
Cr	Chrome
Cu	Copper
N	Nitrogen
CO_2	Carbon dioxide
O_2	Oxygen

ρ	Density
W	Watt
wt/wt	Weight to weight
rpm	Rotations per minute
ºC	Degrees Celsius
PA	Pascal
psi	Pressure per square inch
DC	Direct current
AC	Alternating current
3D	Three Dimensional
MOS-FET	Metal-oxide-semiconductor field-effect transistor
E-field/E	Electric field
LOC	Lab-on-a-chip
DI	Deionized
TAP	Tris-acetate-phosphate media
TAP-N	TAP lacking NH_4Cl
YPD/YEPD	Yeast extract peptone dextrose
TSB	Tryptic soy broth
R2A	Reasoner’s 2A media
DMSO	Dimethyl sulfoxide
PDMS	Polydimethylsiloxane
PAA	Polyacrylic acid

EGaIn	Eutectic Gallium Indium
fps	Frames per second
LED	Light emitting diode
SNR	Signal-to-noise ratio
GFP	Green fluorescent protein
RFP	Red fluorescent protein
DIO	Digital input/output
DAQ	Digital acquisition
PMT	Photomultiplier tube
PCR	Polymerase chain reaction
FDA	Food and drug administration
BODIPY	Boron-dipyrromethene

TABLE OF CONTENTS

LIST OF FIGURES

LIST OF TABLES

Page

1. INTRODUCTION

Drug discovery is an essential, fundamental, and primary component in the large-scale process of drug development, ultimately leading to the production of clinically relevant compounds for combatting a variety of disease, disease states, or pathogens. Without a sound method for discovering, investigating, validating, and developing new compounds, possible therapeutic drugs will fail to reach market potential.

In addition, due to the necessary but large hurdles required for verification and validation of drugs by the FDA, many lead compounds require extensive time and financial investments to become successfully marketable drugs. Also, the development, formulation, synthesization, and mass production of such drugs can have additional obstacles which must be overcome to make these drugs marketable on a mass-scale. In lieu of these facts, many drug compounds with possible clinical relevance fail for a variety of reasons, and the overall process for taking a drug, without a good discovery platform, from discovery to market is often financially infeasible. Considering many of the tests during preclinical research require several years, which include toxicity, mutagenicity, carcinogenicity, and infertility testing, a significant upfront funding is required. In addition, the cost of preclinical research and full phase 1 through phase 3 clinical trials make the chance for a drug to make it to market slim. Any failure along the way can lead to termination of that drug and loss of investment, and for these reasons drug development can costs billions [1, 2].

Furthermore, with the diminishing returns innate to the discovery of novel compounds, especially in the case of antibiotic/antifungal discovery, environmental screening, and library-based screening, finding compounds of interest with conventional drug discovery technology can be risky and is often not financially plausible [3]. Additionally, many lead compounds in the preclinical discovery phase have very low probabilities of being successfully marketable, leading to a need for a platform that can rapidly churn out new compounds of interest. The additional time and cost required to screen for a compound of interest can further exacerbate development costs and can lead to detrimental financial situations for screening approaches and screening companies, and for this reason many have turned to alternative approaches for discovering novel compound [4].

Although there have been many advancements in technology for high-throughput screening applications, many of these new technologies have fell short of their desired goal in producing robust lines of relevant antibiotic/antifungal compounds [5, 6]. The reason for the lack of success is indeed multifaceted, but with the improvement of drug screening technology and approaches, assays could overcome these obstacles and revitalize the world of antibiotic/antifungal discovery. First platforms can be better suited to overcome the issue of compound penetration, which can be done by better investigating, understanding, and characterizing how molecules cross the bacterial cell envelope [7-9]. This could lead to more focused compound libraries, better structure-based compound design, prodrug-like molecules that become active inside cells, and better species-selective screening assays [10-12]. With the rise of antibiotic/antifungal resistance, many companies turned to synthetic antibiotics/antifungals, genomics, combinatorial chemistry, HTS, and rational drug design, but failed to produce robust compounds of interest, especially in the case of Gram-negative bacterial species [13-16]. This in combination with the innate toxicity of many antibiotics/antifungals and small return in investment, the field of antibiotic/antifungal discovery has drastically declined since the 1960's. It is to be noted that every year a few derivatives from old classes of antibiotics/antifungals are produced, which leads one to believe that derivatives of other unknown compounds may produce valuable compounds of interest [17-19]. Considering that we only know a fraction of the actual targets for a few thousand antibiotics/antifungals that have been discovered, there is expected to be a large volume of unknown uses for many of these compounds or undiscovered compounds all together [20-23]. With the advancements in technology, the main problem with drug discovery is still a comprehensive, universal, and adaptable platform or platforms capable of robustly and rapidly investigating large volumes of samples that can produce many lead compounds of interest to take into preclinical investigation [24-27].

1.1. Prior drug discovery methods

In the last millennium, prior to the 20th century, infectious disease was widespread and common. Pathogens such as leprosy, plague, syphilis, smallpox, cholera, yellow fever, typhoid fever, and other infectious disease remained unchecked. With the invention of the microscope in the 1600's, observation of microbes and investigation of microorganisms became possible. In the early 1900's antimicrobial/antifungal drug compounds started being discovered to combat prevalent pathogens. The most famous finding was the random discovery of penicillin by Alexander Fleming in 1928 when an unknown cell showed inhibition of staphylococcus on an agar plate [28]. Although the discovery of penicillin had a large and lasting impact on medicine and began the revolution of antibiotic discovery, a tool to robustly discovery antibiotic/antifungal compounds was still lacking.

The first successful screening system developed was Waksman's platform for antibiotic discovery in the 1940's. Waksman developed a protocol for systematically plating soil derived microbes against streptomycetes which led to the discovery of the first drug against tuberculosis (TB), streptomycin [29]. Using this plate inhibition assay method Waksman and his group were able to discovery 15 novel antibiotic compounds over the course of 20 years. The Waksman screening system lead to the discovery of actinomycin, clavacin, streptothricin, grisein, fradicin, candicidin, candidin, and neomycin. Two of these antibiotics, penicillin and neomycin, were clinically utilized for the treatment of TB and skin bacterial infections, respectively. Although this systematic screening approach was developed more than 70 years ago, inhibition plate assays are still the preferred method for validating and quantifying drug inhibition of a target pathogen. With the wild success of the Waksman platform, society thought we had finally conquered disease pathogens, but after the 1960's no new broad-spectrum antibiotic classes were discovered. Diminishing returns of discovering new antibiotic compounds ultimately lead to the downfall of the Waksman platform [7, 30]. Although new compounds have been discovered using other methods, the last new class of antibiotics was discovered in 1986 (daptomycin) [31]. With the fall of the Waksman platform and increase in antibiotic/antifungal resistance, other alternative methods for discovery of compounds of interest became necessary [32-34]. It became apparent that the war against pathogens was not over and companies began investigating other ways to discover drug compounds [35].

1.2. Conventional drug discovery methods

Later in the 1990's development of a high throughput screening (HTS) strategy was developed for the discovery of new compounds of interest. This strategy often entailed the use of automated instruments and processes for detecting the binding or activity of hundreds of thousands of compounds to an isolated receptor or cell [36]. Although this technology gained great interest and was thought to be a breakthrough technology for drug discovery, little to no clinically useful drugs were discovered, leading to the decline of the HTS system [5]. In addition, rational drug design was sought to be an approach to develop molecules based on the three-dimensional structure of proteins interacting with ligands, but realization of this technology also proved to be difficult and was almost fully abandoned [37-39]. It soon became clear that our lack of understanding of drug interactions, cell penetration, and targets for compounds further hindered our ability to develop sound technology for drug discovery. In lieu of these facts, many drug discovery and large pharmaceutical companies left the drug discovery industry and sought other approaches for discovering compounds of interest.

1.2.1. Environmental drug discovery

The success of the Waksman platform in discovering new antibiotics gave insight to the ability of natural compounds to combat pathogens. Considering the two main approaches for discovering compounds of interest are screening environmental samples or synthetic screening, environmental-based screening assays have several advantages over conventional synthetic screening approaches. First, environmental samples are expected to have some targets for the compounds that are produced [40, 41]. Although many of the compounds and targets may not be known, since they are readily being produced by environmental isolates, there is some expectation that targets to exist. Otherwise, the opposing question would be “why are these compounds being produced, if they have no functionality”? It is true that in some cases these compounds may not have current relevant targets but based on biological evolution there had to have been a reason these compounds began being produced in the past. Furthermore, considering the vastly different biomes, environments, and space, one can theorize that the universe can produce every compound derivation if given enough time. Our planet being billions of years old with different ages, leads one to believe that the Earth may obtain a vast amount of the total population of compounds and many of these have simply not been discovered [42, 43].

Additionally, with recent investigation of cell cultivation there is an understanding that our current biological growth mechanisms are not advanced enough to culture a large class of organisms prevalent in the environment [44, 45]. A whole classification of “unculturables” exists that accounts for at least 50% of the cells present on Earth. For this reason, environmental screening may still have a large population of cells and compounds that have yet to be discovered. This leads one to believe that there are still vast untapped resources of environmental samples for drug discovery that could hold the key to understanding, developing, and defeating emerging pathogens [46].

1.2.2. Synthetic compounds for drug discovery

Considering the downfall of the Waksman platform and lack of success of alternative methods such as HTS and rational drug design, companies began utilizing known successful compounds as backbones to develop a wide variety of synthetic compounds [47]. The synthetic development of fluoroquinolones from nalidixic acid gave hope to the dying field of drug discovery, but this did not last [17]. Later development of bedaquiline in 1997 became the last FDA approved drug against TB and marked the drastic decline of drug discovery.

Recently, other methods for developing libraries of synthetic compounds have been utilized, but it is still uncertain as to how successful these systems will be. Many methods use a backbone molecule and recently developed fractioning technology to create vast libraries of compounds that could have potential clinical use. As with other synthetic discovery methods, the structure of the drug determines the cell penetration mechanism and successfulness of the drug. In addition, the target of many of these synthetic compounds is simply not know and researchers are often screening against a large synthetic library of compounds in hope of discovering a compound of interest [48-50]. Therefore, proper molecule design and understanding the engagement mechanisms of synthetic drugs determine the overall success of these screening technologies.

1.3. Microfluidic/Lab-on-a-chip drug discovery approaches

The advancement of microfluidic lab-on-a-chip based systems have given rise to novel approaches for the discovery or analysis of compounds of interest. Basic microfluidic multiplexed arrays have previously been developed for the screening of cells at a high resolution [51-54]. Utilizing valve controlling layers, cells can be introduced, culture, and harvested under a given drug or stimulus. The integration of such systems with automated processing have given rise to drug screening technologies that can conduct screening assays with minimal cost when compared to conventional multi well plate assay. Furthermore, various pillar or hydrodynamic based trapping structures have been employed to trap cells at a single cell resolution and cultivate these cells while conducting image analysis [55, 56]. This offers the ability to conduct real-time analysis of cells of interest at a fraction of the cost when compared to conventional assays. Continuous perfusion cultures or co-cultivation of species can be conducted and harvested for phenotype confirmation [57, 58]. In addition, the integration of gradient generators for concentration gradient drug analysis assays have offered high-throughput mechanisms for investigating dosage responses, further reducing the cost to conduct preclinical assays. Although many of these technologies offer higher-throughput, lower cost, and a higher resolution when compared to conventional multi well plate robotics pipetting, cells are often not truly isolated[59]. In this bulk flow format, media exchange between cells can occur leading to compound diffusion, compound mixing, and unknown interactions. Essentially, bulk microfluidic assays are not truly isolated in a single-cell format, leading to unexpected results for drug discovery applications.

Recently, the isolation chip (I-chip) was developed as a device capable of culturing the population of “unculturables” leading to a system capable of analyzing cells that researchers have not previously been able to work with. Instead of culturing cells in a conventional laboratory setting, the I-chip uses the native environment of harvested cells to conduct cultures [60]. Harvesting soil derived samples in a microfabricated chip and conducting cultures in the same soil environment where they were harvest allows for the cultivation of these organism inside the device. The I-chip can then be collected later and should contain a larger number of “unculturable” organism than conventional microfluidic or multi well plate assays. Although the I-chip has shown success in cultivation of “unculturables”, the method for conducting screening lacks robustness, and therefore has difficulty churning out many compounds of interest in short timeframes. In addition, deployment of these devices and recollection of the platforms requires manual intervention of researchers. Lastly, the “unculturables” harvested using the I-chip at some point still need to be screened, validated, and investigated in a laboratory setting. Furthermore, with the inability to grow these cells for further analysis, there are limitations in sample volume to conduct follow-up assays.

1.4. Droplet microfluidics-based drug discovery systems

Droplet microfluidics-based screening assays have gained much interested over the past 10 years as they offer the ability to completely isolate cells at a single-cell resolution and conduct assay with high repeatability [61-64]. Millions of identical bioreactors can be generated in a few hours (or less) using a water-in-oil emulsion process [65, 66]. Unlike conventional sonication emulsification, droplet microfluidics entails the generation of identical size emulsions, leading to cells in statistically identical environments [67-69]. Furthermore, with the development of a variety of surfactants to stabilize droplets and prevent small molecule interaction between emulsions, cells can be truly isolated and allowed to accrue compounds of interest. This leads to an ideal case for conducting large-volume high-throughput cell or drug screening assays at a fraction of the cost when compared to conventional multi well plate assays [70-74]. Each droplet containing a picoliter to nanoliter volume confines cells of interest and allows for cultivation and monitoring of these cells in real-time [75-77]. Previous works have shown the ability to conduct complex droplet microfluidic screening assays using functional droplet manipulation techniques such as droplet generation, droplet merging, droplet splitting, droplet detection, and droplet sorting [78-80]. Manipulation of droplets allows for conducting complex assays for drug discovery, mutant screening, chemical interaction analysis, cell-to-cell interaction studies, chemical synthesization, polymerase chain reaction (PCR), and more [81, 82].

Although droplet microfluidics offers many advantages over conventional microfluidics or plate-based assays, many bottlenecks still exist for developing high efficiency systems [83-85]. For instance, droplet merging entails one of the most essential functionalities for conducting quantitative assays using droplet microfluidics. Droplet merging is the cornerstone for any functional assay requiring multiple cells, reagents, drugs, or dye [86-88]. Reaching a high efficiency droplet merging (above 99%) for conducting an assay that is statistically relevant has been a major challenge in the field of droplet microfluidics. Further advancements in the development of microfluidic techniques to improve this efficiency are vital to the overall success of a droplet-based screening platforms [89-91].

Furthermore, complex droplet screening systems with multiple in-series functionalities often suffer from cumulative low efficiency due to additive statistical error from previous manipulation steps. Typical droplet screening systems utilize multiple chips coupled by tubing to conducted complex functional assays [92-94]. This leads to many devices having abrupt interface tubing connections that can lead to droplet merging or shearing, further adding to the statistical error innate to droplet microfluidic screening assays [95-97]. In addition, due to the use of tubing, integration of valving systems for automated platform operation can be challenging but is not impossible. Tethering multiple chips using tubing interfaces can also increase the overall fluidic resistance and dead volume present in the system and therefore should be minimized to prevent adverse effects such as device bulging, delamination, or removal of tubing. In lieu of these facts, there is an inherent need to improve the efficiency of droplet microfluidic screening systems so that they may become marketable platforms for industry screening applications.

2. THREE-DIMENSIONAL ELECTRODE FOR HIGH EFFICIENCY DROPLET ELECTROCOALESCENCE*

2.1. Motivation

Droplet-based merging is one of the most fundamental functionalities for complex droplet microfluidics applications. Furthermore, enhancing the merging of droplets can lead to more stable performance of integrated platforms and downstream droplet manipulation [98-101]. Improving the current standard for droplet merging can lead to a higher droplet merging efficiency and overall higher platform stability. Improving the merging efficiency can eliminate one of the key hurdles that add statistical uncertainty and unnecessary throughput to the platform [102, 103]. In the presence of required stabilizing surfactants that increase surface tension and add platform stability, an external force such as an electric field is required to induce droplet coalescence.

Although there are several device configurations for generating an electric field, we assume that creating a more uniform electric field that aligns with the dipole moment of the droplets to be merged will improve the droplet merging efficiency. Hence, we conducted a systematic comparison of three-dimensional electrode configurations to conventional planar, coplanar, and dual-coplanar electrodes. In doing so, we were able to show evidence and experimentally characterize the generation of a stronger more uniform electric field with a lower input voltage, as well as an improved droplet merging efficiency.

---

*Reprinted with permission from “A three-dimensional electrode for highly efficient electrocoalescence-based droplet merging” by A. R. Guzman, H. S. Kim, P. de Figueiredo and A. Han, *Biomedical Microdevices*, 2015, **17**, 35, Copyright 2015 by Springer Science + Business Media New York.

2.2. Design

A droplet microfluidics device capable of generating an electric field for droplet electrocoalescence of paired droplets is utilized to compare each of the electrode configuration types. The overall droplet merging platform consists of two droplet generators, a droplet merging region, and an observation chamber (Fig. 2.1a). Droplets are generated using T-junction droplet generators to generate droplets ranging from 75-150 µm in diameter depending on the total volumetric flow rate and ratio of oil-to-water. The T-junction droplet generator is comprised of a horizontal continuous carrier oil channel (100 µm wide) and a perpendicular water channel (80 µm wide). Two trains of droplets are generated and brought together in a Y-shaped junction where droplets are paired in preparation for droplet merging. The droplet merging region consists of a 300 µm wide and 500 µm long perpendicular channel that aligns the dipole moment of the paired droplets to the electric field direction of the opposing electrodes. In addition, the merging channel has a 50 µm wide inlet and 100 µm wide outlet to accelerate the droplets before entering and exiting the merging region, enhancing the collision-relaxation force. Each of the electrode designs is comprised of a 500 µm wide electrode that covers the entire width of the droplet merging region, providing sufficient electric field generation for droplet electrocoalescence. The overall gap between the electrodes is set to 1000 µm for each of the electrode configurations to allow enough clearance for all fabrication processes to be identically compared. The observation chamber entails a 10 mm x 3 mm chamber for droplet observation and confirmation of droplet merging efficiencies for data analysis. All the microchannels for each of the devices fabricated to conduct the electrode comparison are set to 100 µm high.

The experimental conditions were set for each of the five electrode configurations (planar, coplanar, dual-coplanar, 3D liquid metal-based, and 3D electroplated) and comparison of the threshold voltage at which droplet merging begins, as well as high efficiency droplet merging was conducted. The planar paired electrode design consists of thin conventional opposing electrodes deposited on a glass slide as a standard for the overall experimental comparison (Fig. 2.1b). The coplanar paired electrodes are configured so that one electrode is at the bottom of the channel and the second electrode is at the top, allowing the electric field to be generated in a diagonal direction across the microchannel (Fig. 2.1c). The dual coplanar design consists of a top and bottom pair of planar electrodes on each side of the microchannel, in a sandwich configuration, providing a more uniform electric field with the middle experiencing 2-times the electric field strength when compared to the conventional planar electrode designs (Fig. 2.1d). The electroplated and liquid metal electrode configurations are solid electrodes the same height as the microchannel that generate a completely uniform electric field throughout the entire height (100 µm) of the merging region (Fig. 2.1e).

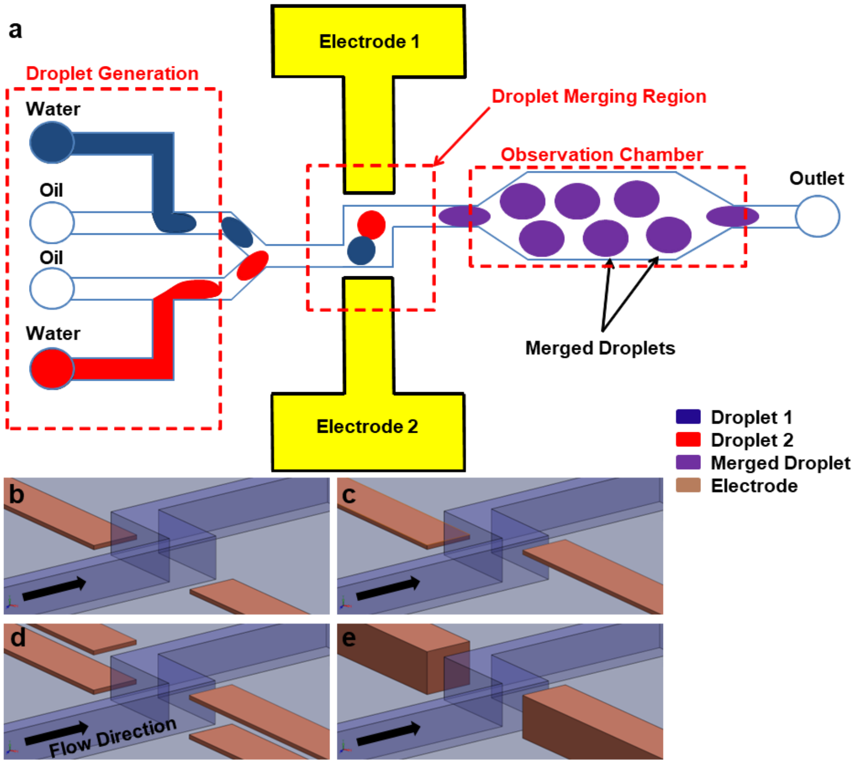

Figure 2.1 Depicts an illustration of the microfluidic design used to test and compare different electrode designs. (a) Shows the overall design of the system. (b) Shows a model of the conventional planar electrode design. (c) Shows a coplanar electrode design. (d) Shows a dual-coplanar electrode design. (e) Shows a 3D electrode design. Reprinted with permission from Springer Science + Business Media New York. [104]

2.3. Fabrication

The 100 µm microfluidic channels are fabricated using conventional soft lithography, where a silicon master is created by spin coating negative photoresist SU-8™ (2075, Microchem Corp., MA) at 1900 rpm, followed by soft baking in two steps at 65 ºC for 60 min and 95 ºC for 20 min. The master is then patterned using conventional photolithography (MA6, Karl Suss, Suss Microtec Se, Garching, Germany) by exposing the pattern using ultraviolet (UV) light, followed by post exposure baking at 65 ºC and 95 ºC for 40 min and 20 min, respectively. The patterned wafer is then developed using conventional SU-8™ developer (Thinner-P, Microchem Corp., MA) and coated with (tridecafluoro-1,1,2,2-tetrahydrooctyl)-1-trichlorosilane (T2492, United Chemical Technologies, Inc., Bristol, PA) for 20 min to prevent pattern removal during PDMS replication.

Planar, coplanar, and dual-coplanar electrodes were fabricated on 50.8 mm x 76.2 mm glass slides (Micro Slides 2947- 75 x 50, Corning Inc., Corning, NY, USA) by first piranha cleaning the glass slides with 1:1 sulfuric acid to hydrogen peroxide, and depositing a Cr/Cu layer (200 Å and 2000 Å thick, respectively) using conventional electron beam deposition (Lesker PVD 75 E-beam Evaporator, Kurt J. Lesker, Co., Jefferson Hills, PA, USA). The glass slides are then spin coated with positive photoresist (S1818, Microchem Corp., Westborough, MA, USA) at 3000 rpm and prebaked at 115 ºC for 5 min. The spin coated glass slides are then patterned using conventional photolithography and wet etched to produce the desired electrode pattern. A thin poly (dimethylsiloxane) (PDMS, Sylgard®, Dow Corning Corp., Midland, MI, USA) layer, mixed at a 1:10 curing agent to polymer ratio, is spin coated on the patterned glass at 3000 rpm for 30 s to obtain a hydrophobic bottom surface necessary for generating droplets.

The planar design is fabricated by pouring 25 g of PDMS on the master mold and replicating the designed microchannels, followed by oven baking at 85 ºC for 1 h. The

PDMS microchannel is then aligned with the bottom planar electrode and bonded using conventional oxygen plasma bonding (Plasma cleaner, Harrick Plasma, Ithaca, NY, USA). Shown in Fig. 2.2.

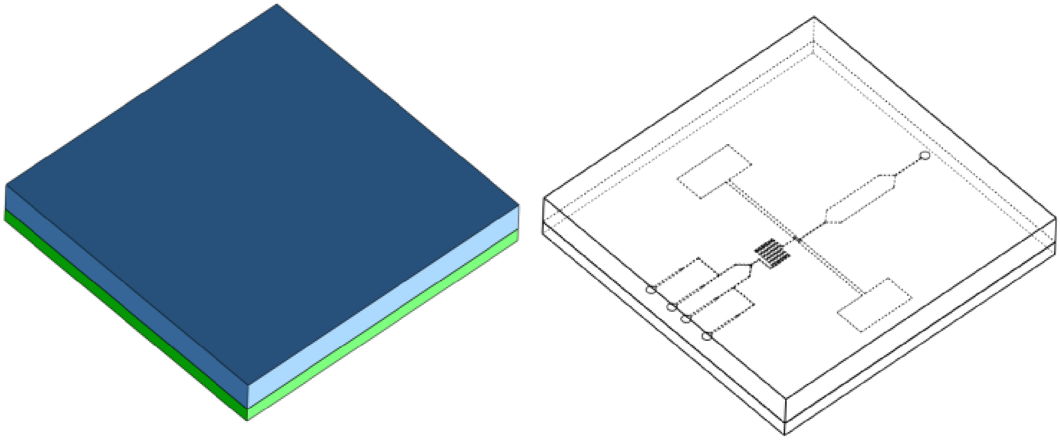

Figure 2.2 A model showing a conventional PDMS/glass device utilized for electrode design comparison (planar electrode and 3D electrode designs). The PDMS layer (blue) is bonded to a glass substrate (green). Reprinted from The Development of a High-throughput Microdroplet Bioreactor Device for Microbial Studies, Texas A&M University Libraries. [105]

The coplanar design is fabricated by spin coating a 130 µm high PDMS slab onto the master mold by pouring 2.5g of PDMS on the wafer and spin coating at 700 rpm for 30 s. The thin PDMS channel layer is then aligned and bonded to the bottom electrode with conventional oxygen plasma bonding (Plasma cleaner, Harrick Plasma, Ithaca, NY, USA), followed by bonding the top electrode with uncured PDMS as an adhesive. After aligning of the bottom and top electrodes, the devices are cured at 95 ºC for 1 h. The dual-coplanar design is fabricated using the same process as described above, but with their being two electrodes patterned on each of the glass slides instead of only one (Fig. 2.3).

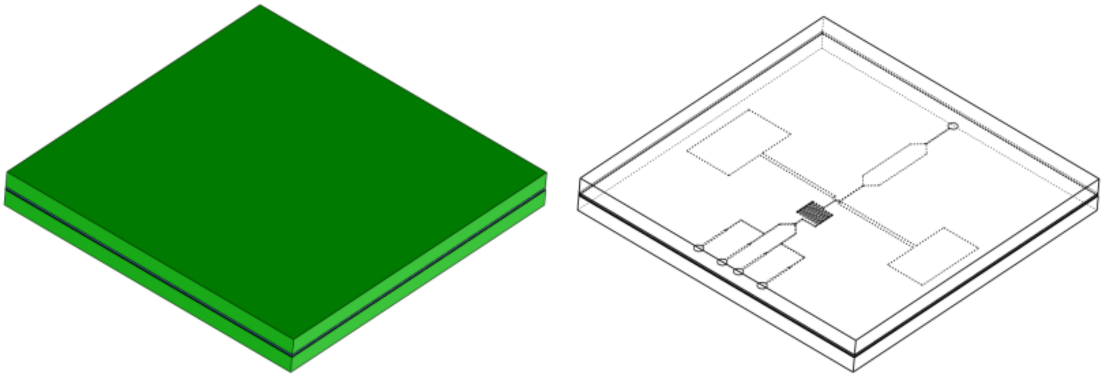

Figure 2.3 A model showing a conventional glass/PDMS/glass device utilized for electrode design comparison (coplanar electrode and dual-coplanar electrode designs). The PDMS layer (blue) is sandwiched between two glass substrate (green). Reprinted from The Development of a High-throughput Microdroplet Bioreactor Device for Microbial Studies. [105]

The liquid metal design device was fabricated by spin coating a bare glass slide with PDMS at 3000 rpm to obtain a 30 µm thick hydrophobic PDMS layer. The PDMS microchannel with patterned channels for the 3D electrodes is bonded to the PDMS spin coated glass slide using conventional oxygen plasma (Plasma cleaner, Harrick Plasma, Ithaca, NY, USA). The electrode channels are filled with EGaIn (Eutectic Gallium Indium 99.99%, Alfa Aesar, Ward Hill, MA, USA) or Field’s metal (RotoMetals, Inc., San Leandro, CZ, USA), creating a three-dimensional electrode.

The three-dimensional electroplated design was fabricated by first spin coating thick photoresist (NR21-2000P, Futurerex Inc., Franklin, NY, USA) at 1000 rpm to create at 100 µm thick layer. The photoresist is patterned using conventional photolithography and developed to create electroplating trenches for copper plating. The electrode device is then electroplated to 100 µm by submersing the device in copper sulphate solution (CuSO4:H2SO4:H2O=250 g:25 mL:1 L), at a current density of 20 mA $(\mathrm{cm}^2)^{-1}$. The photoresist is then removed by submersing the glass slide in acetone and the seed layer is removed by briefly submerging the glass slide in copper etchant (CE-100, Transene Company Inc., Danvers, MA, USA) and chrome etchant (TFE, Transene Company Inc., Danvers, MA, USA), respectively. A PDMS channel layer created using conventional soft lithography is then aligned corresponding with the electroplated three-dimensional electrode and bonded using conventional oxygen plasma treatment (Plasma cleaner, Harrick Plasma, Ithaca, NY, USA).

2.4. Simulation comparison of electric field

An electric field simulation is conducted on each of the four main configurations (planar, coplanar, dual-coplanar, and 3D electrodes) using a finite element method (FEM) software (Comsol® Multiphysics 4.4, The Comsol Group, Stockholm, Sweden). Each of the electrode designs for the simulation correspond to the dimensions of the actual electrodes in the fabrication process listed above (200 µm x 500 µm with a height of 20 nm and 100 µm for the planar and 3D electrodes, respectively). The channel layer is also filled with continuous fluid with dielectric constants matching that of oil and a 1 kV electric potential is set to generate the electric field simulation. These results show a direct comparison of the electric field strength for each of the different electrode configurations and give us insight into the electric field strength given different designs.

Considering the design constraints, all electrode simulation results (shown in Figure 2.4) demonstrated uniform electric fields at the middle of the droplet merging channel but had varying electric field strengths depending on the electrode configuration. The planar paired and coplanar paired electrodes showed very similar results with an electric field strength of .6x10^6 V m^{-1} in the merging region, and the lowest overall electric field strength amongst the various electrode configurations (Fig. 2.4a). The dual-coplanar design showed a higher electric field strength of .8x10^6 V m^{-1}, approximately 30% stronger E-field strength compared to the planar and coplanar electrode designs (Fig. 2.4b). The 3D electrode designs showed the highest electric field strength of 1.1x10^6 V m^{-1}, which is 1.3 times higher than the dual coplanar design, and 1.6 times higher than the planar or coplanar designs (Fig 2.4c). These results show that at the channel dimensions typically utilized for droplet merging, the 3D electrode designs provide a significant improvement in the field strength exhibited by the droplets in the merging chamber, and thus increase the overall merging efficiency at the same applied input voltage (Fig. 2.4d). Conversely, it is also possible to reduce the input voltage required to induce droplet merging when compared to the conventional planar design, allowing for reduced requirements for generating comparable electric field strengths.

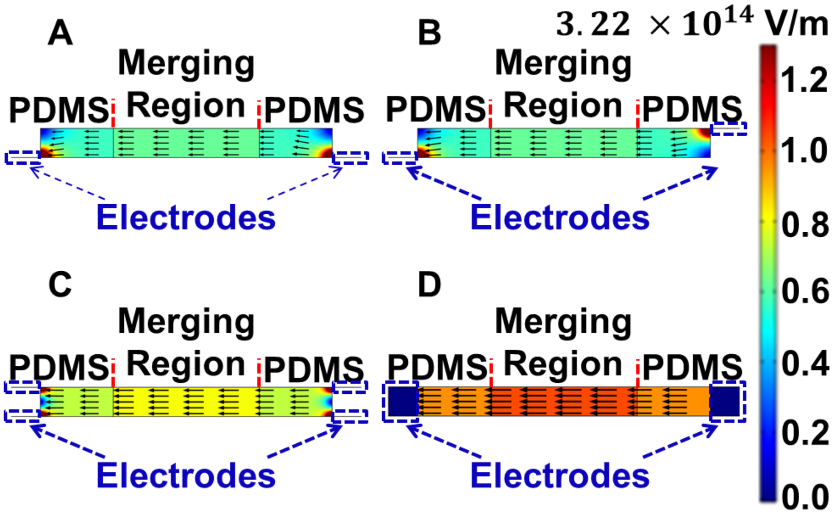

Figure 2.4 Comsol simulation results comparing the E-field using (a) a planar electrode design, (b) coplanar electrode design, (c) dual-coplanar electrode design, (d) and 3D electrode design. Reprinted with permission from Springer Science + Business Media New York. [104]

2.5. Systematic comparison of different electrode types for droplet merging

Each of the electrode types (planar, coplanar, dual-coplanar, 3D field's metal, 3D E-GaIn, and 3D copper electroplated) merging efficiency is characterized using mineral oil (J217 Mineral Oil Light White, Amresco®, OH, USA) with surfactant (Abil EM90, Evonik®, TX, USA) at 2-3% wt/wt as the continuous phase and deionized (DI) water as the encapsulated solution. Without the addition of this stabilizing surfactant droplet will experience spontaneous and random merging when experiencing minimal collision-relaxation or push-pulling forces. The addition of 3% surfactant inhibits this undesired random merging and provides a stability to the droplets that require an external electric field to induce droplet coalescence. It is to be noted that the critical micelle concentration for this oil and surfactant combination is approximately 3% and that above this concentration will often result in undesired micelle formation of the surfactant. Hence, high concentration does not always mean better, and the concentration of surfactant should match the oil, and thus critical micelle concentration varies from oil-to-oil and surfactant-to-surfactant. Two syringe pumps (Fusion 400, Chemyx®, Stafford, TX, USA) are utilized to generate droplets at the T-junction orifice with the oil and water phase ranging from 20 $\mu L\ h^{-1}$ to 3000 $\mu L\ h^{-1}$ and 5 $\mu L\ h^{-1}$ to 1000 $\mu L\ h^{-1}$, respectively. An electric field is induced for each design using a high-voltage DC power supply that provides a constant voltage to a MOSFET relay (G3VM-601BY, Omron®, Kyoto, Japan) that is triggered by a 1 kHz 1 V peak-to-peak sinusoidal wave from a function generator (DG4102, Rigol Technologies, Beijing, China) to generate an electric field. Paired 150 µm diameter droplets are generated at an oil flow rate of 2500 $\mu L\ h^{-1}$

and a water flow rate of 500 μL h^{-1} to compare merging efficiency of each device design (Fig 2.5).

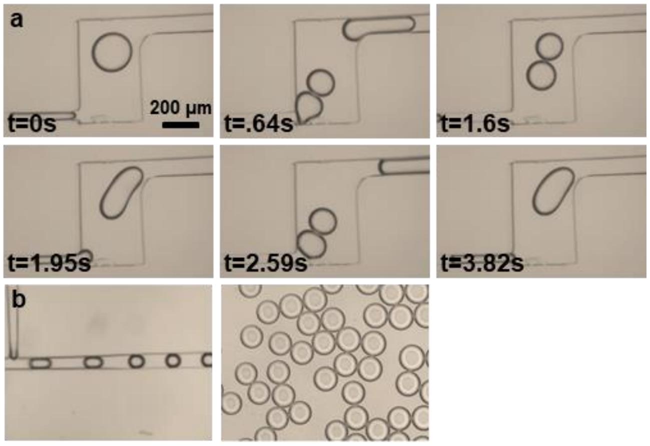

Figure 2.5 Micrographs showing (a) frame-by-frame images of droplet electrocoalescence in the droplet merging region, (b) a droplet generation using a T-junction droplet generator, and droplets analyzed in the observation chamber. Reprinted with permission from Springer Science + Business Media New York. [104]

The overall droplet merging efficiency was analyzed by continuously generating two paired trains of droplets, one-to-one merging these droplets, and observing the number of merged droplets compared to the number of unmerged or double-merged droplets in the microfluidic observation chamber. An applied voltage of 900 V, corresponding to an electric field strength of .9x10^6 V m^{-1} at a total volumetric flow rate of 6000 μL h^{-1}, approximately 550 droplets s^{-1}, was utilized to conduct all comparable droplet merging efficiency experiments. At these experimental conditions the planar electrode designs exhibited a droplet merging efficiency of 80%, with a minimum threshold voltage of 300 V to induce droplet merging (voltage at which droplet merging is observed to begin, although at a very low percentage). Increasing the voltage input above 900 V resulted in a maximum merging efficiency of 82% with the planar electrode design. This merging efficiency serves as a control or reference condition for subsequent alternative electrode designs to be directly compared. At the same experimental conditions, the coplanar design showed very similar results with a minimum threshold voltage to induce droplet merging of 300 V, and a total maximum merging efficiency of 80% at 900 V (Fig. 2.6). Although the designs differ in electrode position and fabrication processes, as expected from the simulation results, the applied electric field strengths are identical, resulting in very similar merging efficiency results under the same experimental conditions. This also gives indication that for this design, the directionality of the two electrode designs with respect to the droplet merging region has very minimal effect on the merging efficiency and the electric field is uniform for each design case. It is to be noted that with shorter electrode-to-electrode conditions there may exist some difference in these designs, as the electric field direction may have a more significant impact on the electric field strength and therefore have an impact on the droplet merging efficiency. It is also to be noted that the coplanar design in this experiment performed slightly worse (2% less) than the planar design, assumed to be due to a slight directionality difference which may have adversely impacted the merging efficiency.

Again, considering the same experimental conditions, based off the simulation results the dual-coplanar design is expected to induce a stronger and more uniform electric field in the droplet merging region and is tested for merging efficiency. The minimum threshold voltage to induce droplet merging was shown to be 150 V, 150 V less than that of the planar and coplanar designs. Therefore, at the same applied voltage the dual-coplanar design exhibited a stronger electric field strength and higher merging efficiency. Overall the dual-coplanar design showed 5 % to 10 % higher merging efficiency at 100 V to 700 V, respectively, compared to the planar or coplanar designs. Furthermore, at the higher input voltage ranges, up to 900 V, the dual-coplanar design showed a maximum merging efficiency of 85 %, which was only slightly higher than that of the planar and coplanar designs (Fig. 2.6). Although this design only showed a 5% increase in the droplet merging efficiency, it is evidence that the uniformity and electric field strength both play a part in the overall merging efficiency of droplet merging and that electrode designs play a critical role in the generated electric field.

The two liquid metals used to create 3D electrodes (EGaIn and Field's metal) showed similar trends comparable to the dual-coplanar design, with threshold voltages to induce droplet merging being 150 V. Although, the EGaIn only had a maximum merging efficiency of 70% at the applied 900 V, while the Field's metal had a higher overall maximum merging efficiency of 86% at the same 900 V (Fig. 2.6). The reason for this difference may be due to the EGaIn always being in liquid form at room temperature, while the Field's metal is a solid at room temperature and is only heated to 65 ^{o}C to become liquid phase for injection into the device. In addition, the Field's metal device only slightly outperformed the dual-coplanar electrode design but is subject to a much easier fabrication process. The dual coplanar design requires electron beam deposition, thin PDMS layer bonding, and liquid PDMS bonding of the top layer, while the liquid metal injection designed channels are fabricated during the normal lithography process required to fabricate the fluidic channels. Essentially the liquid metal designs require one less step compared to conventional planar designs, and two less steps when compared to the dual-coplanar design.

A 3D electroplated copper electrode design, our main design presented here, showed significant improvement in the electric field strength and droplet merging efficiency when compared to the other electrode design configurations. The threshold voltage at which droplet merging was induced was observed to be 50 V, which was 6 times less than that of the conventional planar design, and 66% lower than that of the commonly used 3D liquid metal electrode designs. The maximum merging efficiency observed for the 3D electroplated design was 95%, approximately 10-15% higher than that exhibited by the planar, coplanar, dual-coplanar, and liquid metal designs (Fig. 2.6). In addition, this 95% merging efficiency could be observed at an input voltage as low as 150 V, and vastly outperforms other conventional electrode designs in terms of power input and merging efficiency. It is to be noted that the electroplating design does require one additional step of electroplating of the seed planar electrode layer but provides a significant improvement in the device performance. It is also to be noted that this increase in performance may also be partially attributed to the quality of the pure copper electroplated electrode compared to the alloy of the liquid metal electrodes, and therefore may be partially related to the quality of the electrode and its electrical properties. It is expected that this increase in electric field strength and uniformity with an overall improvement in performance can provide an increase in the stability of future droplet screening platforms.

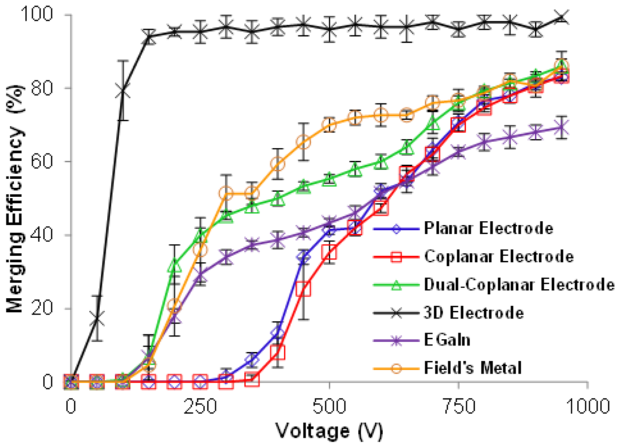

Figure 2.6 Merging efficiency comparison results of planar, coplanar, dual-coplanar, and 3D electrode design. Reprinted with permission from Springer Science + Business Media New York. [104]

In addition, when taking into consideration long duration and high-volume droplet screening assays, it is to be noted that the overall merging efficiency plays a critical role in the overall success, time, and statistical error in the platform performance.

Especially in cases where non-merged or double-merged droplets could count as false positive or false negative units, the overall merging efficiency can have direct implications on the overall success of a high-throughput screening platform. For instance, when conducting a screening assay with $1\text{x}10^6$ droplets at a merging efficiency of 80%, $1.25\text{x}10^6$ droplets are required to obtain the $1\text{x}10^6$ appropriately one-to-one merged droplets for analysis. Alternatively, conducting the same screen with a merging efficiency of 95%, only $1.05\text{x}10^6$ droplets are required to obtain the same volume of one-to-one droplets for appropriate analysis and screening. This is a total of a 16% reduction in the number of droplets of additional throughput that is pushed through the system to find one mutant or compound of interest. Furthermore, considering that many screening assays require single cell encapsulation, and based on the best case of Poisson's distribution or cell ordering, typically a 66% single cell encapsulation rate is considered above average or good, therefore more throughput is needed to achieve the desired $1\text{x}10^6$ merged droplets containing compounds of interest. This is essentially a minimum of a 30% increase in the number of droplets to be generated regardless of the electrode design, and further volume that needs to be pushed through the screening system to find a "hit". Therefore, increasing the merging efficiency can have a significant impact on the assay time, and assuming analysis at 100 events per second, it is then possible to reduce the overall assay time from 10.41 h to as low as 8.76 h. Considering long duration assays where culture time is critical and must be identical for each of the droplet experiment units, this reduction in assay time and characterize of overall assay time is critical in the success and downstream analysis of droplets for screening.

2.6. High-throughput droplet merging efficiency using 3D electrodes

We conducted further investigation to characterize the performance of the 3D electroplated design at high-throughput droplet merging rates to demonstrate the merging efficiency at high flow rates. Beginning at droplet flow rates of 400 µL h^{-1} with increments of 50 µL h^{-1}, while sustaining a 1:3 water to oil flow rate ratio, to a final flow rate of 9800 µL h^{-1}, droplet merging efficiency at four different voltage settings (250 V, 500 V, 750 V, and 900 V) was characterized (Fig. 2.7).

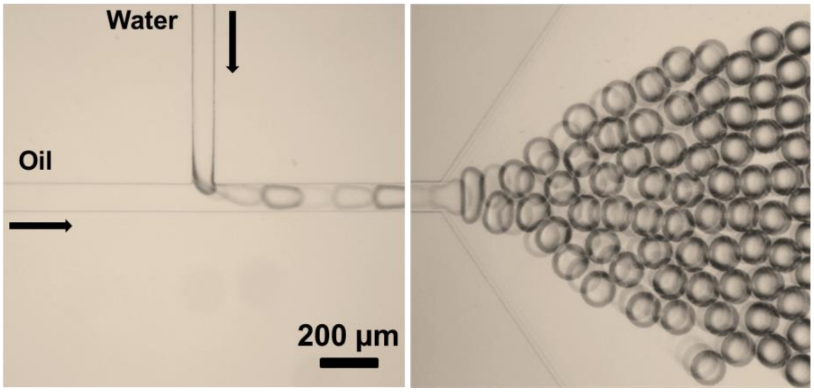

Figure 2.7 Micrographs of high-throughput droplet generation and observation of droplets for high efficiency merging characterization.

At the lowest voltage setting, 250 V, more fluctuation in the droplet merging efficiency was observed, with a decrease in fluctuation at higher flow rates. All voltage conditions showed similar fluctuation results at low throughput conditions with a decrease in fluctuation at high throughputs. Although less fluctuation was observed at voltage conditions of 500 V, 750 V, and 900 V regardless of the flow rate conditions. The overall merging efficiency for the 250 V condition was 85% at high-throughput conditions, with the 500 V condition showing an overall merging efficiency of 90% regardless of the flow rate. The 750 V and 900 V case showed similar merging efficiencies at high droplet merging rates above 700 events per second, reaching 95% at these flow rates and showed some fluctuation at lower flow rates, but still averaging around 95% (Fig. 2.8). The highest flow rate tested, 9800 μL h^{-1}, corresponds to approximately 1,300 droplet merging events per second.

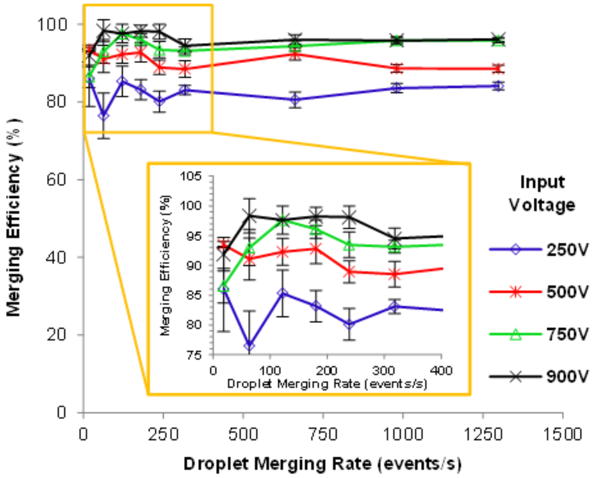

Figure 2.8 Graph comparing the merging efficiency of the 3D electrode design at varying flow rates and E-field input voltages. Reprinted with permission from Springer Science + Business Media New York. [104]

In addition, we conducted a direct comparison with other previously published droplet microfluidic merging works and found that the 3D electrode configuration presented here has the ability to outperform similar electrode merging designs by reducing the minimum applied voltage to induce droplet merging and achieve the same 95% merging efficiency previously exhibited (Table 2.1). It is to be noted, that decreasing the electrode to electrode distance, droplet size, and optimizing the merging region can lead to an even better electric field performance in terms of electric field strength and reduction in the required input voltage, achieving high performance droplet merging.

Table 2.1 Comparison of 3D electrode design and previous droplet merging publications

Electrode Design	Applied Voltage (V)	Electric Field Strength (V/µm)	Droplet Flow Speed (µl/h)	REF
3D cylindrical	2000	0 .1 - 1	15	Chabert, et al
Planar	10 - 120	0.1 – 1.2	electroosmosis	Tresset, et al
Planar	100	0.5	210 - 560	Ahn, et al
Planar	10	1.5	0.8	Priest, et al
Planar	300 - 500	0.375 - 0.975	static	Singh, et al
Planar	50 - 200	0.027 - 0.286	146.2 – 367.2	Tan,et al
Planar	0-800	0 - 1.6	360 - 504	Link, et al
Planar	30 - 1000	~1.2 - 40	200 - 440	Abate, et al
Planar	1500 - 4000	0.19 - 0.51	500	Lai, et al
Planar	200 - 400	1 – 2	4800 - 8400	Schoeman, et al
Planar interdigitated	6 – 100	0.6 - 10	6 - 900	Zagnoni, et al
3D needle	400	1	190	Xu, et al
3D liquid metal	4.5	0.03	1450	Brouzes, et al
3D copper electroplated	50 - 900	0.08 - 1.6	70 - 9800	This Work

Reprinted with permission from Springer Science + Business Media New York. [104]

2.7. Conclusion

The work presented here demonstrates a high-throughput microfluidic droplet-based electrocoalescence electrode design consisting of a three-dimensional electrode that provides higher efficiency droplet merging of paired droplets even in the presence of stabilizing surfactants. A systematic comparison of conventional planar, coplanar, dual-coplanar, liquid metal, and electroplated electrode designs are compared under identical experimental conditions to characterize electrode performance in terms of merging efficiency. A total merging efficiency of 95% or more at a merging rate of 1,300 events per second, with a reduce input voltage of 50 V to 150 V was achieved using the presented 3D electroplated copper electrode design. Although the 3D copper electroplated design required one additional fabrication process, the improved performance in terms of merging efficiency and throughput vastly outperforms previous and similar works. In addition, this electrode merging configuration provides high efficiency merging regardless of the droplet size or surfactant usage and can have a significant impact on future droplet microfluidic platforms that require high performance for droplet screening applications.

3. DROPLET MICROFLUIDICS-BASED PLATFORM FOR MICROALGAL GROWTH AND OIL PRODUCTION SCREENING*

3.1. Motivation

Renewable biofuels derived from microalgae are an attractive energy source for producing oil-based fuel for supplementation of current fuel sources [106, 107]. In particular, renewable microalgal sources are capable of producing identical forms of fuel comparable to conventional petroleum production sources, in addition to providing sources for feed stocks [108, 109]. Furthermore, these microalgae biofuel sources are capable of producing a wide range of oil types which can be refined to gasoline, diesel gasoline, and jet fuel, using conventional refining methods and technology. Feedstocks are comparable to current photosynthetic organisms which include but are not limited to corn, soybean, and sugarcane [110, 111]. Microalgae have higher growth rates and oil production compared to typical first-generation biofuels and do not directly compete with arable land for growing crops. For these reasons, microalgae as a renewable biofuel source is an attractive source for replacement or supplementation of the current fuel sources, but the overall production cost to become competitive with typical petroleum fuel sources is currently not economically feasible. Therefore, improvements in the discovery, development, validation of new microalgal strains, optimization of culture conditions, large scale-up

for mass production, dewatering, and oil extraction methods are needed. Furthermore, low cost high-throughput discovery of mutant microalgae or microalgae having a beneficial phenotype in terms of growth rate and/or oil production can have a significant

---

*Reprinted with permission from "A droplet microfluidics platform for rapid microalgal growth and oil production analysis" by H. S. Kim, A. R. Guzman, H. R. Thapa, T. P. Devarenne and A. Han, *Biotechnology and bioengineering*, 2016, **113**, 1691-1701, Copyright 2016 by Wiley Periodicals, Inc.

improvement in the initial financial investment for discovery. In addition, discovery of higher growth rate and oil accumulating strains can increase the long-term production of oil per square foot of land or liquid volume of microalgae [112, 113]. In this work we sought to develop a high-throughput droplet microfluidics-based microalgae screening system for growth and oil characterization to improve upstream mutant screening/discovery.

3.2. Design

The droplet microfluidics-based microalgae screening platform is comprised of three main functional manipulation regions entailing a microalgae droplet generation, culture chamber, on-chip dye staining, and droplet rinsing with analysis (Fig. 3.1). Utilizing these functional components, the screening system prepares droplets for high-throughput growth and oil analysis.

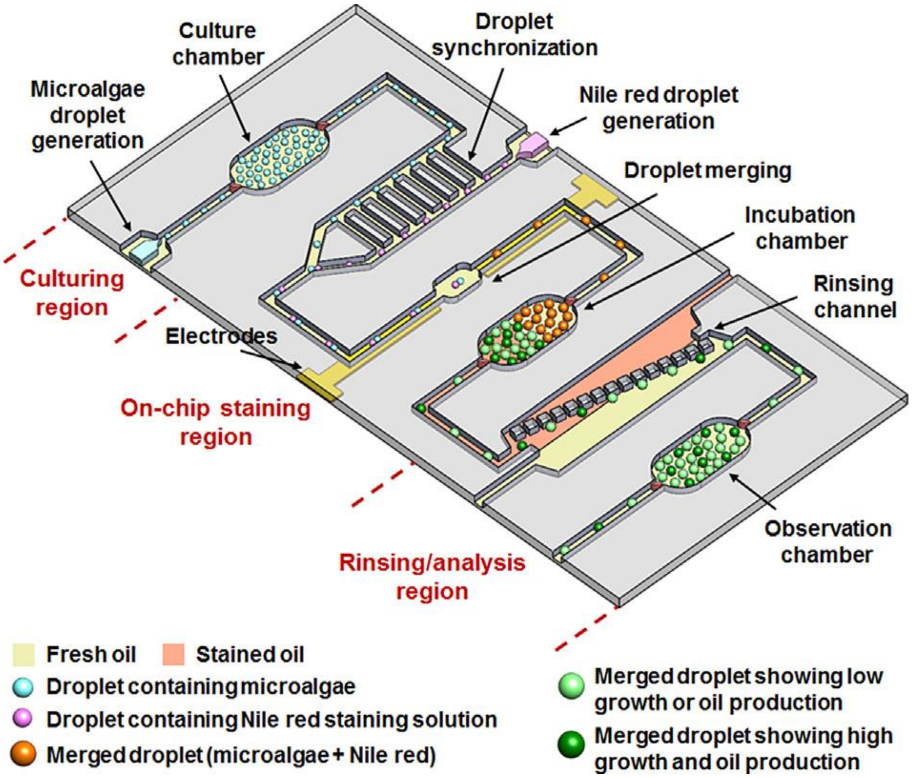

Figure 3.1 Illustration of the droplet microfluidic microalgae staining system for growth and oil accumulation analysis. Reprinted with permission from Wiley Periodicals, Inc. [114]

The initial T-junction droplet generator contains a 200 µm wide channel as the continuous oil phase, or carrier oil, and a perpendicular 160 µm wide orifice for injecting microalgae suspended in culture media (Fig. 3.3b). The T-junction droplet generator is capable of producing 240 µm diameter droplets for encapsulation of microalgae followed by a culture chamber for cultivation of microalgae to allow for the accumulation of cells and oil. The culture chamber also allows for the monitoring of cell growth over time allowing for image analysis of cell growth by characterizing the change in fluorescence of chlorophyll. The 200 µm wide serpentine culture chamber is utilized to ensure that droplets stay in an ordered format and droplets can be easily tracked during image analysis, as well as prevent unexpected droplet merging from occurring (Fig. 3.3c).

On-chip Nile red staining is conducted by suspending Nile red in dimethyl sulfoxide (DMSO) and using a second T-junction droplet generator to continuously generate 240 µm droplets. These droplets are paired one-to-one with reflowed microalgae encapsulated droplets in an adapted fluidic resistance synchronization structure[115]. The railroad-like synchronization structure consists of two parallel 200 µm wide channels carrying trains of droplets, and 100 µm wide rails that are 200 µm apart (Fig. 3.2 & 3.3e). This fluidic structure utilizes fluidic resistances in the two trains to allow for mismatched droplets to become close in proximity prior to being introduced to the droplet merging region.

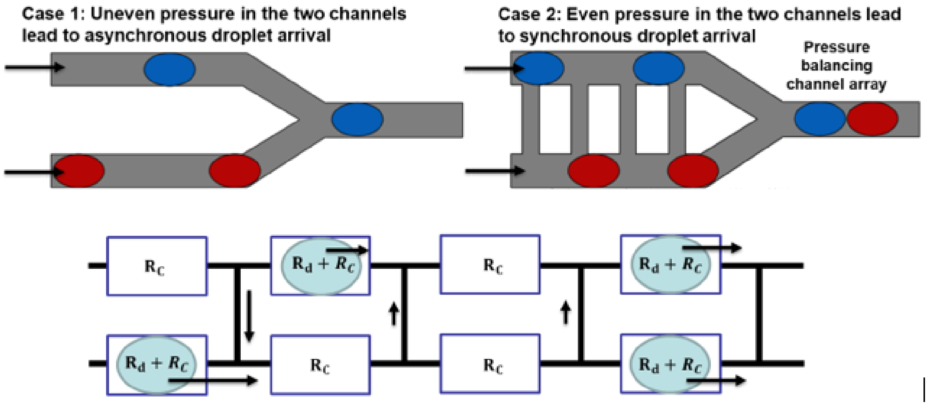

Figure 3.2 Illustration of the droplet railroad-like synchronization region and principal behind fluidic resistance synchronization.

The downstream droplet merging chamber consists of a 500 µm x 500 µm widening structure which slows adjacent droplets to make physical contact and enhance the droplet merging function (Fig. 3.3d). A function generator (DG4102, Rigol Technologies, Beijing, China) was used to generate a 10 kHz 3V peak-to-peak square waveform and was introduced into a high voltage amplifier (Trek 2200, Trek Inc., Lockport, NY, USA) to generate a 150 V AC square wave to induce an electric field causing droplet electrocoalescence. Merged droplets are then stored in a serpentine incubation chamber for 0-10 min to allow for Nile red to appropriately stain encapsulated microalgae.

Nile red molecules have an innate ability to diffuse into the surrounding carrier oil and cause staining of the continuous oil phase, which causes severe fluorescent background and prevents adequate fluorescent imaging or detection of intracellular microalgal oil bodies. This issue was resolved by developing an on-the-fly droplet rinsing process using a 3º angled pillar-based railing structure comprised of 400 µm x 400 µm microposts (Fig. 3.3f). This micropost array was spanned between two laminar flowing oil phases, one containing the reflowed droplets and stained oil to be rinsed, and a second fresh oil flow to rinse the oil surrounding microalgae encapsulated droplets. Droplets roll along the pillar array and are physical transferred from the stained carrier oil to the fresh carrier oil essentially removing all of the background fluorescence. Droplets are finally introduced into a 3 mm x 10 mm observation chamber and oil production is quantified using fluorescence microscopy (Fig. 3.3g).

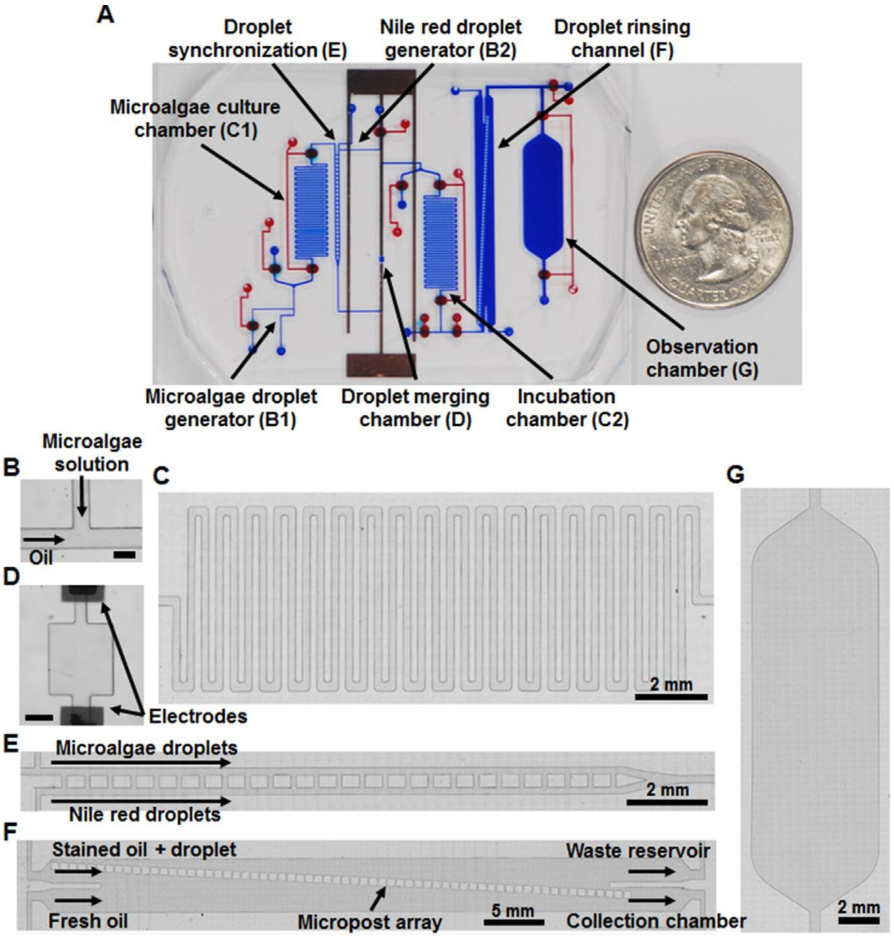

Figure 3.3 (a) An image of the microalgae growth and oil accumulation analysis platform entailing a (b) droplet generator, (c) serpentine culture chamber, (d) merging region, (e) synchronization region, (f) pillar-based rinsing region, (g) and observation chamber. Reprinted with permission from Wiley Periodicals, Inc. [114]

3.3. Fabrication

The droplet staining platform was fabricated using conventional soft lithography techniques where a master silicon wafer was fabricated and PDMS molds were stamped out and bonded to a glass electrode substrate. A master mold for the 160 µm high fluidic channel layer and 250 µm high top valve layer were fabricated using SU-8™ photoresist (SU-2075, Microchem Inc., Westborough, MA, USA). Photoresist was spin coated at 1000 rpm for the fluidic layer and double spin coated at 1000 rpm for the valve layer, followed by 65 ºC and 95 ºC baking for 1 h and 20 min, respectively (the valve layer was also double baked at this same condition between spin coats). The master molds are then patterned using conventional photolithography with a mask aligner (MA6, Karl Suss, Suss Microtec Se, Garching, Germany) and post exposure baked at 65 ºC and 95 ºC for 40 min and 20 min, respectively. After developing, the resulting master molds were coated with (tridecafluoro-1,1,2,2-tetrahydrooctyl)-1-trichlorosilane (T2492, United Chemical Technologies, Inc., Bristol, PA) for 20 min to allow for PDMS replication. The thin PDMS channel layer was spin coated at 300 rpm for 40 s with 4.5 g of liquid PDMS at a 10:1 mixing ratio of polymer to curing agent to obtain a 250 µm thick PDMS channel layer. The valve layer was replicated by pouring 24 g of PDMS pre-polymer and resolving a 4 mm thick PDMS slab. Simultaneously, a Cr/Cu electrode was fabricated on a 50.8 mm x 76.2 mm glass slide (Micro Slides 2947- 75 x 50, Corning Inc., NY) by depositing 200 Å and 3000 Å thick layers using e-beam deposition (Lesker PVD 75 E-beam Evaporator, Kurt J. Lesker, Co., Jefferson Hills, PA, USA), respectively. After conventional photolithography patterning of the electrode using S1818 (Microchem Corp., Westborough, MA, USA) photoresist and Cr/Cu wet etching, the resulting substrate was spin coated with 2.5 g of PDMS at 3000 rpm for 40 s to obtain a 30 µm thick PDMS layer as a hydrophobic substrate for droplet generation. The valve layer and channel layer are then aligned using conventional methanol bonding and bonded using oxygen plasma (Plasma cleaner, Harrick Plasma, Ithaca, NY) treatment followed by curing at 85 ºC for 1 h. The resulting PDMS bonded layers are again treated with oxygen plasma (Plasma cleaner, Harrick Plasma, Ithaca, NY) and the valves are actuated and bonded to the bottom glass electrode substrate resulting in the fabrication of normally closed valves for device operation. After bonding, each device was baked at 85 ºC overnight and allowed to sit at room temperature for 2 days to allow for recovery of hydrophobicity within the microchannel which is necessary for adequate droplet generation.

3.4. Cell preparation

Microalgae *C. reinhardtii, CC-125,* was cultured in Tris-acetate-phosphate (TAP) media at 23 ºC under a light intensity of 80 μmol $\times$ photons $(\mathrm{m}^2)^{-1}\mathrm{s}^{-1}$ with 12 h light-dark cycles. Samples were collected in the exponential phase and diluted to a concentration of 1.38 x 10^5 cells mL^{-1} allowing for a single microalgal to be encapsulated per droplet. Oil accumulation occurred when *C. reinhardtii* was cultured in TAP media without $\mathrm{NH_4Cl}$ (TAP-N) for 4 to 5 days causing stress. A concentration of 8.85 x 10^6 cells mL^{-1} was prepared and used to encapsulate approximately 64 cells per droplet in preparation for Nile red staining. This signifies the typical condition where single cell encapsulation is conducted and cells would be allowed to proliferate to 64 cells in 2 days.

Investigation of the effect of DMSO on the growth rate of *C. reinhardtii* was conducted by comparing the growth rate of encapsulated cells at DMSO concentrations of 0%, 1%, 2.5%, and 50%. Image analysis was conducted by counting the number of cells over the course of a 3-day culture in droplets. The results show that comparable growth was observed for the 0% and 1% case, whereas slower growth was observed for the 2.5% DMSO concentration condition. Furthermore, the 50% DMSO concentration showed a significant decrease in cell proliferation and drastically reduced the cell viability (Fig. 3.4).

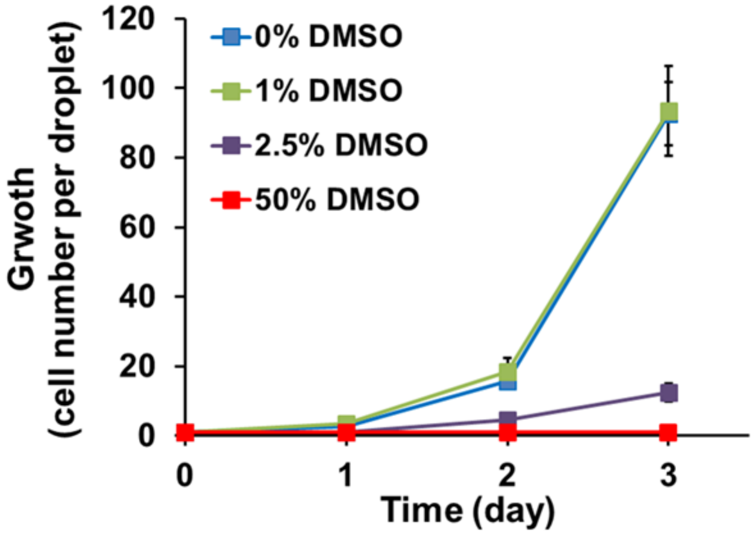

Figure 3.4 Graphical results of the comparison of different DMSO concentrations on cell growth (*n=14*). Data is in mean ± standard error. Reprinted with permission from Wiley Periodicals, Inc. [114]

In addition, a side study was conducted to investigate the DMSO effect on fluorescent intensity of *C. reinhardtii* microalgae by exposing cells to varying concentrations of DMSO (50%, 2.5%, 1%, and 0%) and monitoring the cells for 3 days under 80 μmol $\times \mathrm{photons}\ (\mathrm{m}^2)^{-1}\mathrm{s}^{-1}$ 12 h light-dark cycles. When exposed to 50%, 2.5%, 1%, and 0 % DMSO cells showed a viability of 0%, 74%, 86%, and 90%, where 85% or greater was assumed to be the normal viability standard. Therefore, at DMSO concentrations of less than 1%, cells showed normal viability ranges and DMSO was deemed to have minimal or negligible effects on cell proliferation. It is to be noted that in this experiment only the DMSO concentration was changed and the Nile red concentration was maintained at 5 μL h^{-1} with an incubation time of 10 min. The staining efficiency for the 2.5% and 1% case were 79 % and 63% when compared to conventional off-chip staining, respectively (Fig. 3.5). A DMSO concentration above 20% showed 99% staining efficiency, leading one to believe that addition incubation time is needed for lower concentration of DMSO to allow for complete cell penetration.

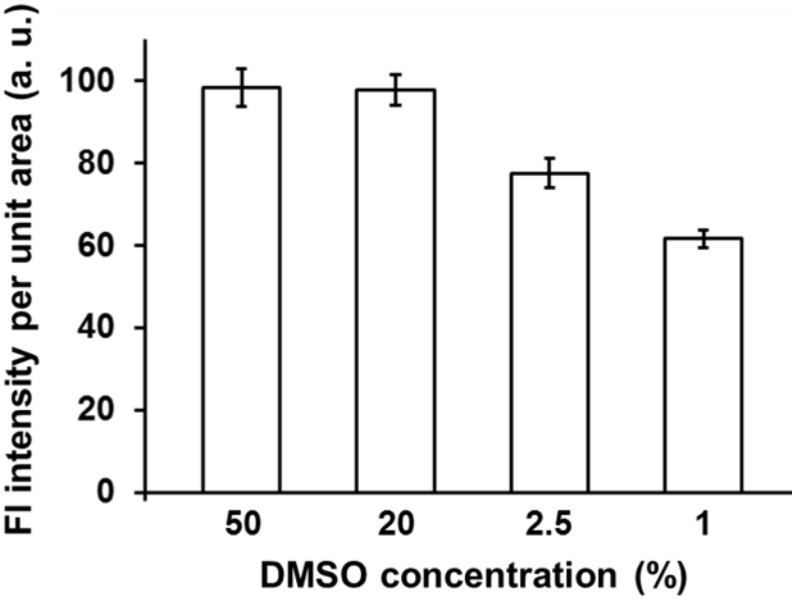

Figure 3.5 Graphical results of the comparison of on-chip Nile red staining at varying DMSO concentrations to conventional off-chip staining (*n=100*). Data is in mean ± standard error. Reprinted with permission from Wiley Periodicals, Inc. [114]

Microalgae *B. braunii* race B, Berkeley was cultured in altered Chu 13 media at 22.5 ºC with similar light intensities and light cycles as those of *C. reinhardtii*. The culture was continuously bubbled with filtered and sterilized air containing 2.5% CO_2. Cells were collected in the exponential phase, filtered for colonies ranging from 70 µm to 100 µm and utilized for on-chip Nile red staining.

3.5. Droplet staining analysis platform operation

The droplet staining platform was characterize using mineral oil (J217 Mineral Oil Light White, Amresco®, OH, USA) with added surfactant (2% wt/wt, Abil EM90, Evonik, Essen, Germany) as the continuous phase to generate droplets. Flow rate characterization was conducted for carrier oil, microalgae solution, and Nile red in DMSO to obtain 240 µm synchronous droplets of microalgae and Nile red solution. All conditions were found experimentally with the final flow rate to obtain appropriate size droplets of microalgae being 272 µL h^{-1} and 55 µL h^{-1}, and 180 µL h^{-1} and 55 µL h^{-1} for Nile red droplets, for oil and water phases respectively. The flow rates of both droplets varied due to the large difference in viscosity of the culture media (.886 cp at 25 ºC) and DMSO (1.990 cp at 25 ºC). Encapsulation of cells followed Poisson's distribution where approximately 30% of droplets contained a single microalgae cell. Microalgae droplets reflowed from the culture chamber are delivered to the synchronization region with a total volumetric flow rate of 327 µL h^{-1}, matching the total volumetric flow rate of the microalgae droplet generator (272 µL h^{-1} + 55 µL h^{-1}). The microalgae train of droplets are synchronized with the Nile red train of droplets at a one-to-one ratio to enhance the downstream droplet merging efficiency. Droplet merging was induced by applying a 150 V AC signal to the droplet merging region for all subsequent experiments and a 95% one-to-one droplet merging efficiency was achieved. Periodically paired droplets do not merge or more than two droplets merge comprising the remaining 5% of droplets. When observing these unmerged or double merged droplets in the downstream chamber, distinguishing these droplets based on their difference in size can be easily observed and eliminated from growth and oil analysis.

3.6. Characterization of On-chip Nile red staining

Droplet staining was characterized by testing combinations of flow rates between the stained and fresh oil to experimentally find a flow rate combination that sufficiently removes stained oil, eliminating background fluorescence. In addition, higher throughput flow rate characterization analysis was conducted to investigate high-throughput platform operation and a continuous platform performance analysis was conducted to validate the system for large-volume microalgae droplet processing. An image analysis was conducted using imageJ (NIH) to analyze the diffusion of Nile red molecules into the surrounding oil and determine which oil combination sufficiently removed stained oil. The fluorescent intensity rinsing measurements were taken across the rinsing channel where the channel was divided into three segments left (X), center (Y), right (Z) for the inlet, middle, and outlet, respectively. Oil flow rates of 225 μL h^{-1}, 450 μL h^{-1}, and 562 μL h^{-1} were tested to flow Nile red droplets with surrounding stained oil into the rinsing channel, and ratios of fresh oil (1: 2, 1: 2.5, 1:3, 1:3.5, and 1:4) were tested and systematically compared to characterize the overall rinsing efficiency. For instance, when a flow rate of 450 μL h^{-1} was tested for stained droplet reflow, an oil rinsing flow rate of 900 μL h^{-1}, 1125 μL h^{-1}, 1350 μL h^{-1}, 1575 μL h^{-1}, and 1800 μL h^{-1} was used for the fresh oil flow rate (Fig. 3.6).

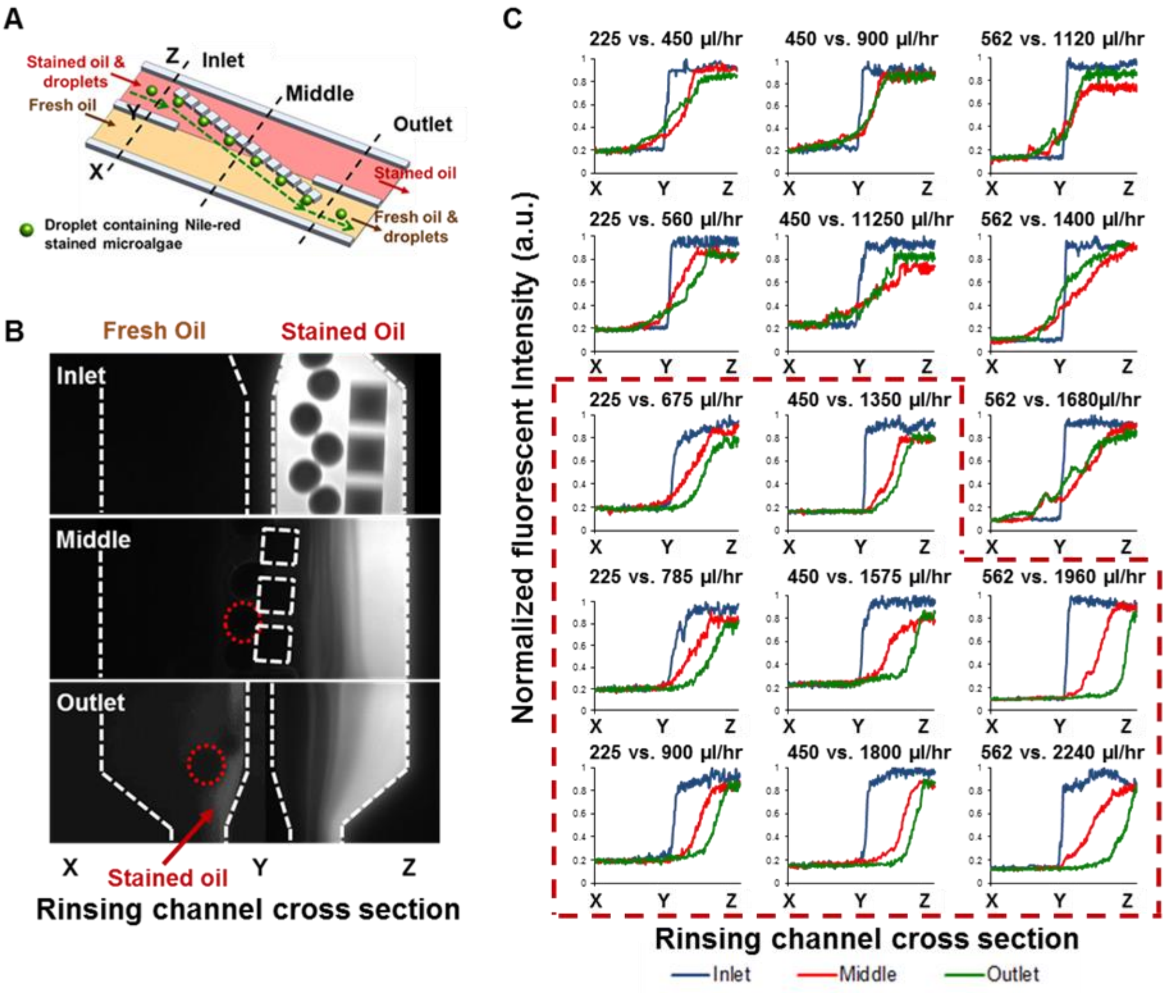

Figure 3.6 (a) Illustration of the operation of the droplet rinsing system where droplets travel along a pillar array and transition from a stained surrounding oil to an unstained surrounding oil. (b) Fluorescent micrographs of the droplet rinsing region showing the removal of stained oil and (c) corresponding fluorescent intensity analysis of surrounding oil using different reflow/fresh oil flow rate combinations. The red box indicates flow rate matches that efficiently rinse stained oil. Reprinted with permission from Wiley Periodicals, Inc. [114]

When a flow rate of 225 $\mu L\ h^{-1}$ was utilized to flow stained droplets into the rinsing channel a fresh oil flow rate of 675 $\mu L\ h^{-1}$ or higher, sufficiently rinsed droplets, approximately three times higher than the stained droplet flow rate. At these flow rate conditions all droplets were completely rinsed and background fluorescence of the stained carrier oil was removed allowing for efficient fluorescent analysis. Alternatively, when the flow rate of the fresh oil was less than three times the stained oil flow, 560 $\mu L\ h^{-1}$ or less, droplets were not sufficiently rinsed and stained oil seeped into the observation chamber leading to undesirable background fluorescence. Similarly, at a stained oil inlet flow rate of 450 $\mu L\ h^{-1}$ a fresh oil flow rate of 1350 $\mu L\ h^{-1}$ or high, three times higher than the stained oil flow, droplets were completely rinsed and successfully transferred into the fresh oil flow region. Furthermore, at a stained oil flow rate of 562 $\mu L\ h^{-1}$, stained droplets were sufficiently rinsed using a fresh oil flow rate of 1970 $\mu L\ h^{-1}$ or high, which corresponds to 3.5 times or higher than the stained oil flow rate. Flow rates lower than 1970 $\mu L\ h^{-1}$ resulted in insufficient rinsing of the stained surrounding oil and severe background fluorescence. Hence, we were able to experimentally find conditions that allowed for adequate rinsing and removal of the background fluorescence for in droplet oil staining quantification, as well as conditions for continuous platform operation and droplet synchronization, merging, staining, and rinsing (Fig. 3.7). A stained droplet flow rate of 450 $\mu L\ h^{-1}$ and rinsing flow rate of 1350 $\mu L\ h^{-1}$ were utilized in all subsequent experiments for on-chip microalgae droplet staining characterization.

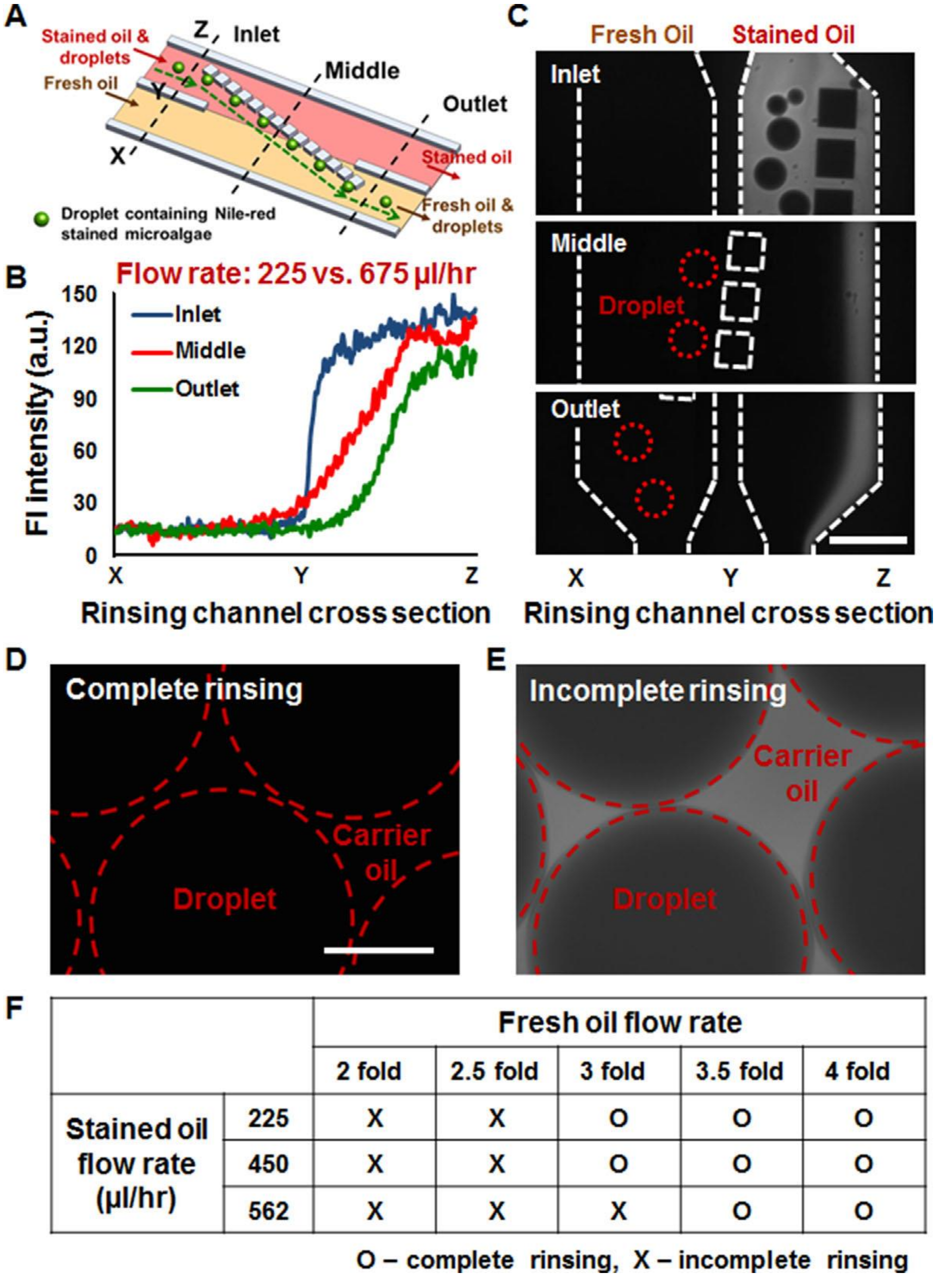

		Fresh oil flow rate				
		2 fold	2.5 fold	3 fold	3.5 fold	4 fold
Stained oil flow rate (µl/hr)	225	X	X	O	O	O
	450	X	X	O	O	O
	562	X	X	X	O	O

O – complete rinsing, X – incomplete rinsing

Figure 3.7 (a) Illustration of the operation of the droplet rinsing system where droplets travel along a pillar array and transition from a stained surrounding oil to an unstained surrounding oil. (b) An example optimized flow rate condition that efficiently removes stained oil, (c) and the corresponding fluorescent micrographs of the optimized condition (Scale bar = 600 µm). (d) Image analysis of completely rinsed droplets and (e) droplets that have not been completely rinsed (Scale bar = 150 µm). (f) Summarization of the flow rate combinations and rinsing outcome. Reprinted with permission from Wiley Periodicals, Inc. [114]

3.7. On-chip characterization of droplet rinsing

On-chip Nile red staining of 64 N-starved (0% nitrogen) encapsulated *C. reinhardtii* cells was conducted to characterize the on-chip staining of the platform. This experiment was conducted to simulate a microalgae screening situation where singe-cell encapsulated *C. reinhardtii* with a doubling time of 8 – 12 h, cultured for 2 – 3 days, will result in approximately 64 cells in a droplet. This culture duration is required to observe a difference in the TAP cultured *C. reinhardtii* and TAP-N cultured *C. reinhardtii*, where the nitrogen limited condition produces sufficient oil bodies for downstream fluorescent analysis. Nile red solution concentrations of 1 μg mL^{-1}, 5 μg mL^{-1}, 10 μg mL^{-1}, 25 μg mL^{-1}, and 100 μg mL^{-1} suspended in DMSO, and incubation times of 0 min, 3 min, 6 min, and 10 min were systematically tested and compared to conventional off-chip staining protocols. Off-chip stained samples were created by suspending 100 μl of *C. reinhardtii* cells with 20 μl of Nile red solution dissolved in DMSO at a concentration of 25 μg mL^{-1} for 10 min, where the final concentration of Nile red and DMSO was 5 μg mL^{-1} and 20 %, respectively. Nile red staining was confirmed by measuring the Nile red fluorescent intensity per unit area of microalgae oil bodies and comparing the average in droplet fluorescent intensity to that of the off-chip stained samples. Nile red fluorescent microscopy characterization was conducted using a Zeiss Axio Observer Z1 microscope (Carl Zeiss Micro Imaging, LLC, Oberkochen, Germany) with a digital camera (Orca Flash 2.9 CMOS Camera, Hamamatsu, Shizuoka, Japan) at excitation wavelengths of 460-500 nm and emission wavelengths of 500-600 nm, as well as chlorophyll auto fluorescent excitation of 400-600 nm and emission > 610 nm.

Comparing the fluorescent intensity to the off-chip stained samples, a concentration of 1 μg mL^{-1} of Nile red achieved only 92% of the fluorescent intensity of the control, even at the maximum incubation time of 10 min. Assume a 95% comparable staining efficiency is required to successfully obtain a statistically relevant staining efficiency, 1 μg mL^{-1} will not reach the desirable staining, regardless of the incubation time. The 5 μg mL^{-1} reached greater than 95% of that compared to the off-chip stained sample for all incubation times of 3 min or greater. At concentrations of 10 μg mL^{-1} or greater, staining efficiency comparable to the off-chip stained sample was achieved regardless of the incubation time or even without any incubation time (Fig. 3.8). It is to be noted that the incubation time defined for these experiments does not include the time required for the Nile red merged droplets to flow through the pillar-based rinsing channel and into the observation chamber for analysis, typically requiring 1.5 min. Therefore, even in the 0 min incubation case, there was still an innate 1.5 min incubation time during which the Nile red molecules have time to stain lipids in *C. reinhardtii* cells. Considering that adding an additional incubation step reduces the overall throughput of the system and prevents continuous flow or the high-throughput screening case from being valid, a concentration of 10 μg mL^{-1} or high was used in all subsequent experiments to eliminate the incubation step and prove the platform viability for high-throughput continuous screening.

All staining procedures for *B. bruanii* were identical to those of *C. reinhardtii* except for an extended incubation time of 20 min and emission filter of 500-550 nm for Nile red fluorescence microscopy. In addition, after on-chip staining *B. bruanii* cells were collected and placed between glass slides to examine whether oil content inside individual cells were stained, as well as confirming extracellular matrix oil were sufficiently stained.

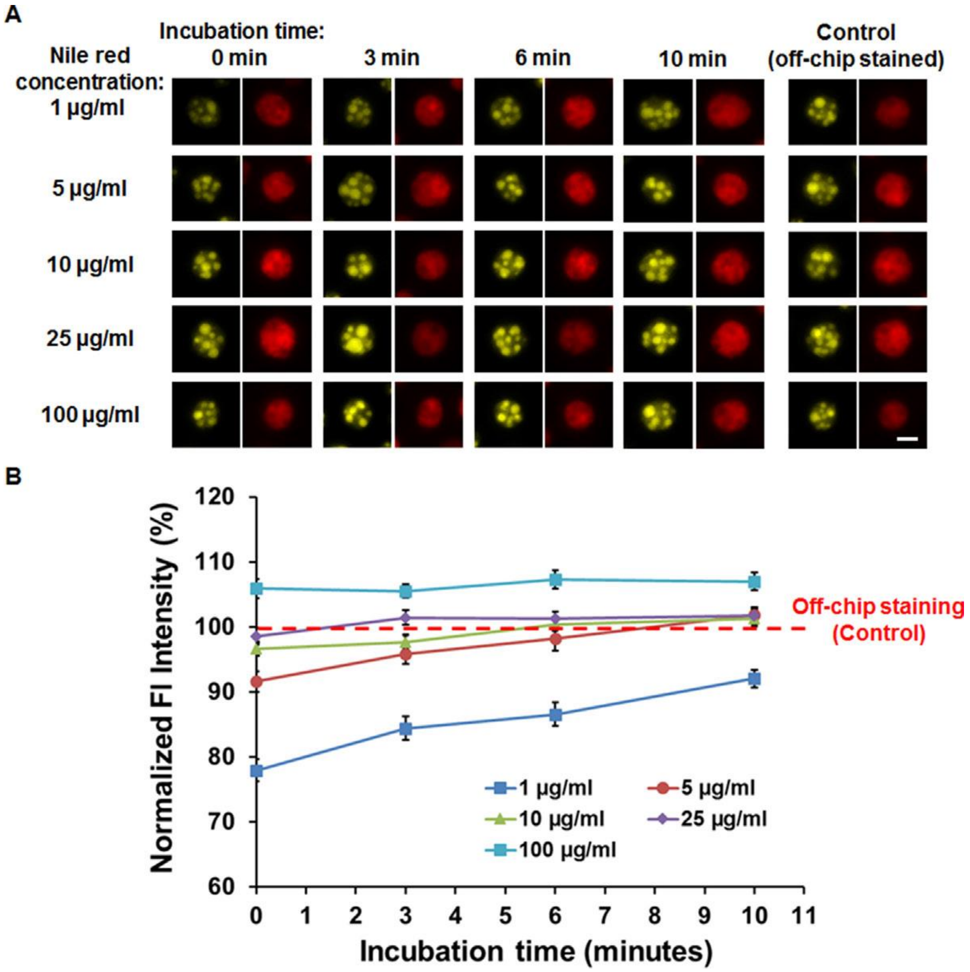

Figure 3.8 (a) Characterization results of the on-chip stained cells in comparison to off-chip stained cells at varying Nile red concentrations (Scale bar = 5 µm). (b) Fluorescent intensity analysis and comparison of on-chip and off-chip stained samples (*n=100*). Data is in mean ± standard error. Reprinted with permission from Wiley Periodicals, Inc. [114]

3.8. *C. reinhardtii* growth and oil accumulation as a model organism for on-chip droplet staining platform

Microdroplets containing a single *C. reinhardtii* suspended in TAP or TAP-N were encapsulated and cultured for 6 days under a light intensity of 80 $\mu\mathrm{mol} \times \mathrm{photons}\ (\mathrm{m}^2)^{-1}\mathrm{s}^{-1}$ with a 12 h light-dark cycle. Time course analysis was conducted by tracking individual droplets and observing cell duplication and corresponding increase fluorescence of chlorophyll autofluorescence. In addition, oil accumulation of *C. reinhardtii* under nutrient limitation conditions was characterized over time by measuring cell fluorescence intensity per unit area by on-chip Nile red staining and time-course image analysis. All conditions were characterized using 12 different samples and analyzed for each using time-course analysis.

Considering the N-replete condition, the average number of cells proliferated inside the microdroplet exponentially for 3 days, and then the growth began to decrease and began saturating. This is assumed to be caused by the nutrient limitation inside the droplet microfluidics format. A doubling time of 8-12 h was observed for days 0-3, which corresponded to the growth rate observed in the off-chip control sample. Conversely, for the N-deplete condition, cell proliferation only occurred for the first day of cultivation and cells stopped doubling as a result of the nitrogen deficiency.

An increase in oil accumulation was observed for the N-deplete condition due to the lack of nitrogen and induced stress, while the N-replete condition showed a negligible increase in oil accumulation from 0-3 days. Considering the adverse effects of DMSO and Nile red staining, even at low concentrations, multiple devices were utilized and sacrificed after each time-course oil analysis to ensure there was no variable in the background fluorescence or leeching of staining from the stained device to surrounding oil or droplets. It is to be noted that Nile red can also stain the hydrophobic PDMS device used in this experiment, giving further reasons for the use of each device only once. In the N-deplete conditions, a maximum oil accumulation was observed after 4 days of cultivation, followed by a subsequent decrease at days 5 and 6, which we assume is due to the cells use of accumulated triacylglycerols as an energy source for sustainability (Fig. 3.9).

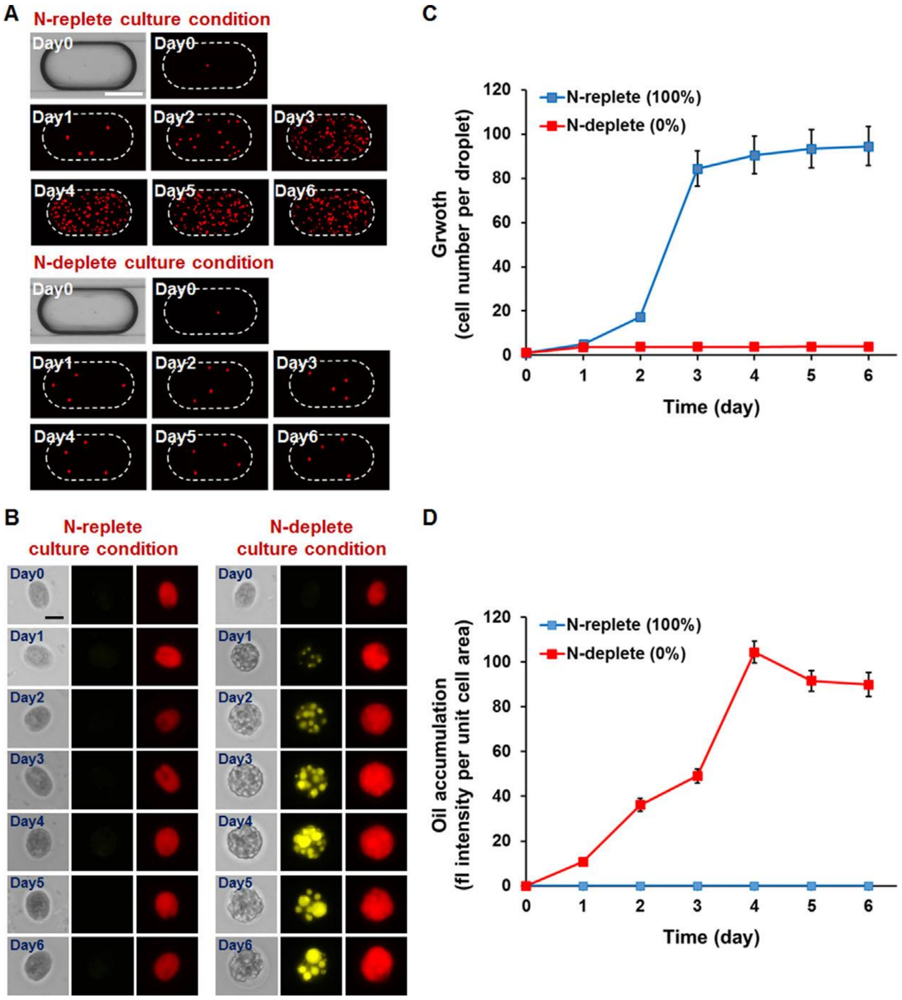

Figure 3.9 In-droplet comparison growth rates and oil accumulation of N-replete and N-deplete conditions was conducted. (a) N-replete time-course fluorescent analysis of chlorophyll conducted and compared to the N-deplete condition (Scale bar = 150 µm). (b) Corresponding Nile red staining and chlorophyll microalgae images were analyzed (Scale bar = 5 µm). (c) Graphical results of growth (*n=12*), and (d) oil accumulation showed a large differential in growth and oil accumulation for the two populations (*n=25*). Data is in mean ± standard error. Reprinted with permission from Wiley Periodicals, Inc. [114]

Furthermore, compared to the N-replete condition, *C. reinhardtii* cells cultured in the N-deplete condition showed a 100%-110% increase in the cell size due to the lack of doubling and accumulation of oil bodies (Fig. 3.10).

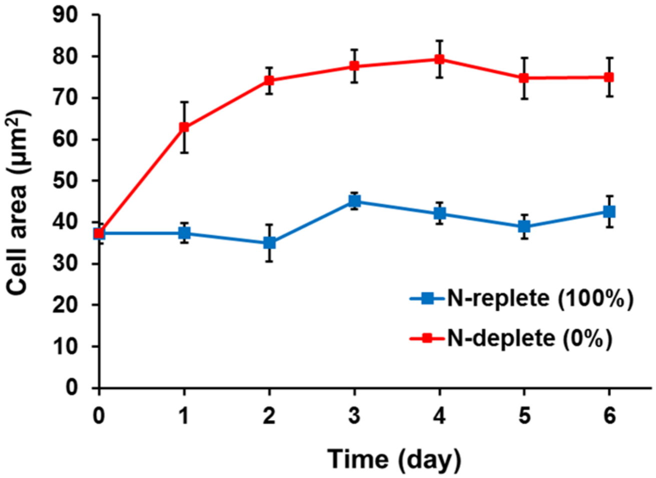

Figure 3.10 Graphical results comparing cell area for N-replete and N-deplete conditions (*n=40*). Data is in mean ± standard error. Reprinted with permission from Wiley Periodicals, Inc. [114]

3.9. Colony forming microalga, *B. braunii* as an additional model organism for platform validation

On-chip analysis of *B. braunii* was demonstrated as a subsequent and different model organism to better validate in-droplet staining for a wide variety of potential microalgal species. Although many different types of microalgae for producing biofuel exist, *B. braunii* is appealing due to its ability to accumulate liquid hydrocarbon oil of up to 50% of its dry weight. Majority of this oil, 90%-95% is accumulated in the colony extracellular matrix with the remaining being inside the individual cells. These cells work together as a network of 100-200 cell colonies to increase the amount of oil per weight. In lieu of this complex network and large number of individual cells, the amount of Nile red required to obtain sufficient staining of all intracellular and extracellular oil bodies is typically much high, with longer incubation times. Often times it is more difficult to find the optimal conditions to stain complex networks of organisms, and this is why *B. braunii* was chosen as a more difficult model to validate the droplet on-chip staining performance. After testing a variety of culture times and concentrations, a Nile red concentration of 2500 μg mL^{-1} and incubation time of 20 min was experimentally found to successfully stain both intracellular and extracellular oil bodies comparable to that of conventional off-chip staining protocols. The average fluorescent intensity analysis for off-chip control and on-chip stained droplets was conducted for a minimum of 25 samples. Further confirmation was conducted by extracting droplets from the chip onto glass slides and squeezing the 3D shaped *B. braunii* to a more spread out 2D format so that individual cell could be observed more readily. Both the intracellular and extracellular oil were successfully stained using the droplet staining and rinsing platform (Fig. 3.11).

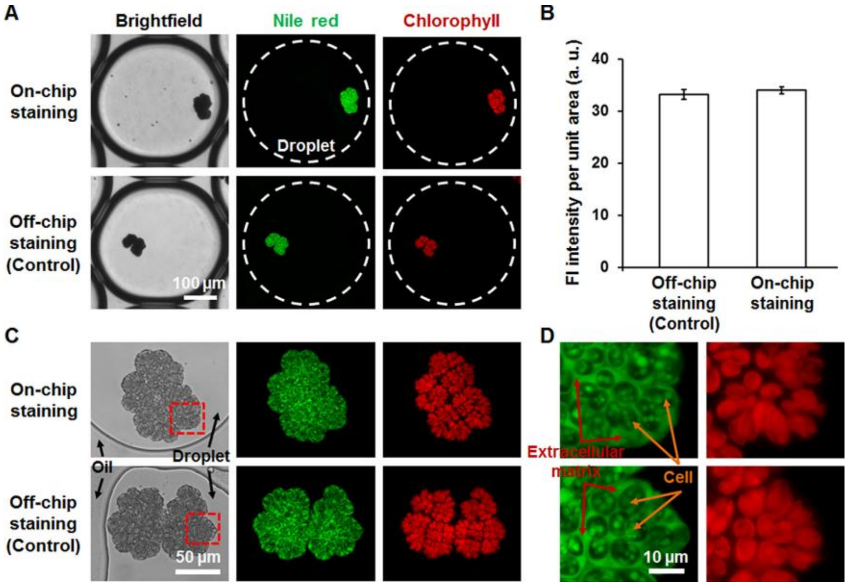

Figure 3.11 (a) *B. braunii* staining comparison of off-chip and on-chip stained samples was conducted through fluorescent image analysis, (b) and showed a similar level of fluorescent intensity *(n=25*). (c & d) Cells were squeezed between glass slides to further confirm that intracellular oil bodies were sufficiently stained. Data is in mean ± standard error. Reprinted with permission from Wiley Periodicals, Inc. [114]

3.10. Conclusion

The work presented here is the first demonstration of a high-throughput droplet microfluidic continuous staining platform for the analysis of growth and oil accumulation of biofuel producing microalgae. Conducting a comparative analysis of on-chip in-droplet on-the-fly microalgae staining under different culture conditions we were able to overcome previous droplet-based microalgae screening limitations and develop a platform for high-throughput screening of microalgal strains of interest. Compared to traditional dilution-based assays or plating screening assays utilized to acquire microalgal mutants, the microalgae droplet microfluidic based screening platform is capable of high-throughput continuous real-time single-cell resolution analysis of oil accumulation and cell growth. In comparison to conventional assays, this droplet screening platform has a drastic reduction in instrument cost, labor, and human error.

The droplet-based screening platform was utilized to characterize growth and oil accumulation of *C. reinhardtii* and *B. braunii* cells with the capability for off-chip retrieval. Although the presented platform can only process several thousands of samples in a batch format, the continuous operating mode successfully allows for the capability of high-throughput screening of $1\text{x}10^6$ samples necessary to find a cell of interest. Although, without complex manipulation many droplet microfluidics platforms have limitations in culture duration due to the lack of replenishing nutrients, for microalgae that typically have slower growth than most bacteria, 5-7 days of cultivation are adequate for distinguishing between microalgae showing improved phenotypes. The droplet platform allows for complete isolation of encapsulated cells and confines daughter cells as to not allow for cross contamination or cell signaling amongst variant species. This leads to a high isolated and robust bioreactor format for quantitative fluorescent analysis of phenotypically beneficial cells.

This work serves as a precursor platform for future high-throughput droplet microfluidic based screening platforms for the investigation and analysis of microalgae and the discovery of new strains or advantageous phenotypic cells to improve the production of biofuels. With this platform downstream development, cell engineering, and mass production can be significantly enhanced, in turn reducing the overall cost for production of biofuels and allowing microalgae to become economically competitive with current petroleum fuel sources. We expect this platform to serve as a vital high-throughput analysis tool for screening large volumes of microalgae in pursuit of rare elusive cells of interest that can have a large impact on the future of biofuel production.

4. LARGE-SCALE INTEGRATED DROPLET INCUBATION CHAMBERS FOR CONSISTENT CELLULAR CULTIVATION*

4.1. Motivation

In most screening applications, statistical models show that a minimum of $1\text{x}10^6$ distinct cells need to be screened to find a single cell of interest that produces a novel compound. Considering this fact, a single droplet microfluidic screening system requires a large volume of microdroplets to process and find a "hit" [116, 117]. Therefore, for integrated high-throughput droplet microfluidic-based screening approaches a droplet culture chamber capable of precisely controlling the culture duration is critical. Considering that screening applications typically require culture durations on the order of hours to obtain noticeable differences in cell proliferation or phenotypes, identical culture durations are imperative to reduce variations and error [118-121].

In conventional droplet microfluidic screening systems an off-chip culture chamber is utilized to culture droplets and these droplets are later reinjected into separate chips for droplet manipulation. Culture chambers such as large channels, serpentine channels, or microchambers are often used as on-chip chambers but are limited in size and volume and therefore not suitable for large screening applications. Also, centrifuge tubes, Pasteur pipettes, or capillaries can be utilized as large volume first-in first-out chambers but cannot be fully integrated into microfluidic based systems for automated fabrication processes, and therefore have limitations in mass fabrication. Furthermore, due to the transfer of droplets from one chamber to a downstream device for manipulation, differences in culture duration can occur between platform interfaces or

---

*Reprinted with permission from "A large-scale on-chip droplet incubation chamber enables equal microbial culture time" by J. Dai, H. S. Kim, A. R. Guzman, W.-B. Shim and A. Han, *RSC Advances*, 2016, **6**, 20516-20519, Copyright 2016 by The Royal Society of Chemistry.

during processing. Consequently, there is a need for an alternative controlled approach with mass fabrication capability that can incubate large volumes of droplets and ensure that each droplet has identical culture duration prior to downstream manipulation. For these long culture duration applications, we suggest an integrated first-in first-out ordered droplet cultivation platform that can precisely control the droplet incubation duration.

4.2. Design

The droplet microfluidics culture chamber capable of culturing a large volume of droplets is comprised of three main components: a top side droplet generator for delivering droplets to the culture chamber in a top down format, the large volume culture chamber with a conical shape to allow for gradual filling of the chamber, and a bottom substrate for flowing droplets out for downstream manipulation. The droplet generator used to generate droplets is a T-junction droplet generator with a continuous phase channel and water orifice, which produces 121 µm diameter droplets for characterization. The culture chamber has a diameter of 1 cm and height of 4.3 cm with a total volume of 2.4 mL, capable of housing $2.32\text{x}10^6$ droplets when filled completely (Fig. 4.1). At this droplet size and a droplet generation rate of 52 Hz, the entire chamber is filled in 12.5 h.

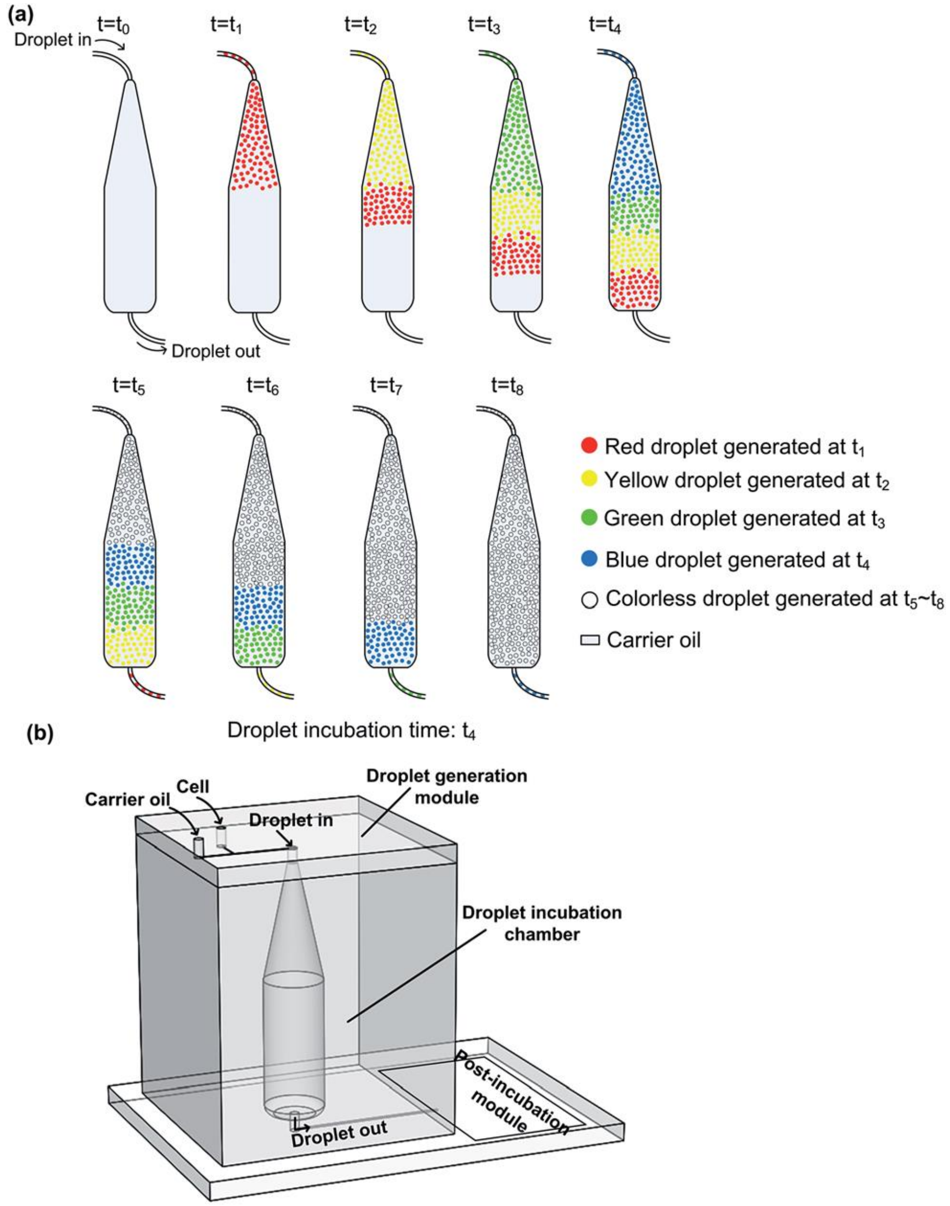

Figure 4.1 (a) Illustration showing the operation of the first-in first-out large droplet culture chamber and (b) integrated droplet culture system. Reprinted with permission from The Royal Society of Chemistry. [122]

4.3. Fabrication

The top droplet generator is fabricated using conventional photolithography techniques where a silicon master mold is spin coated with S-U8 photoresist and patterned using a UV mask aligner (MA6, Karl Suss, Suss Microtec Se, Garching, Germany). The large volume droplet culture chamber is replicated from a master mold printed using a 3D printer (Perfactory Ultra, LS600 resin, EnvisonTEC Inc., Dearborn, MI, USA) that is exposed to UV light (Omnicure S1000, Lumen Dynamics, Mississauga, ON, Canada) for 5 min and baked overnight at 50 ºC. Similarly, the master mold for the bottom channel layer for flowing droplets out for downstream manipulation was fabricated using a 3D printing process (Perfactory Ultra, LS600 resin, EnvisonTEC Inc., Dearborn, MI, USA). Each of the master molds are coated with (tridecafluoro-1,1,2,2-tetrahydrooctyl)-1-trichlorosilane (T2492, United Chemical Technologies, Inc., Bristol, PA, USA) for 30 min to allow for PDMS replication. The large chamber PDMS layer is fabricated by pouring 1:10, crosslinker to elastomer, liquid PDMS and baking for 2 h at 85 ºC. The bottom channel layer was fabricated by pouring PDMS (15:1, elastomer: crosslinker) and baking for 1 h at 85 ºC. The resulting PDMS devices are punched for inlet and outlet holes, bonded, and baked overnight at 85 ºC.

4.4. First-in first-out operation

The first-in first-out long-term droplet microfluidic culture chamber is utilized in a top-down format where droplets are introduced from a top droplet generator layer and droplets are stacked eventually flowing out of the bottom of the chip when the chamber is full. A fluorinated oil (Novec 7500, 3M, Maplewood, MN, USA) with added fluorosurfactant (2 % wt/wt, PFPE-PEG-PFPE, Ran Biotechnolgoies, Beverly, MA, USA) was used to generate water-based droplets using the T-junction droplet generator. This surfactant is used to stabilize droplets and prevent undesirable droplet coalescence. In addition, the fluorinated oil has a greater density than water, causing droplet to float in the presence of fluorinated oil, allowing for the droplets to stack in an ordered top-down format. A syringe pump (Fusion 400 Chemyx Inc., Stafford, TX, USA) was used to generate 121 µm diameter droplets using a continuous oil flow rate of 200 µL h^{-1} and water phase flow rate of 180 µL h^{-1}. Droplet generation rate was characterized using a CMOS camera (C11440, Hamamatsu, Shizuoka, Japan) at 150 fps and 6.67 ms exposure time.

4.5. Characterization of first-in first-out culture chamber

The first-in first-out droplet microfluidic culture chamber is first experimentally characterized by conducting a droplet color dye flow through test using a variety of color dyes and observing the propagation of these dyes through the platform. Due to the buoyancy of droplets, droplets stack in an orderly fashion from the top of the device downward, where new layers of droplets push down previously generated layers. Red, yellow, green, and blue droplet layers are generated at different timepoints (t1-t4), followed by empty droplets to push out these dye stained droplets. A total incubation time of 12.5 h was observed for droplets exiting the chamber. The overall capacity of the chamber was 2.32 x 10^6 with a volume of 2.4 ml (Fig. 4.2). As droplets are gradually introduced into the chamber through the conical top of the chamber, transition color layers are observed to characterize the flow of layers of droplets through the platform.

Image analysis was conducted at the bottom of the chamber to observe the droplet layers as they exited the platform. The first-in first-out and culture time duration was validated by comparing the droplet generation, incubation, and color dye droplets exiting the chamber. Generating empty dummy droplets to push out the droplets of interest allows for a continuous operation format without the need for valving operations.

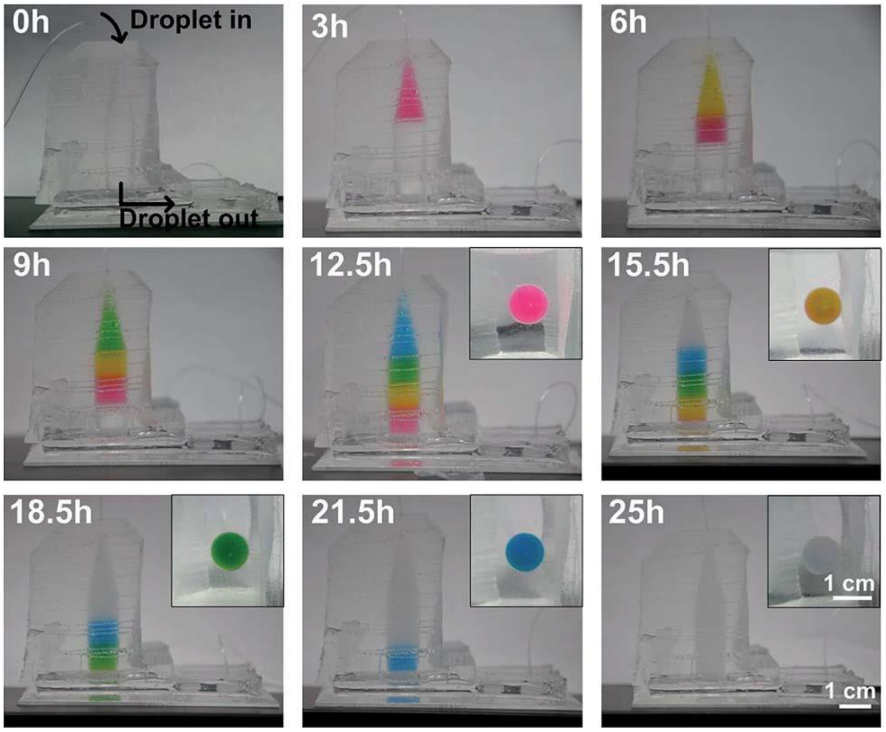

Figure 4.2 First-in First-out chamber characterization: Images of red, yellow, green, blue, and colorless droplets being introduced into the chamber from the top and exiting through the bottom in an orderly fashion. Reprinted with permission from The Royal Society of Chemistry. [122]

Furthermore, the transition of droplets from one color segment to the next was observed and characterized to confirm a first-in first-out order was obtained. Each of the color transitions from red to yellow, yellow to green, green to blue, and blue to colorless was observed and characterized. Each of the transition times varied from 24 min to 62 min, but none exceeded 62 min (Fig. 4.3). Statistical normality and equal variance assumption are conducted using an Anderson-Darling and Barlett's test (Minitab 14, Minitab Inc., State College, PA, USA) The overall variation in the transition time due to Taylor dispersion in the microfluidic channel ranged from 3-8%, which have no statistically significant difference in the culture time and validates the platform.

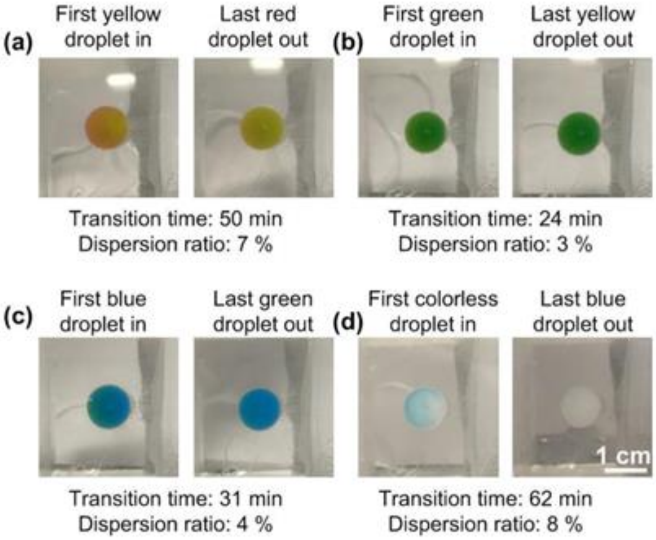

Figure 4.3 Transition of droplets exiting the chamber from (a) red to yellow, (b) yellow to green, (c) green to blue, (d) and blue to colorless. Reprinted with permission from The Royal Society of Chemistry. [122]

The cultivation time was further characterized by encapsulating single spores of *Fusarium verticillioides* (*F. verticillioides*) and culturing these spores in the continuous cultivation chamber. These wild-type *F. verticillioides* spores were suspended in deionized water at a concentration of 5x10^7 spores mL^{-1} and adjusted to a concentration of 5.5x10^5 spores mL^{-1} in YEPD media for encapsulation. These spores were encapsulated at a rate of 48 Hz where approximately 10% contain a single spore based on a diluted form of Poisson's distribution to ensure single cell encapsulation. To ensure spores do not germinate during droplet encapsulation, spores in a syringe are kept on ice during encapsulation. After the 12.5 h incubation time to traverse the entire culture chamber at 23 ºC, cells were analyzed on an inverted microscope (Eclipse TS100F, Nikon, Tokyo, Japan) equipped with a CCD camera (DS-2MV, Nikon, Tokyo, Japan) using a 40x magnification objective in bright-field (Fig. 4.4). Growth analysis was conducted using ImageJ software (NIH) to analyze fungal cell growth at different time points (0, 3, and 6 hours). The cell morphology of droplets in YEPD media was comparable to that of YEPD agar plates with a growth rate of .16 h^{-1} compared to .30 h^{-1}, respectively.

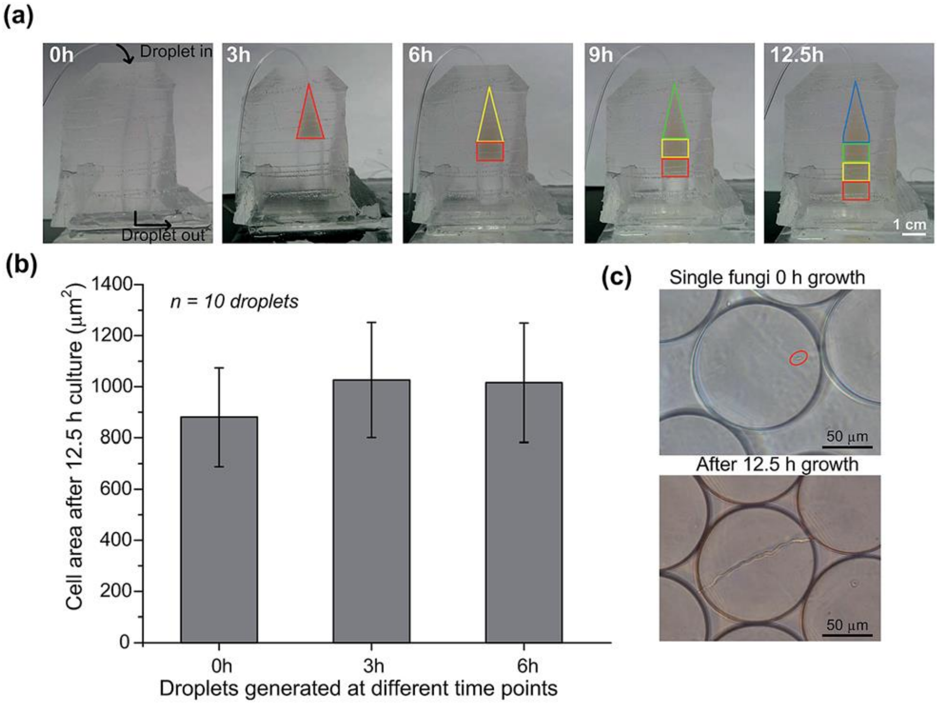

Figure 4.4 Growth of fungi spores was characterized where (a) droplets are tracked at 3, 6, 9, and 12.5 h and (b) cell area is analyzed for growth of cells at each time point. (c) Growth of spores after 12.5 h showed similar filament growth (*n=10*). Data is in mean ± standard deviation. Reprinted with permission from The Royal Society of Chemistry. [122]

4.6. Alternative first-in first-out culture chamber designs

Although the work presented here demonstrates a top-down droplet microfluidic cultivation chamber, there are other similar approaches which can be employed to have the same first-in first-out ordered function. First, the droplet flow scheme for processing large volumes of droplets is highly dependent on the overall assay scheme and application. For instance, the size of the droplet and droplet generation rate have a large impact on the final volume of the chamber that will provide optimal platform performance of the cultivation chamber. In addition, the oil that is to be used in the droplet assay determines if the water-based droplets will float or sink inside of a large volume culture chamber, leading to differences in designing the chamber in a top-down vs. bottom-up approach. For instance, when using a higher density oil, droplets will sink and therefore need to be generated from the bottom to replicate a first-in first-out format as the one shown in this work. It is to be noted that with other more integrated platforms that include valving structures, alternative approaches for semi-continuous first-in first-out chambers, both top-down and bottom-up format, can be employed to better suit more complex assays.

4.7. Conclusion

In the work presented here, we successfully designed and characterized a continuous first-in first-out on-chip droplet incubation chamber capable of processing large volumes of droplets with identical incubation times. This platform was validated by monitoring the propagation of color dye droplets through the system. Furthermore, fungi spores were utilized to further validate the top-down incubation chamber by encapsulating single spores and conducting statistical growth analysis on droplets processed using the culture platform. This work demonstrates a novel approach for developing high-throughput ordered and controlled cultivation chambers with mass fabrication capability for droplet screening applications.

5. MULTI-CHIP DROPLET MICORFLUIDICS-BASED SCREENING SYSTEMS*

5.1. Motivation

In the widening field of droplet microfluidics, screening applications for discovery of novel or mutant strains, undiscovered compounds, antibodies, and drugs have been targeted as key applications that can be enhanced by complex droplet systems. Considering that many droplet microfluidic assays require more than just basic droplet functionalities, multiple processing steps and sequential manipulation is required to successfully conduct complex screens. Many of the previously published droplet screening systems utilize various functional components to manipulate droplets to conduct their assay of interest. These functional components are often highly dependent on the assay that is being conducted, therefore for more complex screening assays, sequential characterization of tethered chips is necessary as building block for ultimately building complex fully integrated systems. Understanding the interaction between the chips and processes on separate tethered chips can give key information as to the overall process being conducted and possible complications that will be innate to the integrated system approaches. Hence, here we investigate separate, but tethered downstream droplet operations for better understanding of issues related to multiple sequential droplet microfluidic functionalities to better understand relevant issues for full platform integration.

---

*Reprinted with permission from “High-throughput droplet microfluidics screening platform for selecting fast-growing and high lipid-producing microalgae from a mutant library” by H. S. Kim, S. C. Hsu, S. I. Han, H. R. Thapa, A. R. Guzman, D. R. Browne, M. Tatli, T. P. Devarenne, D. B. Stern and A. Han, *Plant Direct*, 2017, **1**, e00011, Copyright 2017 by The Authors. *Plant Direct* published by American Society of Plant Biologists, Society for Experimental Biology and John Wiley & Sons Ltd.

5.2. Multi-chip operation design

The overall design of a complex sequential multi-chip assay is highly dependent on the target assay and therefore the work presented here will discuss droplet manipulation techniques and respective chips for conducting assays requiring; droplet generation of an environmental or library sample, incubation of the environmental or library sample to allow for accumulation of growth/drug/toxin/ or antibody, on-chip droplet merging, an additional co-incubation for interaction between organisms/ compounds of interest/ or dye, droplet detection, and subsequent droplet sorting for post processing and validation. A variety of separate chips have been developed to allow for the processing of samples and design of the overall experiment can be easily altered by including or excluding desirable chips as necessary.

5.3. Microalgae mutant screening system

The first system, as an example, is a microalgae-based screening system that first uses a chip entailing a droplet generator and large-volume pillar-based basket trapping cultivation chamber (chip 1/chip 1a & 1b: integrated together or tethered, respectively) for the initial generation and incubation of microalgae to be investigated for high growth and high oil accumulating microalgae cells. A second chip entails on-the-fly generation of a dye and parallel reflow of previously cultured microalgae that are synchronized using a railroad-like structure. Paired droplets are merged using electrocoalescence and incubated in a fluidic delay line for dye staining to occur (chip 2). Downstream chlorophyll and oil accumulation detection is conducted using a blue LED for excitation and dual optical detection system, followed by oil injection droplet sorting to deflect droplets to a collection chamber for harvesting (Fig. 5.1).

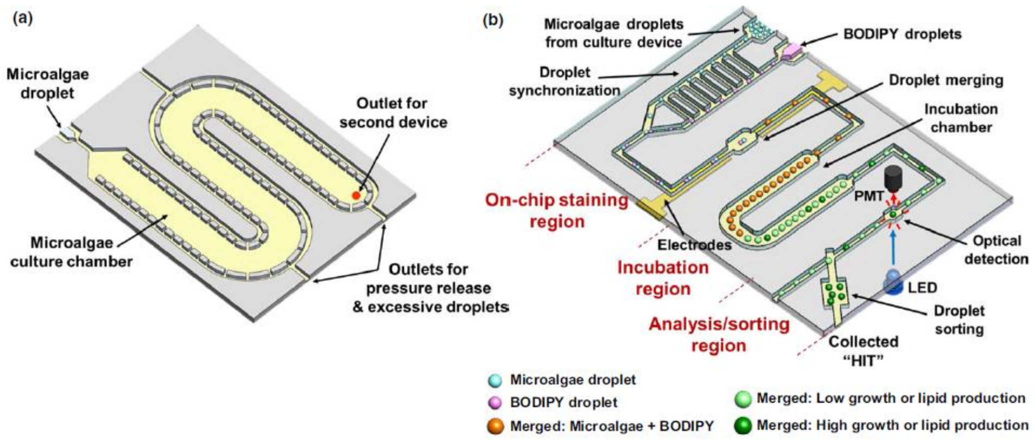

Figure 5.1 (a) A schematic of the large basket trapping culture chamber for conducting microalgae growth analysis and (b) a secondary chip containing on-chip staining, incubation, analysis, and sorting. Reprinted with permission from Plant Direct. [113]

5.4. Novel large-volume basket trapping chamber for bioreactor cultivation

The novel large volume pillar-based basket trapping cultivation chamber is a universal tool that can be used as a system for temporary storage of droplets or long-term cultivation of droplets. In addition, the trapping dynamics allows for droplets to be tightly packed inside of the middle region of the basket, which is highly advantageous for downstream manipulation. Although the original droplet basket trapping cultivation chamber was developed by myself, other variations of this basket trapping structure have been developed within our group to accomplish the same functionality, but with different volume or target droplet size. The design is highly depending on the droplet size, which is determined by the assay and target cells that are to be screened (encapsulated). For instance, larger cells require larger droplets to avoid physical confinement complications and nutrient depletion. In addition, the droplet size determines the overall height of the basket trapping chamber to allow for a monolayer of droplets to be packed in the chamber which is optimal for optional subsequent image analysis or time-lapse image analysis (larger volume multilayer droplet basket structures have been utilized in-house but prevent adequate image analysis due to overlapping of droplets). Furthermore, the pillar size and more importantly the gap between pillars must be optimized based on the droplet size to prevent droplets from escaping from the pillar-based basket structure.

5.4.1. Design

Considering the microalgae screening system where 240 µm diameter droplets are used to cultivate mutant cells, a pillar gap of 40 µm is suitable to prevent droplets from escaping. A typical T-junction droplet generator with a 200 µm wide carrier oil channel and 160 µm wide aqueous phase orifice is used to generate the 240 µm microalgae droplets. Typical pillar sizes for this type of structure are 200 µm x 200 µm and are placed along the side wall with a 200-250 µm gap from the side wall. The inlet has a 45° angled opening to allow for droplets to slow down and progress toward the culture chamber. Excess oil simply flows around the packed droplets and through pillars allowing for the complete packing of the chamber and serving as an overflow function for when the chamber is completely full (Fig. 5.2).

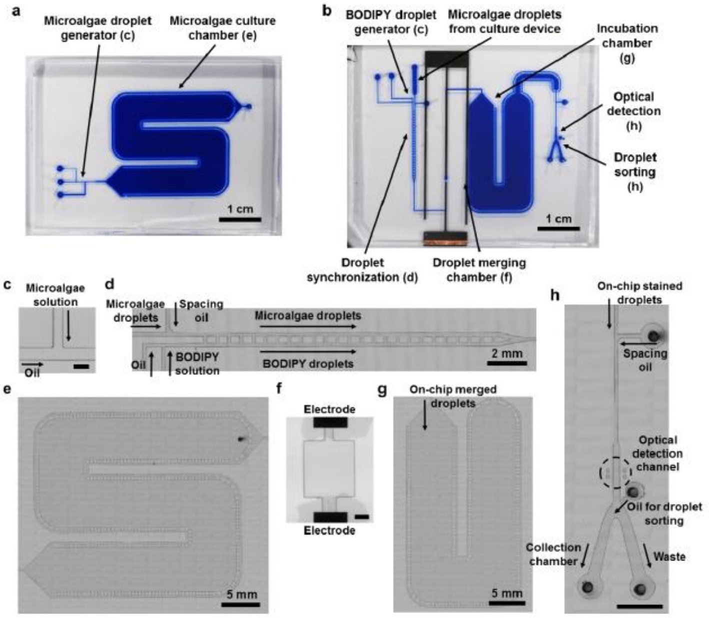

Figure 5.2 Images of the (a) droplet generator and culture chamber and (b) the droplet merging, detection, and sorting chip. Corresponding micrograph images of the (c) droplet generator, (d) droplet synchronization region, (e) droplet incubation chamber, (f) merging region (Scale bar = 200 µm), (g) incubation chamber, and (h) detection/sorting region (Scale bar = 2 mm). Reprinted with permission from Plant Direct. [113]

5.4.1.1. Cultivation of target organisms

Droplets are generated and collected in a first-in first-out format to allow for droplets to have identical culture durations when reflowed from the cultivation chip to downstream processes. At the beginning of the operation of this basket trapping chamber a droplet generator is utilized to generate microalgae droplets and cultivate these droplets in TAP media for 1.5-4 days at room temperature under continuous illumination ($6\ \mu\mathrm{mol} \times \mathrm{photons}\ (\mathrm{m}^2)^{-1}\mathrm{s}^{-1}$), followed by growth and oil accumulation analysis (Fig. 5.3). Similarly, high lipid accumulating cells (*CC-406* and *sta6*) were utilized for characterization of the detection system and were cultivated in TAP-N media to increase lipid production.

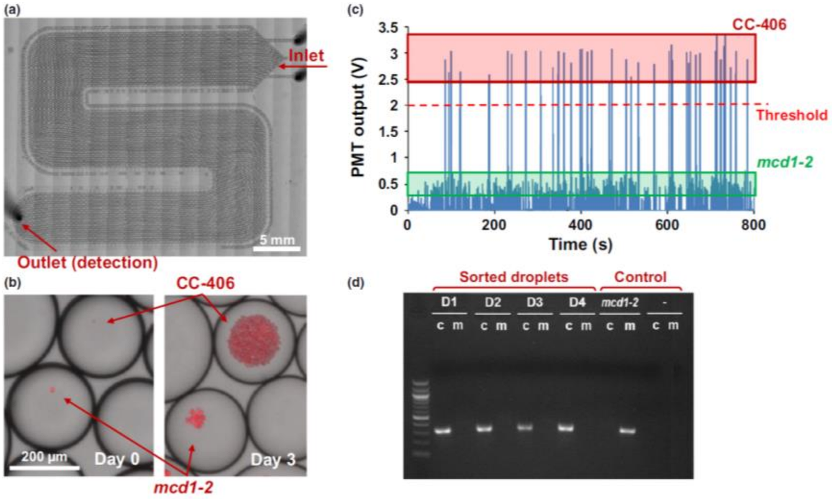

Figure 5.3 (a) Microalgae droplets are generated and incubated in the basket trapping structure. (b) Growth comparison of *CC-406* and *mcd1-2* was conducted for each microalgae strain in droplets, (c) followed by PMT detection of the resulting cultivated microalgae droplets. (d) Further confirmation was conducted using PCR. Reprinted with permission from Plant Direct. [113]

5.4.1.2. Ordered on-demand reflow of droplets to merging chip

In many complex droplet microfluidic screening assays multiple functionalities are utilized to manipulate droplets for on-chip processing. Due to the highly complex nature of sequential integrated systems or tethered systems, precise controllability of droplets and identical flow schemes are required to produce statistically sound results and minimal error rates. In lieu of these facts, having high controllability is an extremely advantageous aspect desired when working with droplet microfluidic screening systems. In particular, the reflow of droplets in a highly packed manner, attained by the basket trapping structure, allow for the input of desirable spacing for downstream manipulation and gives on-demand desirable versatility to the droplet system. Essentially providing controllable standardized spacing and deterministic flow speed/throughput to the system. This controllability is vital to the integrity of the assay for downstream processing and maximizes the likelihood for successful successive operations by reducing error and subsequent false positives/false negatives. In terms of screening applications, this trapping structure has an essential impact on the assay productivity as well as the validity.

Droplets from the first microalgae/environmental basket trapping structure are reflowed to the droplet merging chip containing on-the-fly droplet generation of dye, synchronization, and electrocoalescence. After merging of these droplets, the resulting stained microalgae droplets proceed to a detection and sorting region for harvesting samples of interest.

5.4.2. Fabrication

The microfluidic chips containing a droplet generator/incubation chamber and second droplet generator/incubation/detection/sorting region were fabricated in PDMS at a ratio of 10:1 (polymer to curing agent). The droplet generator/incubation chamber master mold is fabricated by spin coating a silicon wafer with SU-8™ (2075, Microchem Inc., Westborough, MA, USA) at 1000 rpm to produce a 160 µm high resist and are pattern using conventional photolithography to produce the appropriate microstructure. After developing, the master mold is coated with (tridecafluoro-1,1,2,2-tetrahydrooctyl)-1-trichlorosilane (T2492, United Chemical Technologies, Inc., Bristol, PA) and 4 mm thick PDMS molds are produced by pouring 24 g of PDMS prepolymer and curing at 85 ºC for 1 hr. A bare glass slide is PDMS spin coated (at 3000 rpm) to produce a 30 µm thick hydrophobic passivation layer necessary to produce a bottom substrate for droplet generation. Using conventional oxygen plasma (Plasma cleaner, Harrick Plasma, Ithaca, NY), the thick PDMS droplet generator/culture chamber is bonded to a thin PDMS spin coated bare glass slide to produce the finalized device. Aquapel® (Pittsburg Glass Works, LLC, Pittsburgh, PA, USA) is used to coat the device and produce a highly hydrophobic microchannel for stable droplet generation and manipulation.

5.4.3. Device preparation for long-term cultivation and observation

Conducting long-term cultivation of cells inside droplets without continuous perfusion of carrier oil (Novec 7500, 3M, Maplewood, MN, USA) can have issues with evaporation of surrounding oil and/or media in droplets. Especially in the case where higher temperature cultures (30-37 ºC) or long culture durations are required for adequate growth of encapsulated cells, increased evaporation can occur rapidly. This often leads to droplet movement, shrinkage, and/or bubble generator, which leads to difficulty in time-course imaging, low cell growth rates, and/or loss of droplet samples, respectively (Fig. 5.4).

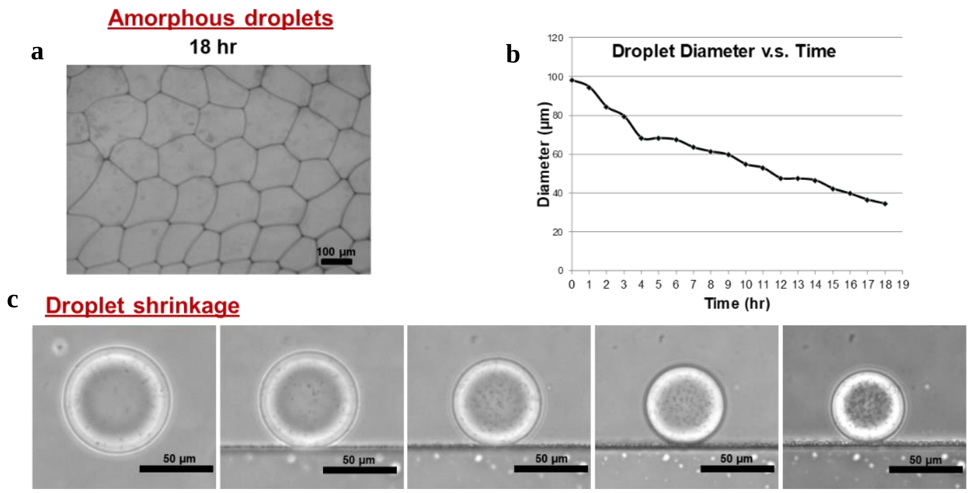

Figure 5.4 (a) Microalgae of droplets becoming amorphous after an 18 h culture. (b) Decrease of droplet size due to evaporation and (c) corresponding micrograph images of droplet shrinkage.

In an effort to ameliorate these issues, we have developed a protocol for eliminating these issues and successfully conducting pre-screening long-term cultivations for growth characterization and analysis of target cells. This is important because each screening assay requires a different host organism with different growth characteristics that need to be analyzed and corresponding voltage thresholds for downstream droplet detection/sorting must be set prior to the droplet screening assays.

Devices are submerged in water and degassed using a desiccator to remove air from the PDMS device. Hydrating the device with water and conducting fully underwater culture for experiments drastically reduces droplet shrinkage, evaporation, and bubble generation (Fig. 5.5).

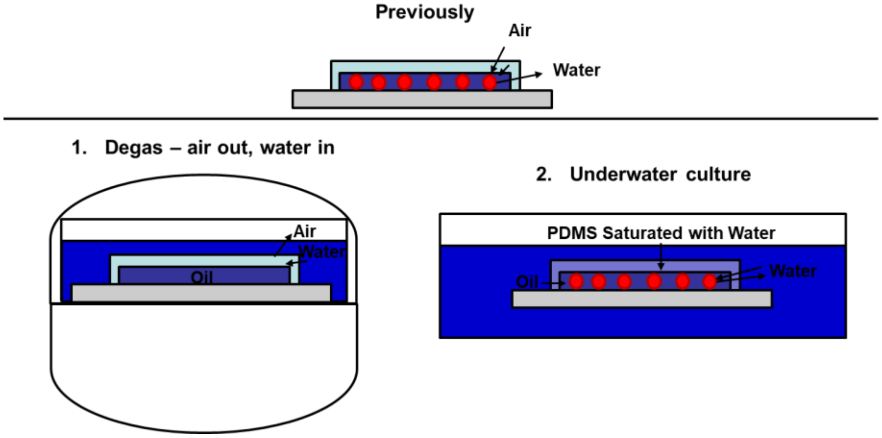

Figure 5.5 Illustration depicting the underwater degassing and culture of the droplet cultivation device to reduce evaporation and bubble generation.

This allows for long-term cultivation and observation of droplets for growth analysis. After 24 h of cultivation droplets showed less than 2% reduction in size and no pressure build-up or bubble generation during cultivation (Fig. 5.6).

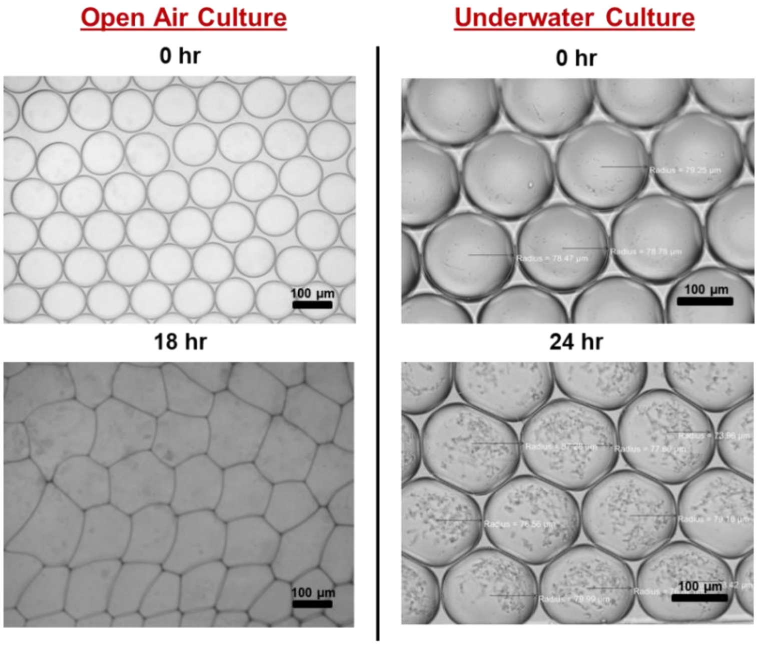

Figure 5.6 Micrograph images of droplets using an open air chamber and droplets using an underwater culture showing no droplet shrinkage or distortion.

5.4.4. Operation and characterization

Device operation is conducted by tethering multiple chips in a sequential format where each chip provides a functional operation and the resulting droplets proceed through the assay. Each chip is individually characterized by optimizing the flow rate conditions for droplet generation, reflow, synchronization, merging, secondary reflow, spacing, detection, delay times, and sorting. Further characterization is conducted for the full system with the chips being tethered to finalize flow rates, resulting in a fully characterized multi-chip droplet microfluidic screening system.

Microalgae droplets are generated using an oil flow rate of 600 μL h^{-1} and cell suspension flow rate of 250 μL h^{-1} and following Poisson distribution which resulted in approximately 25% of single cell encapsulated droplets (Appendix A Fig. 8.1). The resulting droplets are flown downstream to a cultivation chamber where approximately 8,000 droplets are cultured for growth and oil accumulation. Reflow characterization is conducted by flowing droplets out and observing the transition time using an Orca-Flash 4.0 v1 high-speed camera (C13440-20CU, Hamamatsu, Shizuoka, Japan). A reflow rate of 70 μL h^{-1} was used with a spacing oil flow rate of 80 μL h^{-1} to match the combined volumetric flow rate of paired droplets generated downstream on the merging chip.

5.5. Droplet merging chip for co-cultivating host/target

The second chip is comprised of: a droplet reflow inlet to introduce previously cultivated microalgae/environmental droplets from the pillar-based culture chamber, an adjacent oil channel inlet for the addition of spacing of the packed microalgae droplets, an adjacent oil and water inlet and parallel T-junction droplet generator, a railroad-like balancing fluidic resistance channel to allow for droplets to be paired in a one-to-one fashion, and a widening channel to merge droplets. In the case of the microalgae screening assay, an additional optical detection and sorting region is included on-chip.

5.5.1. Design

In the case of the microalgae screen, 160 µm diameter microalgae droplets are merged using electrocoalescence with 160 µm diameter boron-dipyrromethene (BODIPY) droplets and cultured for 11 min in a short fluidic delay line followed by on-chip on-the-fly optical detection and droplet sorting. The analysis and sorting regions are designed with a shallower 100 µm height to decrease the variation in cell position and allow for better focusing of the detection. The optical detection channel is comprised of a 400 µm wide channel coupled to a dual-detection optical housing using a blue LED (NSPB310B, Nichia, Tokushima, Japan) for excitation of both chlorophyll and BODIPY. Emitted light is split through a dichroic bandpass mirror (495DCLP, Chroma, Inc. Bellows Falls, VT, USA) and each signal is acquired using a PMT (H10721-110, Hamamatsu, Inc., Shizuoka, Japan). Droplets showing high growth and oil accumulation are subsequently sorted using a hydrodynamic droplet sorter using oil injection from an adjacent oil reservoir, pushing a target droplet to the collection channel. This automated process is controlled using a LabView® (National Instruments, TX, USA) based program for continuous operation (Fig. 5.7).

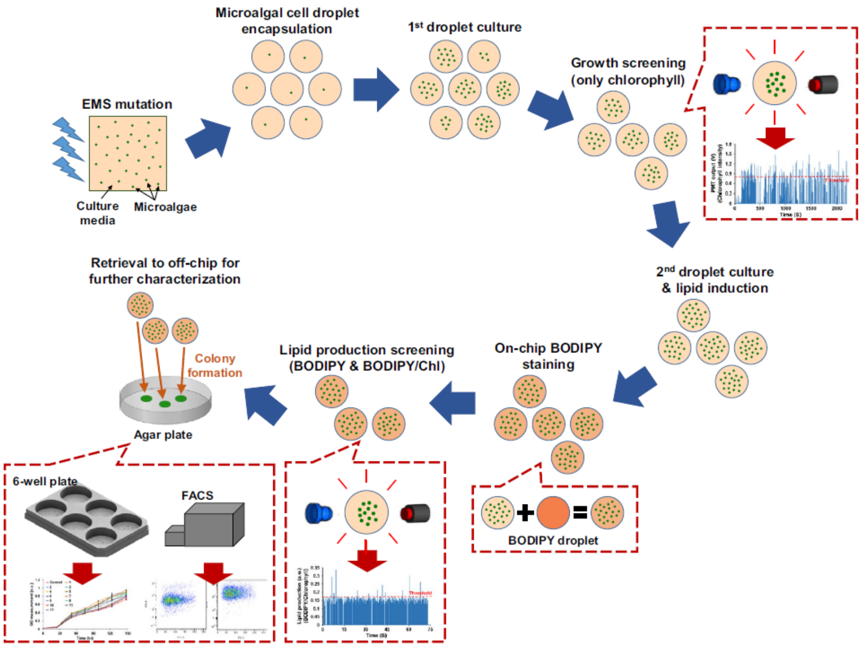

Figure 5.7 The overall workflow of the droplet screening assay. Reprinted with permission from Plant Direct. [113]

5.5.1.1. Droplet synchronization and electrocoalescence

Droplet synchronization and merging characterization is conducted for the on-chip merging device by first matching the droplet diameter of the first droplet being reflowed to the second paired droplet being generated on-the-fly. Considering that the first droplet size is a set desired value, oil and media inlet flow rates are optimized to allow for the second on-the-fly droplet generation to produce a matching droplet size. After the sizes are matched, the droplet spacing of the second train of droplets is observed and the reflow/spacing flow rates of the first droplet train are optimized to match that of the second train of droplets. This process is iteratively conducted until an appropriate combination is obtained. Once droplets are synchronized, the overall spacing of paired droplets is tuned by increasing the desired oil inlet flow rates and droplets are merged using an electric field. Droplet merging efficiency is obtained by comparing the number of merged droplets to the number of unmerged, missed, or double merged droplets.

5.5.2. Fabrication

For the second device, a Cr/Cu planar electrode is produced by depositing 200 Å and 3000 Å (Cr/Cu, respectively) on a 50.8 mm x 76.2 mm glass slide (Micro Slides 2947- 75 x 50, Corning Inc., NY) using e-beam lithography (Lesker PVD 75 E-beam Evaporator, Kurt J. Lesker, Co., Jefferson Hills, PA, USA). S1818 (Microchem Corp., Westborough, MA, USA) is spin coated at 3000 rpm and baked at 115 ºC for 5 min. The electrode pattern is produced using conventional photolithography and developing, followed by PDMS spin coating to produce a 30 µm thick hydrophobic passivation layer to produce a bottom substrate for droplet generation. The second device is aligned and bonded to the glass electrode/thin PDMS substrate using conventional oxygen plasma (Plasma cleaner, Harrick Plasma, Ithaca, NY). Each of the devices were coated with Aquapel® (Pittsburg Glass Works, LLC, Pittsburgh, PA, USA) to produce highly hydrophobic microchannels for stable droplet generation and manipulation.

5.5.3. Operation

The comprehensive microalgae screening system used to screen for high growth and oil producing mutant strains incorporates a spacer to space incoming reflowed droplets, a droplet generator to generate dye droplets, followed by a synchronization region, merging region, delay line, detection region, and sorting mechanism. Previously generated droplets at an oil flow rate of 600 μL h^{-1} and cell suspension flow rate of 250 μL h^{-1} are reflowed at 70 μL h^{-1} into the inlet of the screening system (an oil spacing flow rate of 80 μL h^{-1} was used, total volumetric flow rate of 150 μL h^{-1}). Simultaneously, identical diameter BODIPY droplets are generated in 1% DMSO at 110 μL h^{-1} and 40 μL h^{-1} for the oil and dye solution, respectively. One-to-one pairing is achieved and followed by droplet electrocoalescence using a 200 V high voltage amplifier (Trek 2200, Trek Inc., Lockport, NY, USA) to induce an electric field. A droplet merging efficiency of 95% was achieved using these conditions and an incubation time of 10-11 min at a concentration of 500 μg mL^{-1} was proven to show 97% staining efficiency comparable to conventional methods. After the fluidic delay line, droplets are flown at a rate of 5 droplets s^{-1} into the detection region and a droplet detection sensitivity of 2-3 cells was achieved with greater than two times SNR. An 8-part compact dual-fluorescence system was 3D printed using a material printer (Perfactory Ultra, EnvisiontTEC Inc. Dearborn, MI, USA) to mount the optics for simultaneous dual-excitation of passing droplets using a blue LED (NSPB310B, Nichia, Tokushima, Japan) with an excitation filter (460-500 nm, ET480/40x, Chroma, Inc. Bellows Falls, VT, USA). A dichroic mirror (495DCLP, Chroma, Inc. Bellows Falls, VT, USA) and aspheric lenses (352330-A & LA1540-A, Thorlabs, Inc. Newton, NJ, USA) are used to propagate the light from the source to the sample, and the sample to the PMT (H10721-110, Hamamatsu, Inc. Japan) for detection. Simultaneous detection using a dichroic mirror (590DCLP, Chroma, Inc. Bellows Falls, VT, USA) is used to split the green BODIPY and red chlorophyll wavelengths to their respective PMT's (H10721-110, Hamamatsu, Inc. Japan). A BODIPY emission filter (ET535/10, Chroma, Inc. Bellows Falls, VT, USA) and chlorophyll emission filter (ET610m, Chroma, Inc. Bellows Falls, VT, USA) are used to obtain distinct signals for each of the wavelengths and a reflective mirror (PF10-03-P01, Chroma, Inc. Bellows Falls, VT, USA) is used to bounce the resulting light to the PMT. The relaying signal is acquired through LabView® (National Instruments, Austin, TX, USA) using a data acquisition module (NI9219 DAQ, National Instruments, Austin, TX, USA) for downstream sorting classification. A comparative analysis of the detection voltage output corresponding to normal (*CC-406*) and high oil accumulating (*sta6*) microalgae was conducted to assign a voltage threshold that can be properly assigned to sort the top 2% of droplets showing high growth and oil accumulation (Fig. 5.8). Prior to the droplet detection/sorting region, an oil spacing flow rate of 900 µL h^{-1} is used to space droplets more and maintain single droplet detection and sorting. Upon detection of a droplet above the set threshold, a DIO signal is sent to actuate a solenoid valve to pressurize a vial of oil and inject (27,000 PA, 150 ms) oil to physically deflect the droplet to the sorting channel. Sorted droplets are plated and validated for high growth and oil accumulation phenotypes.

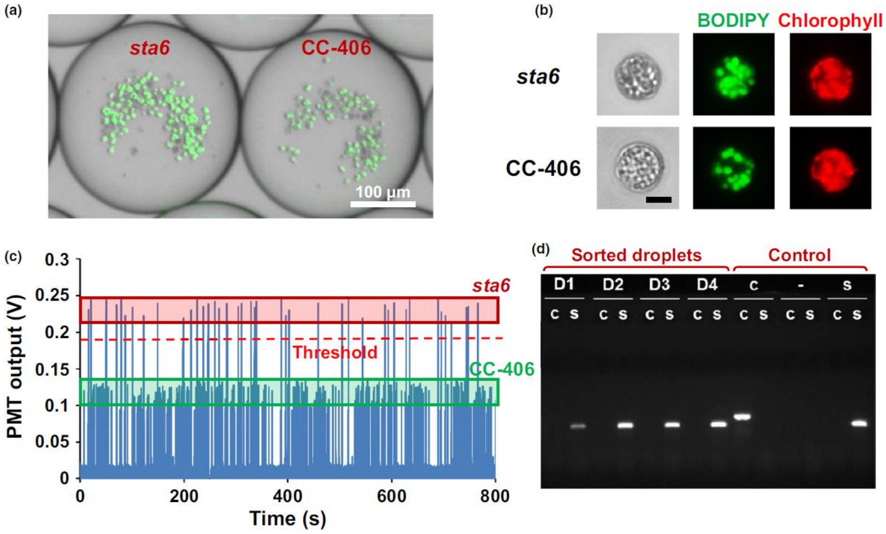

Figure 5.8 (a) Microalgae droplets are generated using *sta6* and *CC-406* strains and (b) BODIPY staining shows the difference in oil accumulation. (c) Resulting populations are flown through the fluorescent detection system and (d) PCR confirmation is conducted to validate the original strains. Reprinted with permission from Plant Direct. [113]

5.6. Droplet sorting chip for recovery of "hits"

Alternatively, droplet detection and sorting can be conducted on a separate chip but should be coupled together to allow for precise control of the droplet introduction, spacing, detection and sorting distance (and corresponding delay time), sorting duration, and downstream trapping of hits. In most instances a much higher oil spacing flow rate is required to add adequate spacing between droplets, which allows for detection and sorting of only one droplet at a time. Detection can be conducted using lower power LED's in a sequential format where growth screening is conducted first and oil accumulation is conducted after, or in a dual-detection format as discussed in the previous section.

5.6.1. Planar electrode for sorting

Considering the limitations of droplet sorting, planar electrode designs have been utilized for reliable sorting of droplets that range from 20-75 µm in diameter. Fabrication requires conventional e-beam electrode deposition and photolithography patterning, as well as PDMS alignment on the order of 10's of µm. Although this method requires an additional deposition step, the electrodes are very robust and almost never fail in terms of connection or propagation of the signal to generation of a proper electric field. When using hard substrates like glass this method is often preferred, but for more complex integrated PDMS-based devices, this may not be suitable as PDMS substrates may be desired (Fig. 5.9).

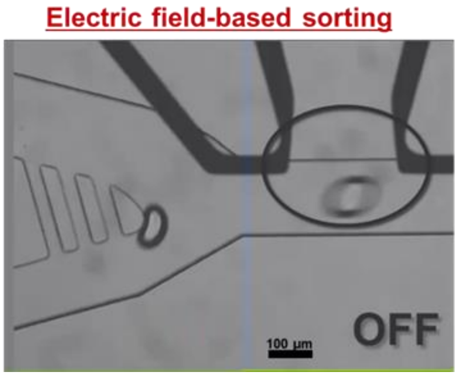

Figure 5.9 Micrograph of droplet sorting using a planar electrode design.

5.6.1.1. Design: Planar electrode for sorting

In the case of smaller droplet assay, resulting droplets are reflowed into a detection and sorting chip with a 100 µm wide channel coupled to an LED or laser-based detection system. An LED (NSPB310B, Nichia, Tokushima, Japan) or laser (LRS-0473-PFM-00100-03, Readylaser, Anaheim, CA, USA) excitation is used to excite the sample and emitted light is detected using a PMT (H10721-110, Hamamatsu, Inc. Japan). A 3D printed (Perfactory Ultra, LS600 resin, EnvisonTEC Inc. Dearborn, MI, USA) optical housing is used to align the dichroic mirror (T495lpxr, Chroma, Inc. Bellows Falls, VT, USA), emission filter (ET525/50m, Chroma, Inc. Bellows Falls, VT, USA), and series of lenses (LA1540-A, Thorlabs, Inc. Newton, NJ, USA). The final signal is collected by a PMT (H10721-110, Hamamatsu, Inc. Japan) and a threshold voltage is used to sort all droplets showing interest.

5.6.1.2. Fabrication: Planar electrode for sorting

The planar electrode sorting device is fabricated using conventional Cr/Cu planar electrodes by e-beam (Lesker PVD 75 E-beam Evaporator, Kurt J. Lesker, Co., Jefferson Hills, PA, USA) metal deposition (200 Å and 3000 Å, Cr/Cu, respectively) on a 50.8 mm x 76.2 mm glass slide (Micro Slides 2947- 75 x 50, Corning Inc., NY). S1818 (Microchem Corp., MA) is spin coated at 3000 rpm and baked at 115 ºC for 5 min, followed by conventional photolithography patterning (MA6, Karl Suss, Suss Microtec Se, Garching, Germany) and developing. PDMS is spin coated at 3000 rpm to produce a 30 µm thick hydrophobic passivation layer necessary for droplet stability. The thick PDMS channel layer is aligned and bonded to the glass electrode substrate using conventional oxygen plasma bonding (Plasma cleaner, Harrick Plasma, Ithaca, NY). Each of the devices are coated with Aquapel® (Pittsburg Glass Works, LLC, Pittsburgh, PA, USA) to produce highly hydrophobic microchannels for stable droplet generation and manipulation.

5.6.1.3. Operation: Planar electrode for sorting

Droplets that have been preculture for their respective assay are reflowed into the detection chip at a set flow rate (20-30 μL h^{-1}). On-chip spacing oil (800-900 μL h^{-1}) at a much higher flow rate is utilized to ensure each droplet has enough space to be detected and sorted as distinct separate entities. As droplets pass the detection region where a light source (LED or laser) excites the sample, droplet producing an acquired emission signal are simultaneously characterized based on their fluorescent intensities using a LabView® program. As desired droplets are detected, an electric signal sent from the LabView® program triggers a function generator (DG4102, Rigol Technologies, Beijing, China) and relays the signal to a high voltage amplifier (Trek 2200, Trek Inc., Lockport, NY, USA) to sort the desired droplet. Using a conventional planar electrode design a 2 V to 9 V, 10 kHz – 40 kHz, signal is generated and relayed to the high voltage amplifier to generate a 200 V to 900 V AC signal that induces an electric field between electrodes. With a correctly characterized flow rate, droplets can be reflowed, spaced, detected, and sorted on-demand to acquire “hits” of interest. As previously mentioned, this electrode design does not generate the strongest electric field due to its position underneath the channel, and therefore high-throughput sorting of larger droplets may suffer from lower droplet sorting efficiencies.

5.6.2. Three-dimensional liquid-metal electrode for sorting

A three-dimensional liquid-metal electrode offers several advantages over conventional planar electrodes, especially in terms of fabrication time and equipment availability. Typical liquid-metal electrodes eliminate the need for deposition processes, which eliminates a whole electronic processing step. Alternatively, electrode channels can be fabricated alongside microfluidic channel layers and only require a liquid metal filling step after PDMS fabrication. Different types of liquid metal also offer different advantages and disadvantages, for instance, room temperature metals such as EGaIn offer the ability to move the liquid during normal processing, while Field’s Metal allows the metal to be hardened at room temperature but becomes liquid around 60 ºC. Therefore, most stationary 3D electrodes require Field’s Metal type liquid metals that are workable but harden at room temperature.

5.6.2.1. Design: 3D electrode for sorting

The three-dimensional design is similar to that of the planar electrode design but with an inlet channel of 150 µm to accommodate larger droplets corresponding to droplets in the 75-150 µm range. A side inlet for droplet spacing allows for droplets to have enough spacing for single droplet detection and sorting. A droplet detection region that slightly widens can be utilized to slow the droplet down, or a narrower height channel can be used to squeeze the droplet for better planar detection. Either LED or laser-based detection can be utilized to conduct the detection. Downstream droplet sorting is conducted in a similar manner as previously discussed where a signal is generated through LabView® and sent to the 150 µm high liquid metal electrodes to generate an electric field for sorting. A waste and droplet collection outlet are used to navigate and acquire droplets of interest for processing.

5.6.2.2. Fabrication: 3D electrode for sorting

The three-dimensional electrode device is fabricated using conventional photolithography processing where a silicon master mold is spin coated with SU-8™ (2075, Microchem Inc., Westborough MA, USA) at 1200-2300 rpm (to obtain a 150-75 µm high channel, respectively) and prebaked for 40 min at 65 ºC and 20 min at 95 ºC. The resulting wafer is exposed using a conventional photolithography mask aligner (MA6, Karl Suss, Suss Microtec Se, Garching, Germany) and post-exposure baked for 40 min at 65 ºC and 20 min at 95 ºC. The wafer is then developed using SU-8™ developer (Thinner-P, Microchem Corp., Westborough, MA, USA) and coated with (tridecafluoro-1,1,2,2-tetrahydrooctyl)-1-trichlorosilane (T2492, United Chemical Technologies, Inc., Bristol, PA) for PDMS replication. Liquid PDMS at a ratio of 1:10 (curing agent: polymer) is mixed and 24 g are poured and cured at 80 ºC for 1 h. An optional 30 µm PDMS spin coated glass slide (50.8 mm x 76.2 mm) can be utilized to create a hydrophobic bottom surface for droplet generation. The thick PDMS channel layer is bonded to the glass slide and the device is put on a hotplate at 65 ºC to inject liquid metal into the electrode channels. The device is coated with Aquapel® (Pittsburg Glass Works, LLC, Pittsburgh, PA, USA) to produce highly hydrophobic microchannels for stable droplet generation and manipulation.

5.6.2.3. Operation: 3D electrode for sorting

In terms of performance, the three-dimensional electrode design has proven to generate a more uniform electric field in the droplet sorting region, which often leads to a high electric field strength when compared to conventional planar electrodes. Also, this enhanced electric field helps larger droplets in the range of 75-150 µm to experience a stronger pulling effect to sort droplets for droplet collection. Larger droplets of 160 µm and greater are still difficult to sort using this three-dimensional electrode design, and other technologies need to be employed to accomplish high efficiency sorting for larger droplets.

5.6.3. Oil pushing for droplet sorting

The droplet sorting method utilized for the microalgae assays was an oil-based droplet pushing method. Here a side channel connected to a pressure driven oil reservoir is utilized as an inlet for on-demand high speed injection of oil to deflect droplets to the collection channel for downstream processing. Considering that larger droplets have limitation in the electric field experienced when using conventional planar or three-dimensional electrodes, this oil pushing method is used as a high efficiency alternative for sorting droplets larger than 150 µm. Although this design was originally utilized to sort larger droplets, it is still capable of conducting mediocre throughput droplet sorting for smaller droplets down to 50 µm.

5.6.3.1. Design

The design of the oil-based pushing sorting chip entails a 200 µm inlet for droplets to be reflowed into the device, followed by a 50 µm side channel inlet to increase droplet spacing for single droplet detection and sorting. The T-junction at the spacing region is chamfered at 45º to ensure large droplets are not cleaved during addition of oil for spacing. The droplet detection region widens for whole droplet detection, and droplets passing through the Y-shape outlet are deflected using a side channel oil inlet (Fig. 5.10). An array of fluidic balancing channels can be used between the two outlet channels to stabilize the device during sorting when droplets are being processes through the channels.

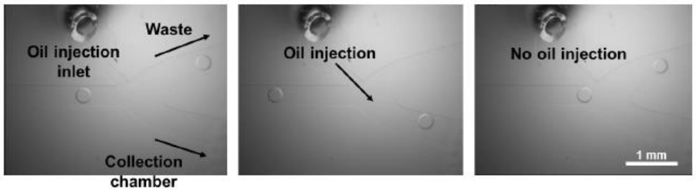

Figure 5.10 Micrograph images of droplets being sorted using an oil pushing device. Reprinted with permission from Plant Direct. [113]

5.6.3.2. Fabrication: oil-pushing for sorting

The oil-based droplet sorting device is fabricated by double spin coating a silicon master with SU-8™ (2075, Microchem Inc., Westborough MA, USA) at 1900 rpm (to obtain a 200 µm high channel), followed by prebaking for 40 min at 65 ºC and 20 min at

95 ºC. The wafer is patterned using conventional photolithography (MA6, Karl Suss, Suss Microtec Se, Garching, Germany) and post-exposure baked for 40 min at 65 ºC and 20 min at 95 ºC. The wafer is developed using SU-8™ developer (Thinner-P, Microchem Corp., Westborough, MA, USA) and coated with (tridecafluoro-1,1,2,2-tetrahydrooctyl)-1-trichlorosilane (T2492, United Chemical Technologies, Inc., Bristol, PA) for 20 min to allow for PDMS replication. Liquid PDMS is mixed at a ratio of 1:10 (curing agent: polymer) and 24 g are poured into a petri dish containing the master and is cured at 85 ºC for 1 h. An optional 30 µm PDMS spin coated glass slide (50.8 mm x 76.2 mm) can be utilized to create a hydrophobic bottom surface for droplet generation. The thick PDMS channel layer is bonded to the glass slide using conventional oxygen plasma bonding (Plasma cleaner, Harrick Plasma, Ithaca, NY). Lastly, the device is coated with Aquapel® (Pittsburg Glass Works, LLC, Pittsburgh, PA, USA) to produce a highly hydrophobic surface for stable droplet generation and manipulation.

5.6.3.3. Operation: oil-pushing for sorting

Droplets are reflowed from a previous cultivation chip to the detection/sorting chip using a set reflow rate (70 µL h^{-1} for the microalgae assay) and a set oil droplet inlet flow rate (900 µL h^{-1} for the microalgae assay). Upon detection of a droplet above the set threshold, a DIO signal is sent to actuate a solenoid valve to pressurize a vial of oil and inject (at 27,000 PA) oil for 150 ms to physically deflect the droplet to the sorting channel. Sorted droplets are plated and validated for high growth and oil accumulation phenotypes.

5.6.4. Graphical interface for sorting

A LabView® program is designed to conduct both droplet detection and sorting simultaneously, requiring an analog input and digital or analog output with variations in the functions used, which depends on the application of program. Considering droplet detection, the acquire signal is sent through a series of daqmx functions which utilize a while loop to continuously plot the output PMT voltage. In the same loop, a threshold value is set to turn on a global function that controls a case loop for droplet sorting. A second while loop is designed with a case structure and case sequence inside (and delay interval) that sorts the droplet when the global variable “on”, signifying the signal is above the threshold voltage. The first type of program would be to generate an electric field for droplet sorting, and this requires the generation of a trigger signal or directly relaying a sinusoidal function to a high voltage relay (G3VM-601BY, Omron®, Kyoto, Japan). Alternatively, a digital signal can be output with the desired voltage to actuate a solenoid valve to add pressure that pressurizes a reservoir creating a pressure driven pump for oil injection and droplet deflection.

5.6.5. Microalgae screening results

The microalgae screening is conducted by exposing microalgae to a chemical treatment, randomly mutating select cells in the population and conducting the screening assay. Cells are encapsulated in microdroplets for isolation and cultivation (Fig. 5.11).

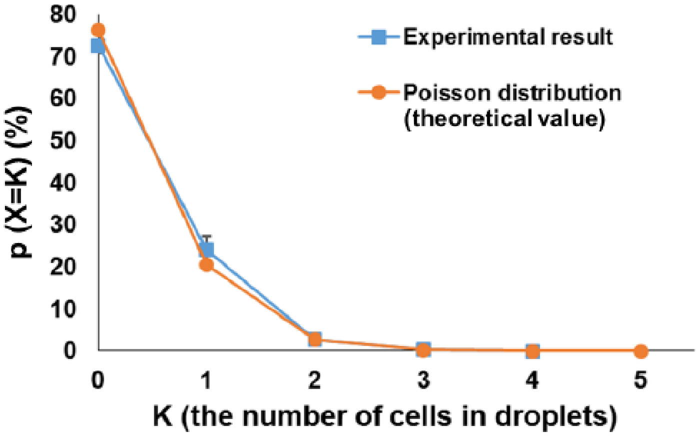

Figure 5.11 Cell encapsulation distribution of microalgae showing the encapsulation distribution follows the expected Poisson's distribution. Reprinted with permission from Plant Direct. [113]

After cultivation the resulting cell droplets are flown through the droplet staining chip which merges droplets with BODIPY droplets on-the-fly to allow for staining of oil that was accumulated during the cultivation. Downstream detection is conducted for both growth and oil accumulation using chlorophyll and BODIPY fluorescent systems (Fig. 5.12). A dual detection optical housing system was developed to conduct both fluorescent analyses simultaneously.

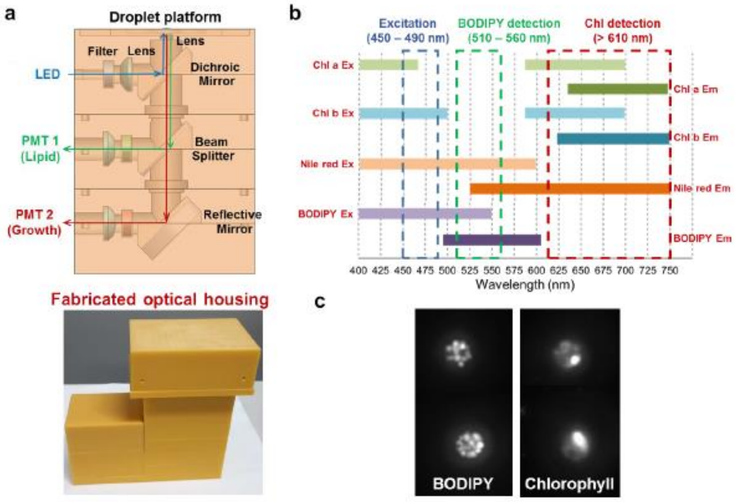

Figure 5.12 (a) Illustration of the dual detection system, operation, and the corresponding 3D printed optical housing. (b) Filter strategy for conducting simultaneous fluorescent detection of chlorophyll and BODIPY. (c) Fluorescent micrograph images of microalgae cells using chlorophyll and BODIPY filter sets. Reprinted with permission from Plant Direct. [113]

The resulting detection assay exhibited several droplets of interest that are later sorted for collection (Fig. 5.13). An appropriate threshold is set to minimize error and only obtain the droplets with high growth and high oil accumulation.

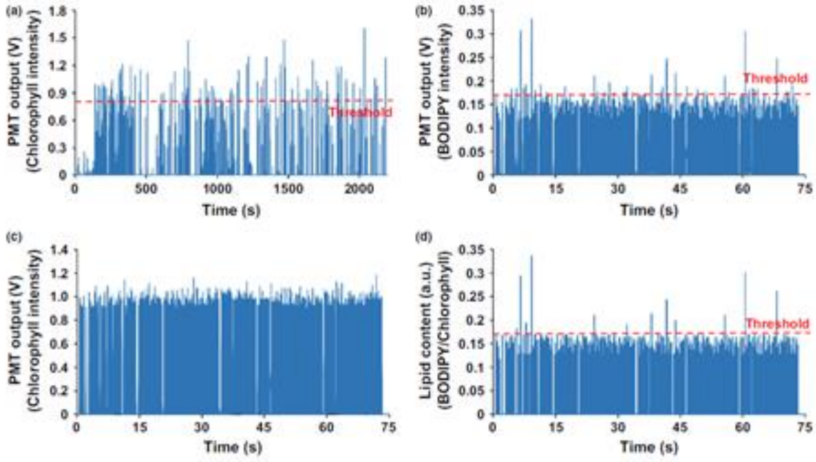

Figure 5.13 Detection signals from the PMT dual detection system for (a) chlorophyll after 36 h of culture. Additional detection voltage output of (b) BODIPY, (c) chlorophyll, (d) and BODIPY/chlorophyll after 60 additional hours of cultivation. Reprinted with permission from Plant Direct. [113]

The resulting 12 variant isolates were characterized for growth and oil accumulation using a six-well culture plate. A control condition and all variants were cultured for 6 days, after only 3 days of culture 7 variants showed 30% or more increased growth when compared to the control (Fig. 5.14). Flow cytometry was also conducted to compare the lipid content of each of the variants to the control (Appendix Fig. 8. 8).

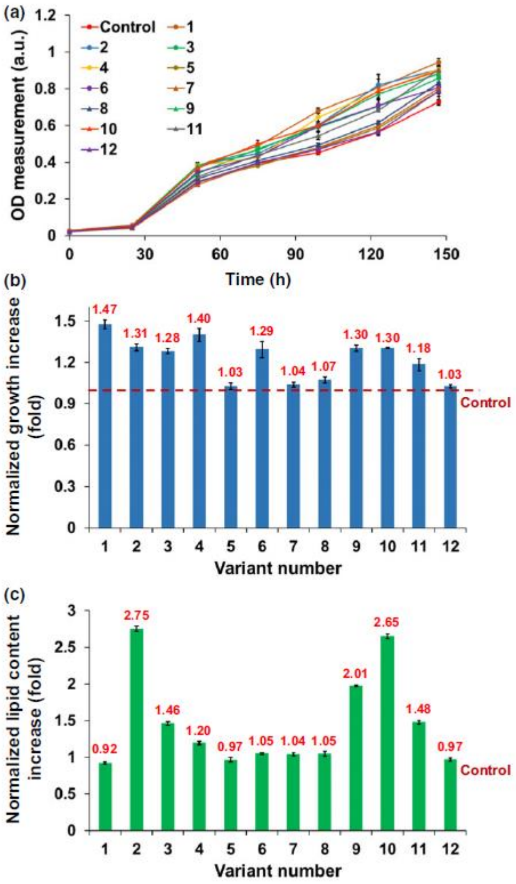

Figure 5.14 (a) Comparison of the growth rate of the 12 variants after 3 days is compared to a control sample using an off-chip multi well plate format (*n=3*). (b) Growth rate comparison showed that variant 1, 2, 3, 4, 6, 9, and 10 showed larger than 30% increase in growth rate when compared to the control. (c) Comparison of lipid accumulation of the 12 variants to the control using flow cytometry analysis (*n=150*). Data is normalized to the control and is in mean ± standard error. Reprinted with permission from Plant Direct. [113]

5.7. *Acinetobacter baumannii* screening

An *A. baumannii* screening assay was conducted by encapsulating environmental samples followed by cultivation to accrue compounds of interest. The resulting droplets are flowed to the merging chip where *A. baumannii* droplets are paired and merged with environmental droplets.

The merging chip is comprised of: a droplet reflow inlet to introduce previously cultivated environmental droplets from the pillar-based culture chamber, an adjacent oil/surfactant (Novec 7500, 3M, Maplewood, MN, USA)/ (Picosurf 1, Sphere Fluidics, Monmouth Junction, NJ, USA) channel inlet for the addition of spacing of the packed environmental droplets, an adjacent oil and water inlet comprising a parallel T-junction droplet generator, a railroad-like balancing fluidic resistance channel to allow for droplets to be paired in a one-to-one fashion, and a widening channel to merge droplets. This chip allows for high efficiency droplet merging of paired droplets which is critical for functional droplet screening assays. Droplets are then co-cultivated in a second large basket trapping structure to allow for phenotype analysis.

After co-cultivation each of the remaining droplets are flown through a GFP-fluorescent laser-based detection system and droplets showing low GFP (*A. baumannii* inhibition or death) are sorted for confirmation.

5.7.1. Design: *Acinetobacter baumannii* screening

The *A. baumannii* screening system utilizing a first chip for droplet generation and incubation (chip 1) of an environmental library to allow for accruement of elicited drugs. The second chip is a large basket trapping chamber (chip 2) for incubation of droplets (Fig. 5.15). The pillar-based trapping structure has a gap of 25 µm and height of 160 µm which is more optimal to prevent droplets from escaping and allow for monolayer droplet image analysis. A 200 µm x 200 µm pillar size is utilized with a 200 µm gap from the wall to the pillar array.

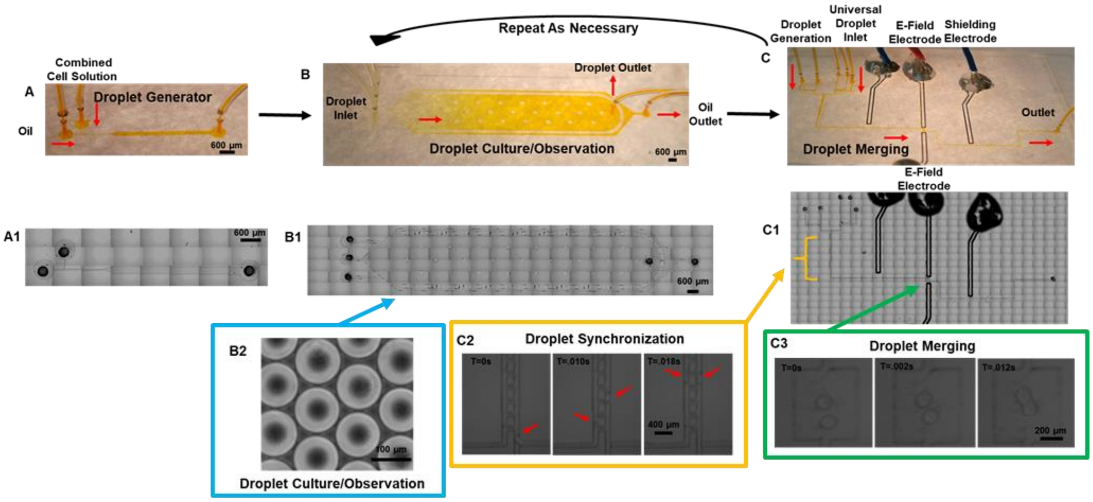

Figure 5.15 Images and corresponding micrograph tiled images of the droplet generator and incubation devices utilized for the *A. baumannii* screening.

A third chip for on the fly droplet merging (chip 3) entails a reflow inlet for previously cultivated environmental microbes with an adjacent oil spacer and parallel droplet generator for *A. baumannii* encapsulation. These droplets are flown parallel and synchronized in a railroad-like fluidic resistance structure and merged in a one-to-one fashion using droplet electrocoalescence (Fig. 5.16). The resulting droplets are then flown into a fourth chip comprised of a larger volume basket trapping structure for co-cultivation of cells (chip 4). Lastly, resulting droplets containing “non-hits” and “hits” are reflowed to a fifth detection/sorting chip (chip 5) where a blue 473 nm laser (LRS-0473-PFM-00100-03, Readylaser, Anaheim, CA, USA) based optical detection system and oil injection sorting mechanism are utilized to investigate and harvest droplets showing low GFP-*A. baumannii* signal (chip 4).

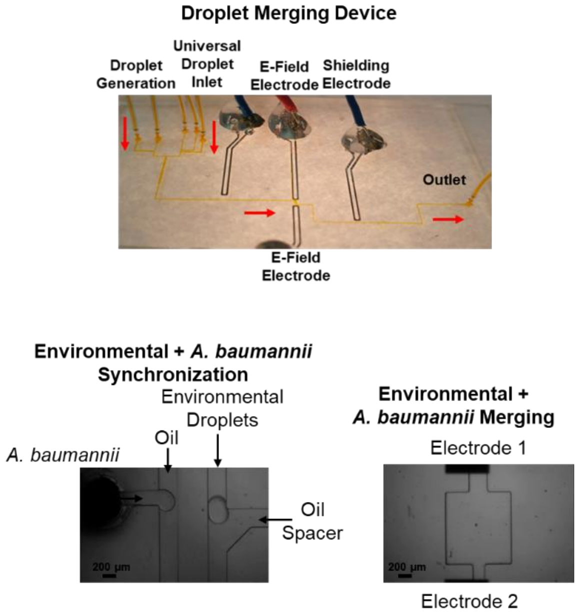

Figure 5.16 Image of the droplet merging chip and micrograph images of the synchronization and merging region.

Resulting droplets that have been collected as “hits” are then plated on agar plates and incubated to allow for the surrounding carrier oil to dissolve causing cells to adhere to the plate and produce colonies of target cells of interest. Additional confirmation of the hits was performed by picking single colonies and further plating of the colonies for homogenous cell line production, followed by phenotypic/drug confirmation. Although the *A. baumannii* assay is conducted with multiple environmental cells per droplet (5 cells per droplet), this multiplexed style assay allows for more cells to be analyzed in a similar format/time. The resulting assay output needs to be demodulated to decipher which microbes produce a phenotypic response. Furthermore, there may be complex interactions between cells in a variety of scenarios which result in combinatorial effects that may produce advantageous phenotypic responses but when reduced to the single-cell level may be lost. In those instances, additional assays would need to be conducted to further characterize combinatorial effects.

5.7.2. Fabrication: *Acinetobacter baumannii* screening

The microfluidic chips containing a droplet generator/incubation chamber and second droplet generator/incubation/detection/sorting were fabricated in PDMS at a ratio of 10:1 (polymer to curing agent). The droplet generator and incubation chamber master mold are fabricated by spin coating a silicon wafer with SU-8™ (2075, Microchem Inc., MA) at 1000 rpm to produce a 160 µm high resist and patterned using conventional photolithography to produce the appropriate microstructures. After developing, the master mold is coated with (tridecafluoro-1,1,2,2-tetrahydrooctyl)-1-trichlorosilane (T2492, United Chemical Technologies, Inc., Bristol, PA) and 4 mm thick PDMS molds are produced by pouring 24 g of PDMS prepolymer and curing at 85 ºC for 1 h. A bare glass slide is PDMS spin coated to produce a 30 µm thick hydrophobic passivation layer to produce a bottom substrate for droplet generation. Using conventional oxygen plasma (Plasma cleaner, Harrick Plasma, Ithaca, NY), the thick PDMS droplet generator/culture chamber is bonded to a thin PDMS spin coated bare glass slide to produce the finalized device. Aquapel® (Pittsburg Glass Works, LLC, Pittsburgh, PA, USA) is used to coat the device and produce a highly hydrophobic microchannel for stable droplet generation and manipulation.

5.7.3. Operation: *Acinetobacter baumannii* screening

Prior to conducting the screening assay, *A. baumannii* is cultivated in R2A media at 37 ºC and fluorescence is confirmed. Utilizing a droplet generator and basket trapping structure, droplets containing approximately 5 environmental cells per droplet are generated using an on-chip droplet generator and the droplets are cultivated in 50% TSB/50% R2A media for 2 h at 30 ºC to allow for drug accumulation. Environmental sample droplets are generated using an oil flow rate of 300 µL h^{-1} and cell media flow rate of 100 µL h^{-1}, producing 150 µm diameter droplets containing approximately 5 environmental isolates per droplet. Resulting environmental droplets are cultivated for 2 hours at 30 ºC and reflowed at 25 µL h^{-1} with 500 µL h^{-1} spacing flow rate to have one train of droplets flowing at a total volumetric flow rate of 525 µL h^{-1}(Fig. 5.17).

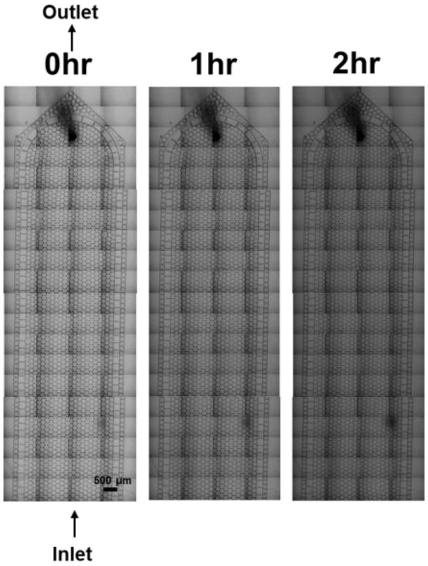

Figure 5.17 Micrograph tiled images of the encapsulated environmental microbes for *A. baumannii* screening.

The *A. baumannii* screening assay is conducted where previous 150 µm cultivated environmental library droplets containing 40-80 cells are reflowed into a merging chip (third chip) where *A. baumannii* droplets are generated on-the-fly and synchronized in preparation for droplet merging. The adjacent droplet generator using an oil flow rate of 400 µL h^{-1} and *A. baumannii* inlet flow rate of 100 µL h^{-1} produces a 150 µm diameter droplet containing 5 *A. baumannii*. A 200V AC signal is used to generate an electric field using a high voltage amplifier (Trek 2200, Trek Inc., Lockport, NY, USA). After droplet merging, the resulting 240 µm droplets are reintroduced into a pillar-based trapping culture chamber (fourth chip) and cultivated for 8 h at 30 ºC to allow for environmental elicited drugs to react with *A. baumannii* (Fig. 5.18).

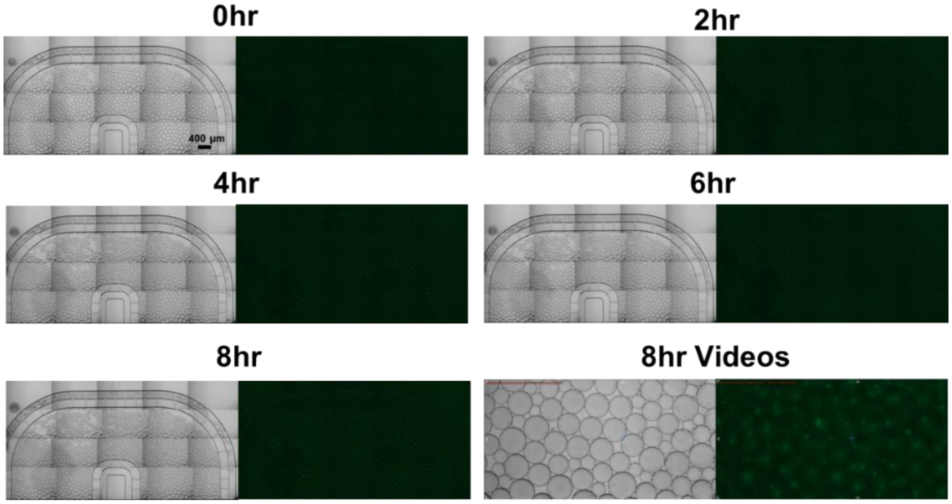

Figure 5.18 Bright-field and fluorescent images of co-cultivated droplets after 8 h of cultivation and prior to droplet detection/sorting.

5.8. Droplet sorting chip for recovery of “hits”

Although detection can be conducted using lower power LED’s, there are often limitations in the excitation/detection limit and light scattering/spot size. Alternatively, we utilize laser-based detection approaches which allow for the detection of low light fluorophores, such as GFP induced cell strains (Fig. 5.19). Additional detection methods can be employed to conduct single photon acquisition, but require additional photon counters, higher end PMT’s, and demodulation of the acquired signal. Furthermore, droplet sorting can be conducted in a relatively easy manner using conventional planar electrodes or 3D electrodes, but often have limitations in the size of droplets that are capable of reliably being sorted. We found that for larger droplet assays, an oil pushing is more suitable to reliably sort droplets with less error. Alternative approaches for electric field sorting could be utilized, such as different electrode dimensions or structures, different channel structures or orientations, and stronger electric field strengths. The trade-off is throughput, as oil pushing requires mechanical actuation and suffers from throughput limitations, whereas electric field-based sorting can be conducted at tens to hundreds of Hertz and have less throughput limitations.

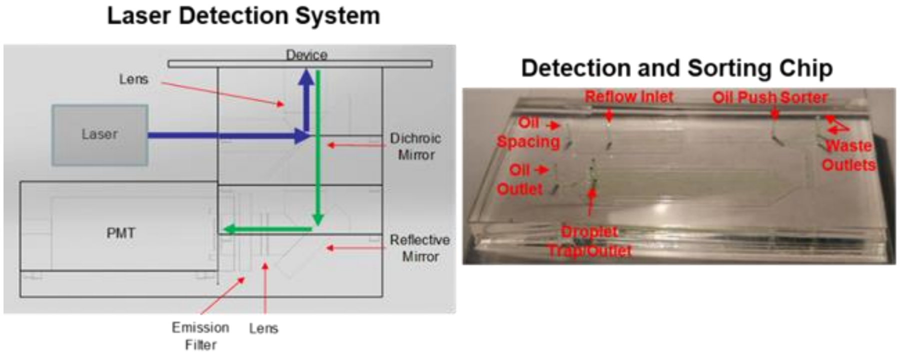

Figure 5.19 Illustration of the laser-based detection system and detection/sorting device for harvesting droplets of interest.

Droplets are reflowed from a previous cultivation chip to the detection/sorting chip using a set reflow rate of 20 $\mu\text{L h}^{-1}$ and a set oil droplet inlet flow rate of 800 $\mu\text{L h}^{-1}$. Upon detection of a droplet below the set threshold, a DIO signal is sent to actuate a solenoid valve to pressurize a vial of oil and inject (at 27,000 PA) oil for 200 ms to physically deflect the droplet to the sorting channel (Fig. 5.20). Sorted droplets are plated and validated for inhibition against *A. baumannii*.

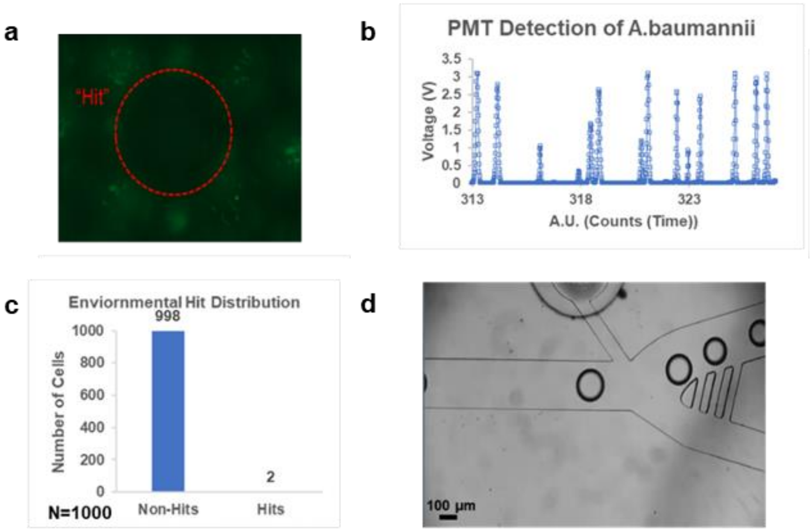

Figure 5.20 (a) Micrograph image of example "hit". (b) Voltage output of *A. baumannii* fluorescent droplets being flown through the laser-based detection system. (c) Distribution of "hits" after incubation. (d) Droplet sorting region showing push valve sorting of droplets.

Droplets are spread plated onto a TSB agar plate and colonies are picked for isolation. Each of the colonies were cultivated in 50% TSB/50% R2A media overnight at 30 °C. Two rounds of picking colonies and cell isolation are conducted to confirm each of the isolates are homogenous populations. A total of 20 isolates were obtained and cultivated overnight in TSB/R2A media followed by inhibition plate assays to observe killing of *A. baumannii*. An aspiration inhibition assay was carried out and 2 isolates showed large void zones of *A. baumannii* inhibition (Fig. 5.21).

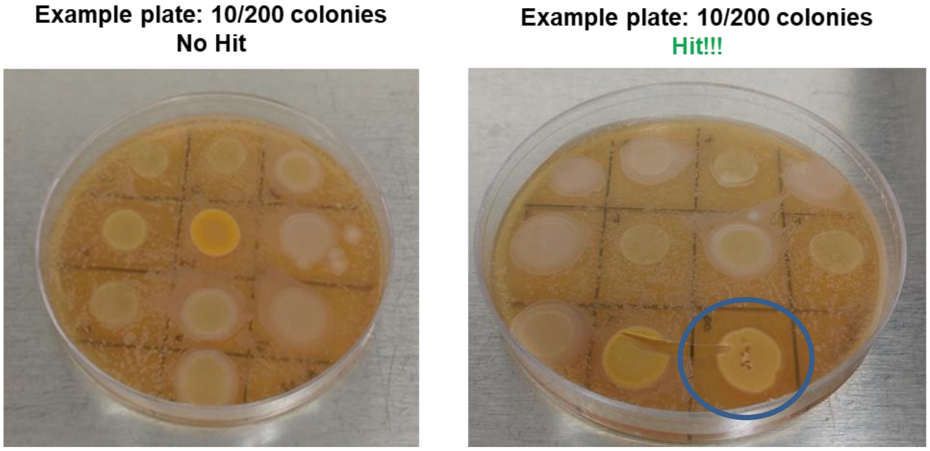

Figure 5.21 Images of the 20 isolates harvested using the droplet sorting chip, showing a hit of interest.

Further analysis was conducted to determine the cell species showing *A. baumannii* inhibition. Secondary confirmation was conducted using the same cell strain (Fig. 5.22).

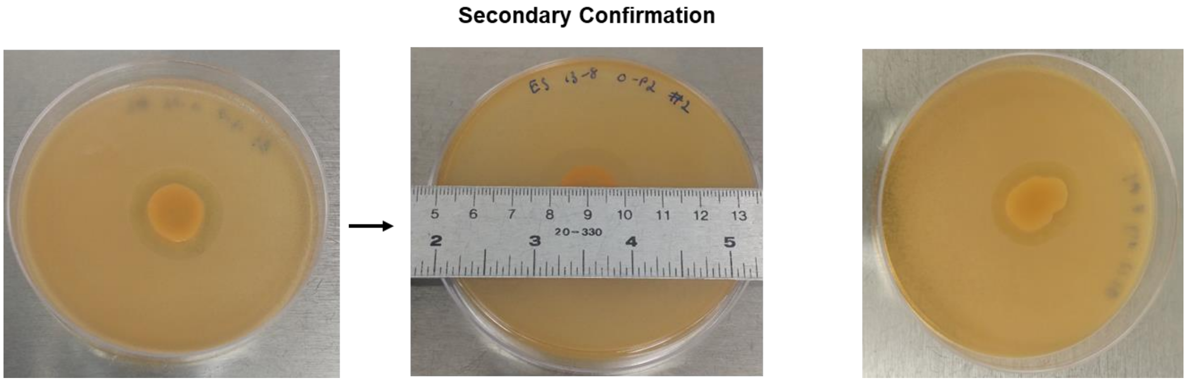

Figure 5.22 Images showing triplicate repeats of hit and inhibition of *A. baumannii* on a TSB agar plate.

Results of 16s sequencing were analyzed for two repeats of each of the two isolates and all isolates were confirmed to classify at 92-97% to the same genus (Table 5.1).

Table 5.1 Table showing the percent of genus classification read outs of 4 samples.

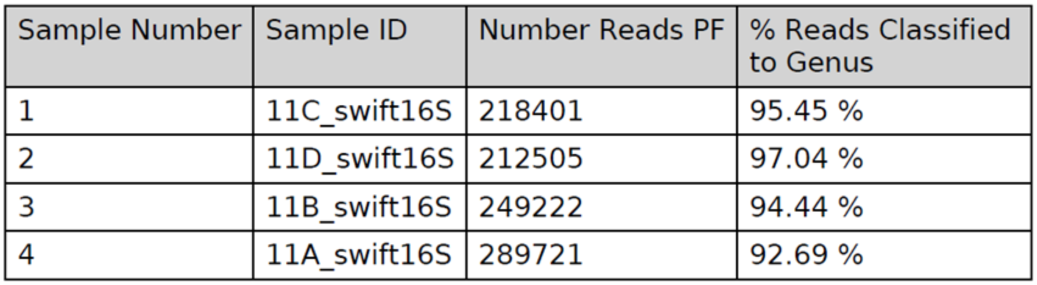

Sample Number	Sample ID	Number Reads PF	% Reads Classified to Genus
1	11C_swift16S	218401	95.45 %
2	11D_swift16S	212505	97.04 %
3	11B_swift16S	249222	94.44 %
4	11A_swift16S	289721	92.69 %

All samples tested classified as *Microbacterium* with approximately 95% of the reads tested (Table 5.2 & Fig. 5.23).

Table 5.2 Table showing the percent of species classification reads of sample 1.

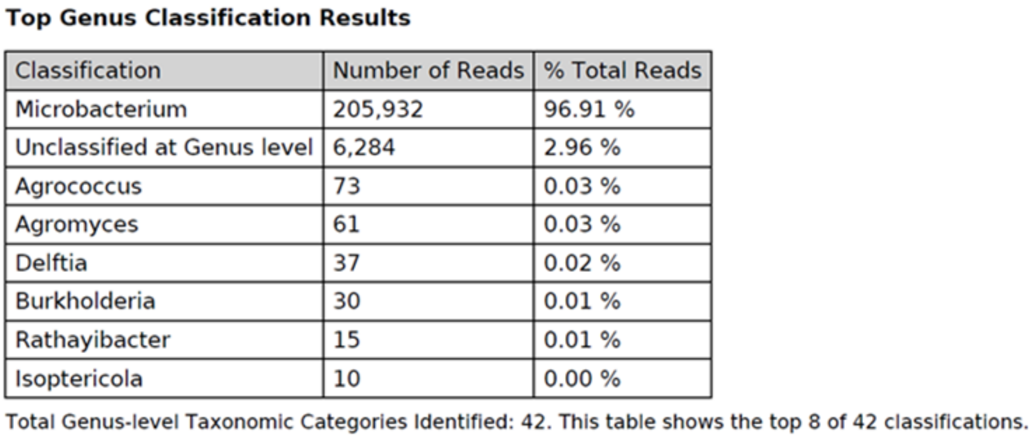

Top Genus Classification Results

Classification	Number of Reads	% Total Reads
Microbacterium	205,932	96.91 %
Unclassified at Genus level	6,284	2.96 %
Agrococcus	73	0.03 %
Agromyces	61	0.03 %
Delftia	37	0.02 %
Burkholderia	30	0.01 %
Rathayibacter	15	0.01 %
Isoptericola	10	0.00 %

Total Genus-level Taxonomic Categories Identified: 42. This table shows the top 8 of 42 classifications.

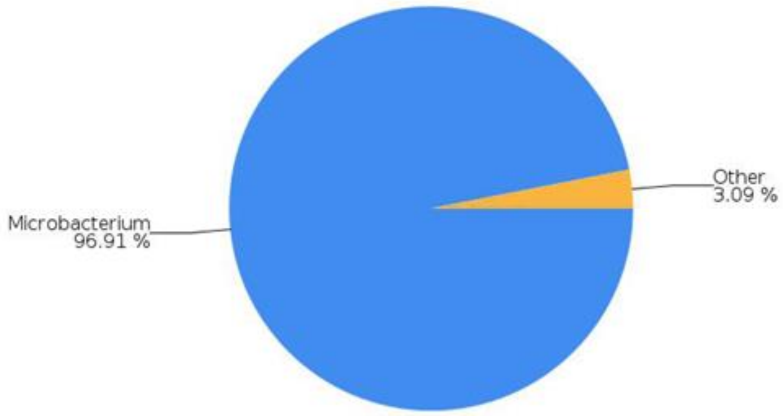

Figure 5.23 Pie graph of resulting genus classification of sample 1 of 4.

In addition, the final species was found to be *Microbacterium arborescens*, with approximately 75% of the reads being classified under this species. It is to be noted that the 16s sequencing data misclassified many of the reads as *Microbacterium chocolatum* due to the close genetic structure of *M. chocolatum* and *M. arborescens*. After further analysis and investigation, the resulting 16s sequencing was determined to be mainly *M. arborescens* (Fig. 5.24).

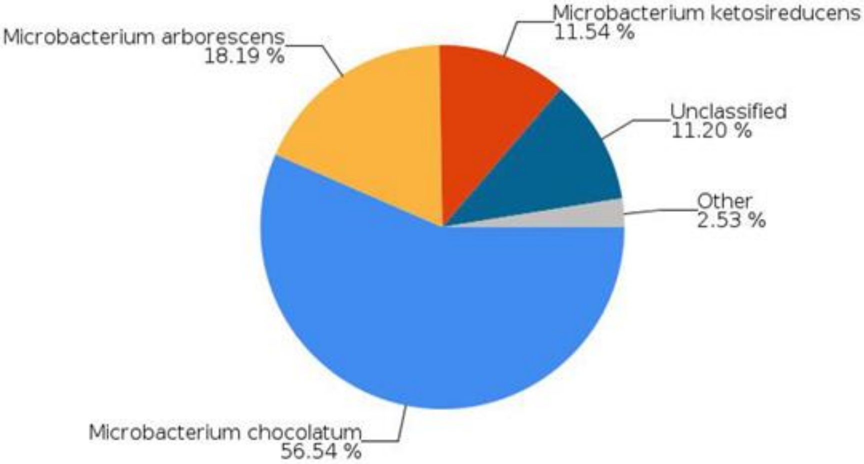

Figure 5.24 Pie graph of resulting species classification of sample 1 of 4.

Here we were able to demonstrate a high-throughput multi-chip droplet screening system for the screening of microalgae or environmental samples. Utilizing this strategy we were able to find high growth and oil accumulating microalgae that can improve the production of oil for biofuel refinement. In addition, a similar strategy was successfully utilized to screen for environmental isolates which inhibit the growth of *A. baumannii* and could produce a novel compound to combat resistant strains of *A. baumannii*. Typical screening applications require days, weeks, or months to screen through 10's of thousands of samples and find a hit of interest. Using this multi-chip system we were able to conduct similar screening and find hits of interest in a matter of hours. Further inhibition assays are currently being conducted to determine the compound novelty for the *M. arborescens* strain. **The *A. baumannii* screening work is currently being submitted for publication.**

6. A FULLY INTEGRATED HIGH-THROUGHPUT DROPLET MICROFLUIDICS PLATFORM FOR POLYMICROBIAL INTERACTION SCREENING

6.1. Basket trapping structure

A monolayer basket trapping structure is utilized to cultivate thousands to 10's of thousands of droplets in a single layer, allowing for droplets to be imaged and analyzed using a time-lapse imaging microscope. The basket trapping structure is optimized for the droplet size by creating gaps small enough to hold droplets of the desired size. Upon complete filling of the chamber, excess droplets are allowed to flow out of the sides of the chip, and inlet/outlets are closed to maintain droplets inside of the basket for observation

6.1.1. Motivation: Basket trapping structure

Considering droplet screening assays, prior to conducting complex screening assays, characterization of the droplet size and corresponding flow rates to produce these droplet sizes must be conducted to match the droplet size chosen for the respective assay. Additionally, the host growth rate characterization needs to be conducted to quantify the fluorescent signal corresponding to a particular number of cells. In addition, environmental control samples must be chosen and utilized in droplets to characterize the growth rate and expected number of cells for a given set assay duration. Furthermore, the interaction between the host/environmental samples needs to be characterized to identify the appropriate time for killing/suppression of growth that has a suitable differential for distinguishing “hits”. Each of these characterization experiments are vital to the success of a droplet screening assay and provide information about the host/target organisms that are necessary for assigning a threshold value for downstream droplet fluorescent sorting and a sorting duration.

6.1.2. Design: Basket trapping structure

The monolayer droplet basket trapping structure described herein entails a 3 mm x 10 mm culture chamber with one inlet and two outlets. The chamber is 45 µm high, appropriate for 37-50 µm droplets, which is the size range of droplets before and after on-chip merging. Additionally, the chamber is lined with 100 µm x 100 µm pillars having 20 µm gaps between pillars and 100 µm from the side wall of the chamber. The first outlet is at the end of the basket to release droplets in a packed format after the basket has been filled. This is useful if conducting a culture followed by droplet flow-through fluorescent analysis, which is often required to assign an appropriate PMT gain and threshold range for downstream detection and sorting. The second outlet is at the end of the chamber after a short 200 µm wide fluidic channel, which is utilized to flow out excess droplets after the chamber is full and as an oil perfusion outlet to maintain the chamber pressure during cultivation/imaging. This can help to prevent droplet evaporation/shrinkage and air bubble generation during cultivation.

6.1.3. Fabrication: Basket trapping structure

The basket trapping chamber is fabricated by preparing a master wafer with the patterned chamber for PDMS replication. First, a silicon wafer is spin coated with SU-8™ (2050, Microchem Inc., Westborough, MA, USA) at 2300 rpm to produce an approximately 45 µm high resist layer for the device to be fabricated from. The wafer is prebaked for 40 min at 65 °C and 20 min at 95 °C and exposed using a mask aligner

(MA6, Karl Suss, Suss Microtec Se, Garching, Germany) to pattern the culture chamber using a conventional photolithography process. The wafer is post exposure baked for 40 min at 65 °C and 20 min at 95 °C, followed by developing. The wafer is coated for 20 min with (tridecafluoro-1,1,2,2-tetrahydrooctyl)-1-trichlorosilane (T2492, United Chemical Technologies, Inc., Bristol, PA) using a desiccator to allow for PDMS replication. The master mold is put into a petri dish and 24 g of 10:1 (polymer: curing agent) liquid PDMS is poured using conventional soft lithography fabrication. After 85 °C baking for 1 h the PDMS is removed from the master and inlet/outlet holes are punched. The PDMS device is then bonded to a glass slide using conventional oxygen plasma bonding (Plasma cleaner, Harrick Plasma, Ithaca, NY). Tygon® (AAD04091, Saint Gobain, Courbevoie, France) tubing is attached to the device inlet/outlets and Aquapel® (Pittsburg Glass Works, LLC, Pittsburgh, PA, USA) is flushed through the device to make the channels hydrophobic for droplet generation/cultivation.

6.1.4. Droplet flow and size characterization comparable to platform operation

Utilizing a cross junction droplet generator with a 25 µm orifice and two 20 µm side channels (27 µm high), 35 µm droplets are generated and introduced into the droplet culture chamber. The droplet size is optimized to match the droplet size used in the later screening assay by adjusting the inlet flow rates. A flow rate of 20 $\mu\mathrm{L\ h^{-1}}$ for the aqueous phase and a flow rate of 70 $\mu\mathrm{L\ h^{-1}}$ for the fluorinated oil with fluorosurfactant (Novec 7500, 3M, Maplewood, MN, USA)/ (Picosurf 1, Sphere Fluidics, Monmouth Junction, NJ, USA) is used to generate droplets.

6.1.5. Interrogation of environmental and host organisms as model organisms for in-droplet growth characterization

A culture well plate assay is first conducted with yeast (*Saccharomyces cerevisiae*) alone (as a control condition), yeast with *PK* (antifungal producing cell), and yeast with *Escherichia coli* (*E. coli)* to characterize the model system (Fig. 6.1). The resulting growth phenotype are utilized as a base reference for the in-droplet cultivation assay under the same experimental conditions. Additional assays were conducted with *Botrytis cinerea* (*B. cinerea*) and can be found in Appendix B.

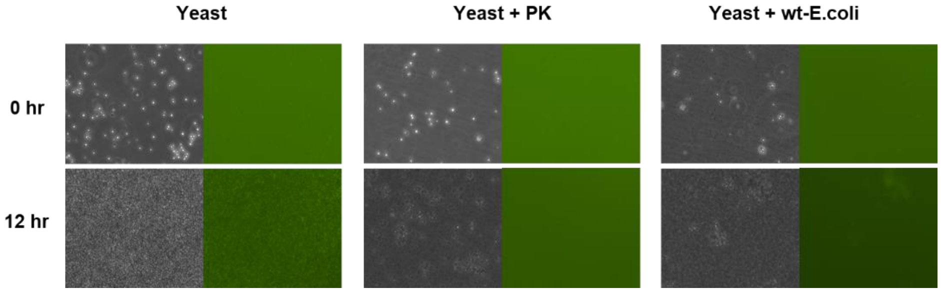

Figure 6.1 Bright-field and fluorescent images of yeast, yeast grown with *PK* (antifungal producing cell), and yeast with *E. coli* for growth characterization.

6.1.6. Cell cultivation using a novel basket trapping structure for pre-platform characterization

Growth rate characterization and corresponding fluorescent intensity is investigated by cultivating host and/or microbes in 35 μm droplets and conducting image analysis. Additionally, the cell encapsulation distribution is optimized to 5 host GFP-yeast cells per droplet, mimicking the cell number encapsulated at the start of the droplet screening assay. Time-course analysis is conducted using a fluorescent microscope (Carl Zeiss Micro Imaging, LLC, Oberkochen, Germany) to characterize the increase in GFP fluorescence related to yeast cell proliferation. The average cell number increase due to cell growth correlates directly to the fluorescent intensity. Therefore, by conducting a 2-4 h culture for *E. coli* (modeling environmental samples) and 4-6 hours culture for yeast, we can ascertain the approximate expected cell number range and corresponding average fluorescent intensity for the respective cell number. This will help to set a gain voltage for the PMT used for droplet detection, and a threshold value for droplet sorting.

In preparation for the Poly-chip screening assay, GFP-yeast proliferation and corresponding fluorescent intensity is interrogated simultaneously in a multi-well plate format and a droplet-based format. Three conditions are prepared to compare the growth rates of GFP-yeast when GFP-yeast is cultivated alone, GFP-yeast is cultivated with *PK* (acting as an antifungal), and GFP-yeast is cultivated with *E. coli* (no effect). Cell proliferation (budding) of yeast is characterized in each of the conditions and directly compared to determine the expected GFP-yeast cell number after co-cultivation during the screening assay. Here we show that GFP-yeast encapsulated alone can proliferate from approximately 5 cells per droplet to more than 25 cells per droplet when cultivated for 6-8 h. Furthermore, when encapsulated with approximately 20 antifungal-*PK* (signifying encapsulation of 1 *PK* cell that is cultivated for 2 hours prior to droplet merging) GFP-yeast cell only increase from 1-2 cells to 2-3 cells when cultivated for the same 6-8 h. In addition, when 20 *E. coli* cells are encapsulated with 2-3 GFP-yeast, the GFP-yeast increases to approximately 15-20 cells in 6-8 h of cultivation (Fig. 6.2 & 6.3).

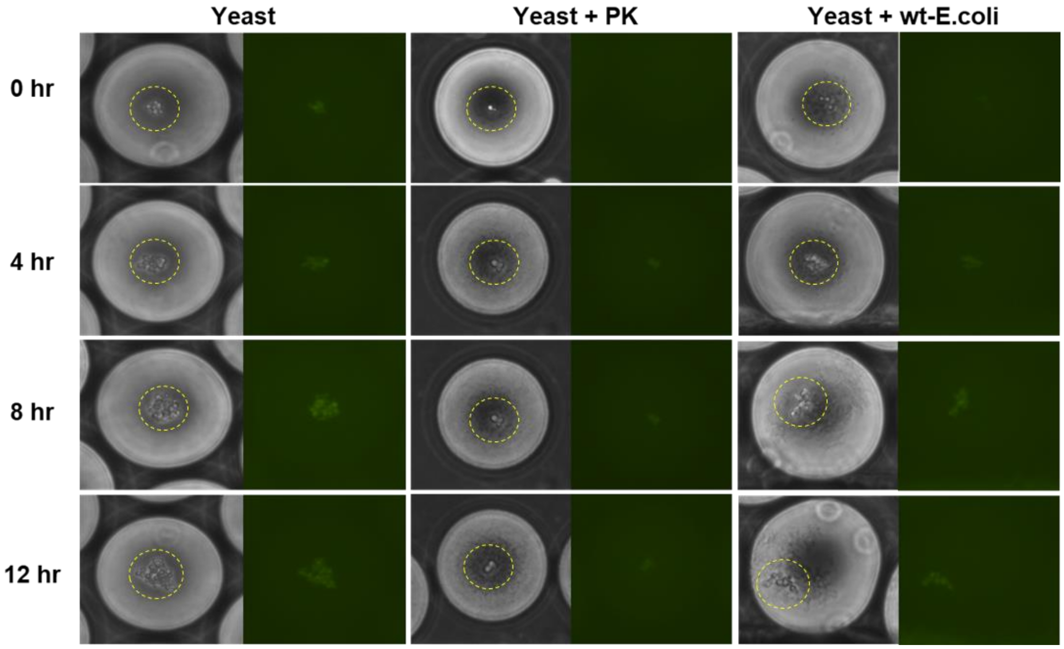

Figure 6.2 Micrograph images of cultivated droplets containing yeast, yeast with *PK*, and yeast with *E. coli*.

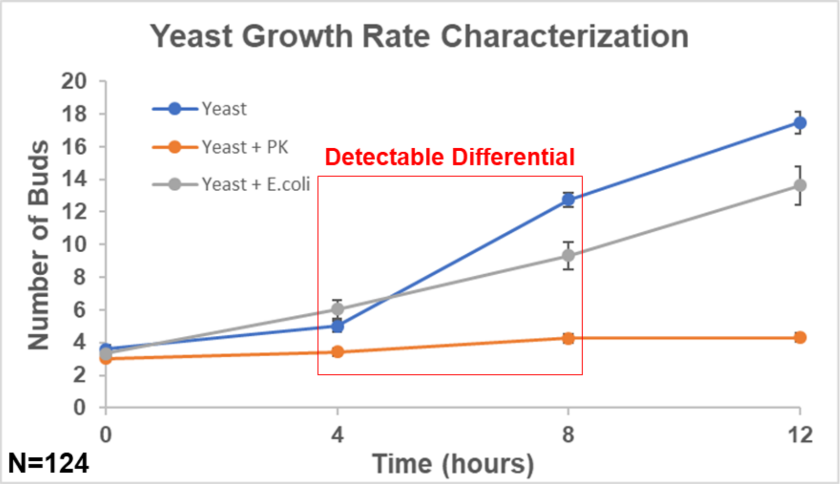

Figure 6.3 Growth comparison analysis of yeast, yeast with *PK,* and yeast with *E. coli* as a model organism for Poly-chip screening.

These results prove that GFP-yeast encapsulated in droplets doesn't cause a significantly different growth profile when compared to a conventional multi-well plate culture. Furthermore, we can expect that in a real droplet screening assay where approximately 5 GFP-yeast are encapsulated per droplet, a normal growth rate will result in a cell range of 15-25 cells after 6 h of cultivation. Also, since a difference in growth between the conditions can be observed at 4-6 h, this give indication that a culture time of 6 h should be plenty to illicit the desired killing/suppression response. As mentioned before, this provides us with an estimate on the number of cells at the end of the assay (5-10 cells for the killing case, and 15-25 cells for the non-killing case). This same sample is flown through a laser based-detection system after cultivation to acquire the desired threshold voltage necessary to efficiently sort droplets.

6.2. Bottom-up culture chamber

Integration of a fully functional droplet-based microfluidic screening system for high-throughput drug/compound discovery requires combining a variety of complex functionalities in a seamless workflow. Considering aqueous droplets surrounded by fluorinated oil, droplets are known to have a higher buoyancy than the surrounding oil phase, and therefore float. Therefore, for the Poly-chip droplet screening system a bottom-up droplet culture chamber is most suitable for being integrated into the screening system. Droplets can be generated in a bottom layer and allowed to freely float up to a top outlet. Droplets reflowed out of the top of the chamber can be coupled to an adjacent fluidic layer for further manipulation.

6.2.1. Motivation: Bottom-up culture chamber

A large-scale droplet cultivation chamber is necessary for conducting a large volume screening and incorporation of a bottom-up chamber can provide several advantages over conventional culture chambers. In addition, considering the need for downstream manipulation (droplet synchronization/merging), packing droplets at the top of the cultivation chamber and reflowing these droplets allows for maximum control. Hence, a desired spacing can be input while conducting reflow leading to stable one-to-one synchronization and high efficiency downstream droplet merging. This allows for the full integration of a controllable large-scale droplet culture chamber capable of housing millions of droplets for conducting a drug discovery screening assay.

6.2.2. Design: Bottom-up culture chamber

The integrated large-scale bottom-up culture chamber is comprised of 7-9 layers that are divided into three main sections. The bottom section is utilized for droplet generation and release of excess oil. A blank PDMS slab base layer is used as the bottom substrate, on which a 19 µm deep fluidic channel layer is bonded. A cross-junction droplet generator entailing a 25 µm wide aqueous phase inlet and two 20 µm wide oil junction inlets is used to generate approximately 35 µm diameter droplets. These droplets are propagated down a fluidic channel to a 2 mm diameter large vertical reservoir that is utilized as a culture chamber. A perpendicular 200 µm channel leads from the bottom of the large vertical reservoir to an outlet where excess oil is removed. The 3D printed culture chamber (Perfactory P3 mini, HTM 140v2 resin, EnvisonTEC Inc., Dearborn, MI, USA) can be divided into three stacked layers, a bottom, middle, and top layer where the bottom and top layers have conical sloped transitions from the final 2 mm diameter culture chamber to a 1 mm diameter.

This allows for a smoother transition of droplets, reduces the dead volume in the chamber, and keeps the droplets in a first-in-first-out format while conducting the assay. Simulation results of various culture chambers diameters and slopes were directly compared to determine which chamber minimizes abrupt changes in the droplet flow. Minimizing this transition is important because it reduces the changes in flow which cause droplets to merge or split when traversing from one layer to another. The top portion of the design entails a base layer to bond a channel layer to that allows for the release of droplets into an adjacent fluidic channel layer. The top and bottom channels layers each have valves to control the aqueous inlet phase (stopping/starting droplet generation), oil exiting the bottom layer, and droplets being on-demand released from the top of the chamber. The valves are incorporated using a normally-closed valving structure where pressure/vacuum is applied to close/open a pillar used to block/allow flow.

6.2.3. Operation: Bottom-up culture chamber

The bottom-up large-scale culture chamber is first filled with droplets by closing the valve at the top of the chamber, causing droplets to pack at the top of the chamber. The bottom valves for the aqueous phase and oil outlet are both left open so that droplets generate and float to the top of the chamber, but excess oil flows out through the bottom outlet. Once the chamber is full, the valve for the aqueous inlet is close and the corresponding syringe pump is turned off to stop droplets from being generated. The oil flow used to generate droplets is then reduced from 70 $\mu L\ h^{-1}$ to 20 $\mu L\ h^{-1}$ until excess droplets are removed and internal pressures are stabilized. When ready to release the droplets, the bottom outlet where excess oil is escaping is closed and simultaneously the top valve is opened to release droplets out the top of the chamber.

6.2.4. Integration of semi-continuous bottom-up first-in first-out droplet cultivation chamber

A semi-continuous bottom-up first-in first-out cultivation chamber can be integrated by using a novel bottom-up fabrication process to create highly aligned modular systems. Conventional photolithography-based alignment marks can be stamped in the PDMS device using conventional soft-lithography processes. These alignment marks embedded in conventional fluidic layers can be aligned to alignment/3D alignment marks at the top and bottom of each channel layers. Since each chamber layer has a 3D alignment mark (Perfactory P3 mini, HTM 140v2 resin, EnvisonTEC Inc., Dearborn, MI, USA) and conventional alignment mark, each of these layers can be stacked iteratively in an endless manner. This leads to culture chambers of the desired volume and the ability to modularly stack chamber layers to the desired height. Furthermore, incorporating valving structures into the inlet and outlet of the large-scale cultivation chamber allows for the on-demand filling/release of droplets. Using this operation method, droplets can be generated, reflowed, and then generated again to fill the chamber in a semi-continuous operation manner (Fig. 6.4).

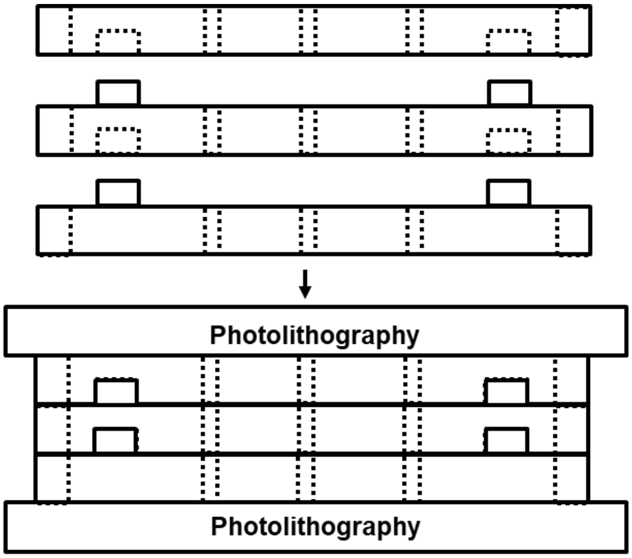

Figure 6.4 Illustration of the device fabrication process using photolithography and 3D alignment marks to iteratively stack PDMS layer for fabrication of the Poly-chip platform.

6.3. Integration/characterization reflow, synchronization, merging

Using the integrated stacking fabrication process, a highly complex integrated droplet microfluidic system can be designed to include all droplet functionalities on a single chip. Although integration of various functions can be difficult to employ, separating different stages using valving structures can allow for separate operation of sections of the device and make operation/characterization straight forward. Here we use this complex integration and valving scheme to separate the droplet generation and incubation of environmental samples from the droplet synchronization/merging layer. This essentially allows us to characterize the necessary flow rates for generating appropriate size droplets at the appropriate rate, which is required to match the processing speed of downstream functions.

6.3.1. Motivation: Integration/characterization reflow, synchronization, merging

Integration of the Poly-chip system provides some inherent advantages over conventional multi-chip function assays. First, integration removes the need for interface tubing between functionalities, leading to high efficiency platform performance. This can be seen in the reduction of unwanted merged or split droplets during platform operation. Furthermore, integration allows for a more compact and automated system that can be controlled using the complex valving operation and corresponding LabView® program to control flow through the platform. The integration of a large-scale bottom-up culture chamber provides one with the ability to reflow packed droplets and add the desired droplet spacing that matches a second droplet generator rate/spacing. Matching the flow of these two trains of droplets can be tuned using different reflow rates, spacing flow rates, and water/oil generation flow rates. Controlling each of these flows allows for characterization of the system and high efficiency one-to-one synchronization, leading to high efficiency downstream droplet electrocoalescence.

6.3.2. Design: Integration/characterization reflow, synchronization, merging

The integrated synchronization/merging layer is comprised of a base layer which has a hole that aligns to the environmental culture chamber, a microfluidic channel layer to manipulate droplets, and a valve layer to control inlet and outlet flow. Droplets enter the channel layer, travel down a 200 µm wide channel, past a set of two valve (one going to an outlet for waste during generation, and one to the synchronization region). An oil inlet (50 µm wide) adding spacing to droplets traveling down a narrowed 50 µm wide channel to the synchronization region. The synchronization region is comprised of an array of 100 µm x 100 µm pillars between two parallel channels (50 µm wide), making a railroad-like structure. These two channels are combined using a Y-junction, where paired droplets flow into a 50 µm wide channel to the droplet merging region. The droplet merging region entails a 150 µm long x 100 µm wide channel with curved corners to reduce dead volume in the region. Merged droplets then flow out to a 200 µm channel and into the bottom of the second (co-cultivation) culture chamber (Fig. 6.5).

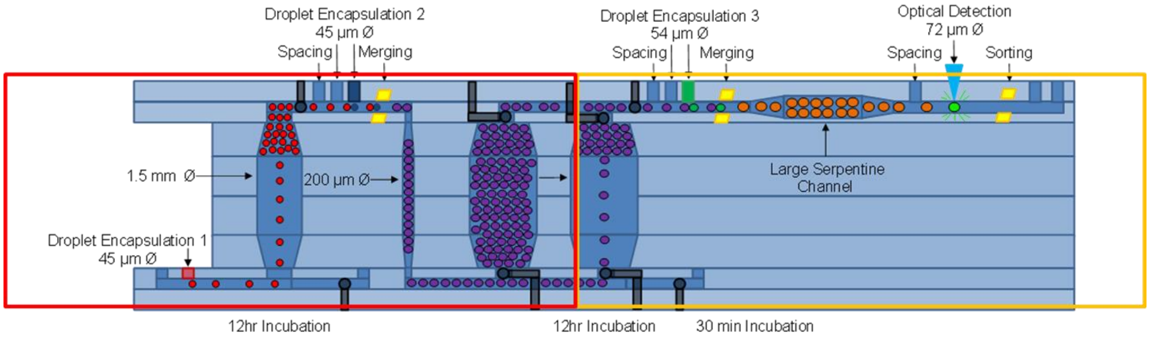

Figure 6.5 Illustration of a sandwich Poly-chip system where droplets are generated on a bottom layer, cultivated, merged with a second droplet, further cultivated, optionally merged with a third dye staining droplet, flown through the detection region, and sorted.

6.3.3. Fabrication: Integrated Poly-chip systems

All valve layers are fabricated by spin coating a silicon wafer with SU-8™ (2075, Microchem Inc., Westborough, MA, USA) at 1900 rpm to produce an approximately 75 µm high resist layer for the device to be fabricated from. The wafer is prebaked for 40 min at 65 °C and 20 min at 95 °C and exposed using a mask aligner (MA6, Karl Suss, Suss Microtec Se, Garching, Germany) to pattern the culture chamber using a conventional photolithography process. The wafer is post exposure baked for 40 min at 65 °C and 20 min at 95 °C, followed by developing. The wafer is coated for 20 min with (tridecafluoro-1,1,2,2-tetrahydrooctyl)-1-trichlorosilane (T2492, United Chemical Technologies, Inc., Bristol, PA) using a desiccator to allow for PDMS replication. Approximately 20 g of liquid PDMS prepolymer at a ratio of 10:1 (polymer: curing agent) is poured to produce a 3mm thick PDMS layer. After 85 °C baking for 1 h the PDMS is removed from the master and methanol bonded to the corresponding channel layer using conventional oxygen plasma bonding (Plasma cleaner, Harrick Plasma, Ithaca, NY), followed by baking at 85°C for 1 h.

The Poly-chip is fabricated by preparing a master wafer for the channel layers (bottom, middle, top) for PDMS replication. First, a bottom/middle channel layer silicon wafer is spin coated with SU-8™ (2025, Microchem Inc., Westborough, MA, USA) at 2300 rpm to produce an approximately 27 µm high resist layer for the device to be fabricated from. The wafer is prebaked for 40 min at 65 °C and 20 min at 95 °C and exposed using a mask aligner (MA6, Karl Suss, Suss Microtec Se, Garching, Germany) to pattern the culture chamber using a conventional photolithography process. The wafer is post exposure baked for 40 min at 65 °C and 20 min at 95 °C, followed by developing. The wafer is coated for 20 min with (tridecafluoro-1,1,2,2-tetrahydrooctyl)-1-trichlorosilane (T2492, United Chemical Technologies, Inc., Bristol, PA) using a desiccator to allow for PDMS replication. The master mold is spin coated with 2.5 g of 10:1 (polymer: curing agent) liquid PDMS at 700 rpm to obtain a 50 µm thick PDMS layer. After 85 °C baking for 1 h the PDMS is removed from the master and methanol bonded to the corresponding valve layer. After 85°C baking for 1 h the valves are actuated and bonded to a bottom substrate using conventional oxygen plasma bonding (Plasma cleaner, Harrick Plasma, Ithaca, NY), followed by baking at 85°C for 1 h.

Second, a top channel layer silicon wafer is spin coated with SU-8™ (2050, Microchem Inc., Westborough, MA, USA) at 2300 rpm to produce an approximately 45 µm high resist layer for the device to be fabricated from. The wafer is prebaked for 40 min at 65 °C and 20 min at 95 °C and exposed using a mask aligner (MA6, Karl Suss, Suss Microtec Se, Garching, Germany) to pattern the culture chamber using a conventional photolithography process. The wafer is post exposure baked for 40 min at 65 °C and 20 min at 95 °C, followed by developing. The wafer is coated for 20 min with (tridecafluoro-1,1,2,2-tetrahydrooctyl)-1-trichlorosilane (T2492, United Chemical Technologies, Inc., Bristol, PA) using a desiccator to allow for PDMS replication. The master mold is spin coated with 2.5 g of 10:1 (polymer: curing agent) liquid PDMS at 700 rpm to obtain a 50 µm thick PDMS layer. After 85 °C baking for 1 h the PDMS is removed from the master and methanol bonded to the corresponding valve layer. After 85°C baking for 1 h the valves are actuated and bonded to a bottom substrate using conventional oxygen plasma bonding (Plasma cleaner, Harrick Plasma, Ithaca, NY), followed by baking at 85°C for 1 h.

Finally, Bottom substrates are fabricated by spin coating a silicon wafer with SU-8™ (2075, Microchem Inc., Westborough, MA, USA) at 1900 rpm to produce an approximately 75 µm high resist layer for alignment marks to be replicated in PDMS. The wafer is prebaked for 40 min at 65 °C and 20 min at 95 °C and exposed using a mask aligner (MA6, Karl Suss, Suss Microtec Se, Garching, Germany) to pattern the culture chamber using a conventional photolithography process. The wafer is post exposure baked for 40 min at 65 °C and 20 min at 95 °C, followed by developing. The wafer is coated for 20 min with (tridecafluoro-1,1,2,2-tetrahydrooctyl)-1-trichlorosilane (T2492, United Chemical Technologies, Inc., Bristol, PA) using a desiccator to allow for PDMS replication. Approximately 15 g of liquid PDMS prepolymer at a ratio of 10:1 (polymer: curing agent) is poured to produce a 2 mm thick PDMS layer. After 85 °C baking for 1 h the PDMS is removed from the master and bonded to the opposing side of the corresponding channel layer using conventional oxygen plasma bonding (Plasma cleaner, Harrick Plasma, Ithaca, NY), followed by baking at 85°C for 1 h.

Lastly, all chamber layers are fabricated by 3D printing (Perfactory P3 mini, HTM 140v2 resin, EnvisonTEC Inc., Dearborn, MI, USA) a master and coating the master for 40 min with (tridecafluoro-1,1,2,2-tetrahydrooctyl)-1-trichlorosilane (T2492, United Chemical Technologies, Inc., Bristol, PA) using a desiccator to allow for PDMS replication. Approximately 15 g of liquid PDMS prepolymer at a ratio of 10:1 (polymer: curing agent) is poured to produce a 3 mm thick PDMS layer. After 85 °C baking for 1 h the PDMS is removed from the master and bonded to the PDMS valve or substrate layers using conventional methanol oxygen plasma bonding (Plasma cleaner, Harrick Plasma, Ithaca, NY), followed by baking at 85°C for 1 h.

The final device is additionally baked at 85°C for 3 days to regain hydrophobicity and Field’s metal is injected into the electrode channels. Wires are connected to each electrode and sealed with epoxy glue while solidifying to prevent disconnection of the electrode.

6.3.4. Operation: Integration/characterization reflow, synchronization, merging

The integrated synchronization and merging layer is operated by first opening the valve at the top of the environmental incubation chamber and releasing packed droplets in a controlled manner. Through experimental flow characterization, a flow rate of 20 $\mu L\ h^{-1}$ is utilized to reflow droplet from the environmental cultivation chamber. As droplets travel down a microchannel toward the railroad-like synchronization region, a perpendicular oil spacing channel flow rate (70 $\mu L\ h^{-1}$) is optimized to match the speed, rate, and spacing of on-the-fly generated and paired yeast host cell droplets. An adjacent cross-junction droplet generator (25 µm wide aqueous phase inlet and two 20 µm wide oil junction inlets) is utilized to generate 35 µm yeast host droplets. As these two trains of droplets travel down the railroad-like synchronization structure, a highspeed camera (Orca Flash V3.1 Hamamatsu, Shizuoka, Japan) at a frame rate of 500 fps is used to acquire 20 s videos for analysis. Frame-by-frame analysis is conducted to obtain the synchronization efficiency of paired droplets. Furthermore, after droplets have been paired and join in a Y-shape junction, the final efficiency of synchronized droplets is quantified. During characterization, flow rates are adjusted to maximize the synchronization efficiency, which has a direct effect on the downstream droplet merging efficiency. Additionally, at the droplet electrocoalescence region, highspeed videos are taken when the electric field is on and off. Frame-by-frame analysis is conducted to obtain an overall merging efficiency of paired droplets entering the merging region. Droplets that do not merge or are mismatched and double merged are both designated as failed mergers and account for a decrease in the merging efficiency. An electric field can be generated using a voltage range from 50 V to 900 V using a function generator (generating a 10 kHz square wave) and high voltage amplifier (amplifying 100x, Trek 2200, Trek Inc., Lockport, NY, USA). At a droplet throughput of 10 droplets s^{-1}, a voltage of 200 V to 250 V is typically required to induce an electric field strong enough to maintain a 90% or greater merging efficiency in the Poly-chip platform. Considering higher throughput operation, a higher frequency, higher voltage, and stronger corresponding electric field is necessary to maintain this high efficiency droplet merging. After merging, droplets are flown into a second incubation chamber where co-cultivation of merged droplets occurs.

6.1. Asynchronous culture chambers

Environmental droplets that have been cultivated in the first stage of the chip to allow for accruement of drugs/compounds must be reflowed, synchronized, and merged with host droplets, followed by an additional culture duration. Since the second cultivation duration is 6 h, if only one culture chamber exists at this stage, then no additional droplets can be generated and cultivated until this chamber has been fully released to the downstream droplet detection/sorting functions. Therefore, one approach to resolving this issue is to add an additional chamber that functions separately, but in parallel to the second culture chamber.

6.1.1. Motivation: Asynchronous culture chambers

Avoiding throughput limitation due to generation and reflow of environmental droplets from the first chamber, multiple second chambers that fill one after another can be utilized to create a staggered second stage cultivation/reflow. Adding a second chamber removes the throughput limitation that is inherent to the system due to generation, packing, and reflow. The additional chamber essentially doubles the throughput of the second half of the system and further complex staggered systems can be utilized to further enhance this throughput. Therefore, we incorporated an identical parallel chamber that shares the same main inlet/outlet but can be filled or released separately using valves. This double chamber design can be utilized to culture one set of droplets while filling the second chamber. Additionally, each of the chambers can be operated separately and therefore can be reflowed at any given time without effecting the adjacent chamber.

6.1.2. Design: Asynchronous culture chambers

The asynchronous droplet culture chambers are 1.5 mm in diameter with two inlets on the bottom, one oil outlet on the bottom, and one outlet at the top of the chamber. The inlet channels to each of the chambers originate from the same source channel and are 200 µm wide and 27 µm high, with a normally closed valve allowing for one chamber to be filled at a time. Each of the chambers has a side bottom oil reflow inlet (50 µm wide) with a normally closed valve to independently reflow droplets after cultivation. Similar to the bottom chamber, a bottom excess oil outlet (50 µm wide) with a valve is utilized to flow out oil during droplet introduction and packing into the chamber. Introduction and exit valves that traverse droplets are intentionally larger (200 µm x 300 µm elliptical shaped) in size to prevent droplet breakup or merging during generation and reflow. Alternatively, simple aqueous/oil inlets/outlets are opened and closed using a small square valve (100 µm x 100 µm), which often maintains the integrity of the surrounding plasma bonding between layers better and has a longer operation lifetime than the larger droplet valves. In addition, these small square valves are capable of being operated at a higher device pressure, which is often experienced in complex integrated devices, without valve leakage or bulging (Fig. 6.6).

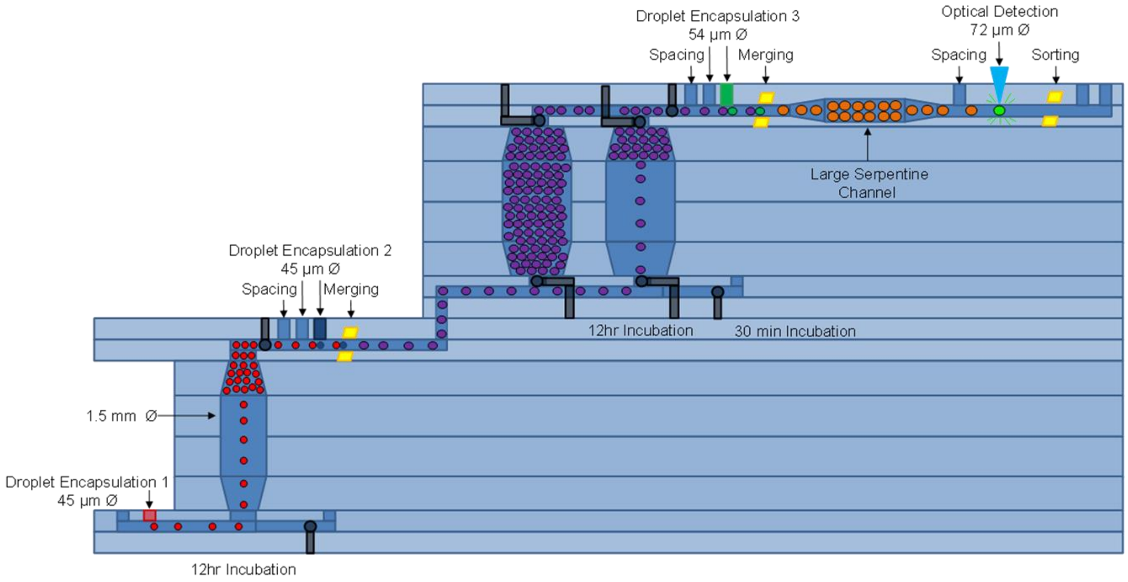

Figure 6.6 Illustration of a stacked Poly-chip design where droplets float up to adjacent layers to prevent droplet merging.

6.1.3. Operation: Asynchronous culture chambers

The asynchronous culture chambers are operated in a similar format as the bottom environmental culture chamber, where droplets are flown into the chamber from a bottom channel layer and flown out of the chamber in a packed manner from the top of the chamber. Droplets that are synchronized and merged are introduced into one of the culture chambers that has their corresponding inlet valve open, while the adjacent culture chamber has its inlet valve closed. The excess oil outlet valve is open to allow for removal of oil and packing of droplets, while the top outlet of the chamber is closed. Droplets fill the entire first chamber and overflow droplets escape through the excess oil outlet. All valves for the first chamber are simultaneously closed while the droplet inlet valve for the second chamber and the excess oil outlet for the second chamber are opened, allowing droplets to begin filling the second chamber while the first chamber droplets are incubated. When each of the chambers are filled, all valves on the second chamber are closed and incubation for this chamber is started. At any given time, the oil reflow inlet valve and top droplet exit valve of the first chamber can be simultaneously opened and droplets can be reflowed to the downstream detection/sorting regions.

6.1.4. Asynchronous culture chambers for co-cultivated host/environmental microbes

Considering the final assay of encapsulating single environmental microbes in droplets, cultivating these droplets for 2 h, merging these droplets with GFP-yeast encapsulated droplets containing 5 yeast buds, and culturing the resulting droplets for 6 h, two larger-scale cultivation chambers are required. In order to allow for continuous operation, the second cultivation chamber has an identical parallel culture chamber with valves at the inlet and outlet to allow for on-demand filling and releasing. Therefore, when the first chamber is filled with droplets that are being cultivated for 6 h, the inlet/outlet valves can be closed and inlet valves for the identical parallel chamber can be simultaneously opened to allow for droplets to begin filling the second chamber. When the co-cultivation is concluded, droplets can be released from one chamber without effecting the adjacent parallel chamber. This operation strategy allows for multiple chambers to be filled/released simultaneously, leading to semi-continuous operation where the screening system can process more droplets in the same amount of time. Furthermore, advanced multiplexed designs can be employed using this staggered operation strategy to allow for continuous operation of multiple chambers to be screened.

6.2. Integration laser-based optical detection

A fluorescent-based optical detection system is then integrated into the Poly-chip droplet microfluidic-based screening system to analyze the fluorescent content of droplets for downstream sorting. A droplet detection region with a set distance from the droplet sorting function is utilized with an in-house 3D printed (Perfactory Ultra, LS600 resin, EnvisonTEC Inc., Dearborn, MI, USA) compact fluorescent-based system to detect droplet fluorescent intensities and relay the corresponding droplet fluorescence to a LabView®-based graphical interface. This integrated optical detection system allows for highspeed on-the-fly characterization of in-droplet content which is necessary for on-the-fly phenotypic analysis of droplets for drug screening applications.

6.2.1. Motivation: Integration laser-based optical detection

A detection method is required to analyze the content of droplets for characterization of in-droplet content, which is necessary for quantifying phenotypic responses due to complex polymicrobial interactions. Furthermore, a high resolution and high-throughput detection method is most suitable for highspeed screening applications, as rapid screening systems often require higher sensitivity for adequate characterization. Although other detection modalities exist, fluorescent analysis offers the most versatility in terms of conducting a variety of assays using different host organisms, dye, or tagging methods. Hence, for the Poly-chip screening platform, a fluorescent-based detection system is utilized to develop a versatile system that can be used for conducting various screening assays.

6.2.2. Design: Integration laser-based optical detection

The droplet detection system entails a blue laser (LRS-0473-PFM-00100-03, Readylaser, Anaheim, CA, USA) as an excitation source, that is coupled directly to a 5-part in-house 3D printed (Perfactory Ultra, LS600 resin, EnvisonTEC Inc., Dearborn, MI, USA) optical system for housing all of the optics components. The laser reflects off a dichroic mirror (DiO-R488-25x36, Semrock: IDEX Health & Science, LLC Rochester, NY, USA) onto the device and emitted light is focused using a lens (LA1540-A, Thorlabs, Inc. Newton, NJ, USA) back onto the dichroic mirror. An additional collection lens (LA1540-A, Thorlabs, Inc. Newton, NJ, USA) is utilized to refocus light onto a fully reflective mirror (PF10-03-P01, Chroma, Inc. Bellows Falls, VT, USA), and toward a green emission filter (ET525/50m, Chroma, Inc. Bellows Falls, VT, USA). Lastly, filtered light is recollected using a final lens (LA1540-A, Thorlabs, Inc. Newton, NJ, USA) and focused into a PMT (H10721-110, Hamamatsu, Inc. Japan) for droplet detection (Fig. 6.7). The focal lengths (15 mm) of all lenses are optimized to the exact distance between components and provide the most ideal light excitation/emission acquisition, providing the highest sensitivity possible with the optical system. The output signal from the PMT is input into an amplifier (OPA350PA, National Instruments, National Instruments, Austin, TX, USA) to change the acquired signal from a current output to a voltage output and increase the corresponding voltage output. This final signal is acquired using a DAQ (NI9219 DAQ, National Instruments, Austin, TX, USA) and a LabView® graphical interface displays the acquired signal in real-time.

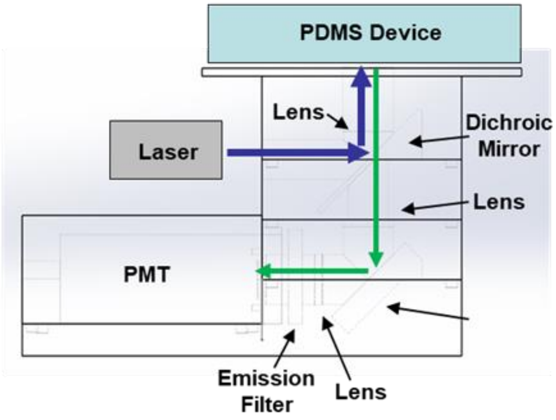

Figure 6.7 Illustration of the first-generation laser-based detection system.

6.2.3. Operation: Integration laser-based optical detection

A microfluidic device containing a detection region is aligned to the optical detection spot of the optical detection system, and the resulting signal is acquired for assigning a threshold voltage for downstream sorting. The output signal from the PMT is input into an amplifier (OPA350PA, National Instruments, Austin, TX, USA) to change the acquired signal from a current output to a voltage output and increase the corresponding voltage output. This final signal is acquired using a DAQ (NI9219 DAQ, National Instruments, Austin, TX, USA) and a LabView® graphical interface displaying the acquired signal in real-time. The detection signal is optimized for a specific cell type by tuning the gain of the PMT (.6-.9 V) and tuning the output power of the excitation light source, resulting in the highest resolution possible using the described detection system.

Although an LED-based detection system is suitable for detecting high autofluorescence cells, fast growing GFP strains (e.g. GFP-*E. coli*), and dye stained samples, slow growing strains and weak fluorescent strains suffer from low resolution (e.g. GFP-yeast). Therefore, considering the high-throughput Poly-chip screening assay, a laser-based detection system is more suitable for conducting on-the-fly detection of GFP-yeast. Providing a higher excitation power source increases the signal-to-noise resolution approximately 10-times, leading to the ability to detect 2-3 GFP-yeast cells which was unattainable using the LED-based detection system.

6.2.4. In-droplet laser-based characterization and SNR optimization

The laser-based detection system is characterized and optimized using identical conditions of those expected in the Poly-chip GFP-yeast screening assay. Droplets 45 µm in diameter containing only TSB or YPD media are generated and packed into a monolayer droplet basket trapping structure, reflowed, spaced, and flown through the detection region at a rate of 10 droplets s^{-1}. The PMT gain is adjusted from .6-.9 V and the laser power is adjusted from 1.5 to 1.7 V (with 1.9 V being a maximum of 120 mW power input). Different combinations of PMT gain and laser power are utilized to determine a reasonable value that provide high resolution detection, but do not fully saturate the PMT (Table 6.1). Additionally, populations of droplets encapsulating 5-10 cells and 20-30 cells are generated and flown through the system in an identical manner to determine the appropriate gain and laser power for high resolution detection. A SNR comparison shows that TSB media provides the highest SNR, while YPD media has slightly higher inherent background noise.

Table 6.1 Table showing the percent of species classification reads of sample 1.

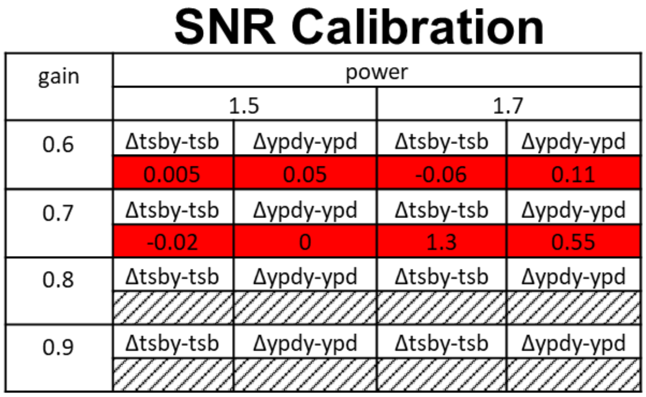

SNR Calibration

gain	power			
	1.5		1.7	
0.6	Δtsby-tsb	Δypdy-ypd	Δtsby-tsb	Δypdy-ypd
	0.005	0.05	-0.06	0.11
0.7	Δtsby-tsb	Δypdy-ypd	Δtsby-tsb	Δypdy-ypd
	-0.02	0	1.3	0.55
0.8	Δtsby-tsb	Δypdy-ypd	Δtsby-tsb	Δypdy-ypd
	▨	▨	▨	▨
0.9	Δtsby-tsb	Δypdy-ypd	Δtsby-tsb	Δypdy-ypd
	▨	▨	▨	▨

6.2.5. Media, dye-staining, GFP-cells, and background fluorescence

Although TSB media was chosen as the primary media for performing a model droplet microfluidic screening assay using GFP-yeast, other medias were also investigated for future screening assays. It was observed that other medias which have more yellow hues often suffer from lower SNR due to high background fluorescence (Appendix B Fig. 8.19). In addition, minimal media can be utilized to have a higher SNR, but often have a significant impact in the growth rate of cells (usually slower growth rates) and therefore also have a lower SNR when conducting co-cultivation for the same duration. Obviously, the growth portion of the assays can be increased to allow for more cell proliferation, but this will also reduce the overall throughput of the assay.

When conducting dye-staining assays, green live-dead staining assays using Fun1 (F7030, Thermo Fisher Scientific, Waltham, MA, USA) and BCECF-AM (B1170, Thermo Fisher Scientific, Waltham, MA, USA) were used to investigate the staining efficiency, fluorescent intensity, and background fluorescence (Fig. 6.8). When utilizing yellow media (e.g. LB, TSB, YPD), the dye staining background noise is often increased. We suspect this increase in background fluorescence is due to the combination of yellow media and dye that have an interaction when conducting fluorescent analysis. Furthermore, some slight non-specific staining can be observed, especially when conducting long-term assays where dye is present for greater than 30 min (and often increases over time). In lieu of this high background fluorescence (Appendix B 8.18), investigation and a comparison of GFP-yeast was conducted to determine which scenario offers the highest SNR.

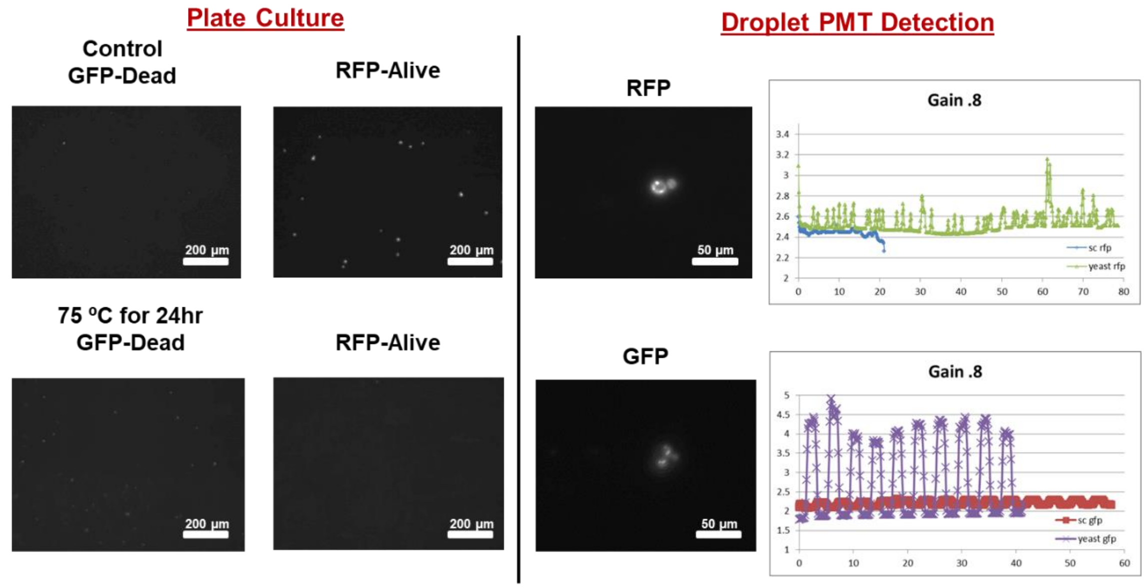

Figure 6.8 Characterization of dye-based fluorescent detection using the laser-based detection system, Fun1 dye, and yeast (other gain voltages were tested, but .8 V provided the highest SNR).

Droplets containing GFP-yeast are encapsulated with the same number of cells as the droplet dye staining experiment above and flown through the laser based optical detection system. After optimization of the detection, GFP-yeast in TSB media showed 1.3-times SNR and provided a better resolution than any of the dye staining conditions. This is due purely to the adverse impact of high background fluorescence innate to dye-staining assays and the interaction of the dye with surrounding media. Therefore, due to the ease of use, the GFP-yeast (eliminates the need for an additional droplet merging and incubation step for dye-staining) is chosen as the host cell to conduct the Poly-chip screening assay and provides the highest resolution for the platform (Fig. 6.9).

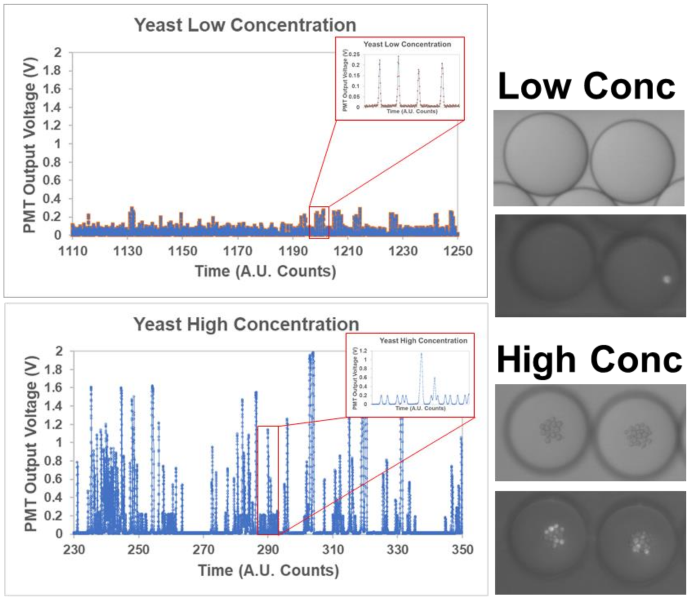

Figure 6.9 Encapsulation and flow through of high concentration and low concentration GFP-yeast using the laser-based detection system.

6.2.6. Development of two-part optical system for Poly-chip platform

Considering that the integrated Poly-chip system uses the droplet buoyancy to release droplets to adjacent top layers, droplet detection is ideally conducted in the most top PDMS layer. Therefore, the previously discussed, bottom-up, detection system is not adequate for conducting on-the-fly detection of droplets using the Poly-chip screening platform. We developed an inverted, top-down, integrated optical alignment and observation system capable of exciting droplets from the top of the device and perfectly aligning the laser spot to the desired detection region. Additionally, a long-range objective (MY5X-802, Thorlabs, Inc. Newton, NJ, USA), mirror (PFR10-P01 , Thorlabs, Inc. Newton, NJ, USA), lens (LA1540-A, Thorlabs, Inc. Newton, NJ, USA), and camera (Orca Fusion, C14440-20UP, Hamamatsu, Shizuoka, Japan) system are incorporated on the bottom of the device to allow for observation of the laser spot and alignment of the device (Fig. 6.10).

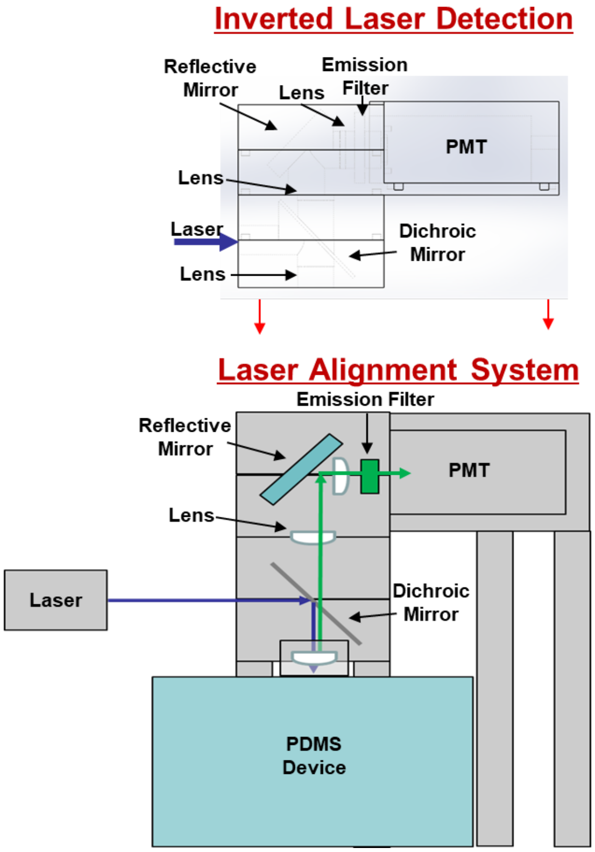

Figure 6.10 Design of an inverted optical housing system to excite the Poly-chip from the top, and laser alignment system for optimal detection, observation, and sorting.

6.2.6.1. Device-to-laser alignment

Laser alignment is conducted by first designing a new inverted 3D optical housing (Perfactory Ultra, LS600 resin, EnvisonTEC Inc., Dearborn, MI, USA) to align all optics components and excite the sample from the top of the device. An additional 2-piece 3D printed (Perfactory Ultra, LS600 resin, EnvisonTEC Inc., Dearborn, MI, USA) laser-to-optical housing alignment tool is printed to automatically align the laser to the 5-piece inverted optical housing that is dropped into the top of the laser-to-optical housing. The opposing end of the laser-to-optical housing has four holes to mount (UBP2/M, Thorlabs, Inc. Newton, NJ, USA) the entire system to an XYZ-stage (PT1/M (Quantity:2) & MVS010/M, Thorlabs, Inc. Newton, NJ, USA) that is mounted to an adjustable post (PH150/M & TR200/M, Thorlabs, Inc. Newton, NJ, USA). This allows for the laser to always remain aligned to the housing and optics but provides the user the ability to move the laser spot to a desired location. An additional mounting post (PH150/M & TR200/M, Thorlabs, Inc. Newton, NJ, USA) and 3D printed holder is used to stabilize the laser-head but can be freely moved as to not interfere with the XYZ-movement. The bottom optics/camera allows for real-time observation of the device and ensuring optimal positioning of the laser to the detection region (Fig. 6.11).

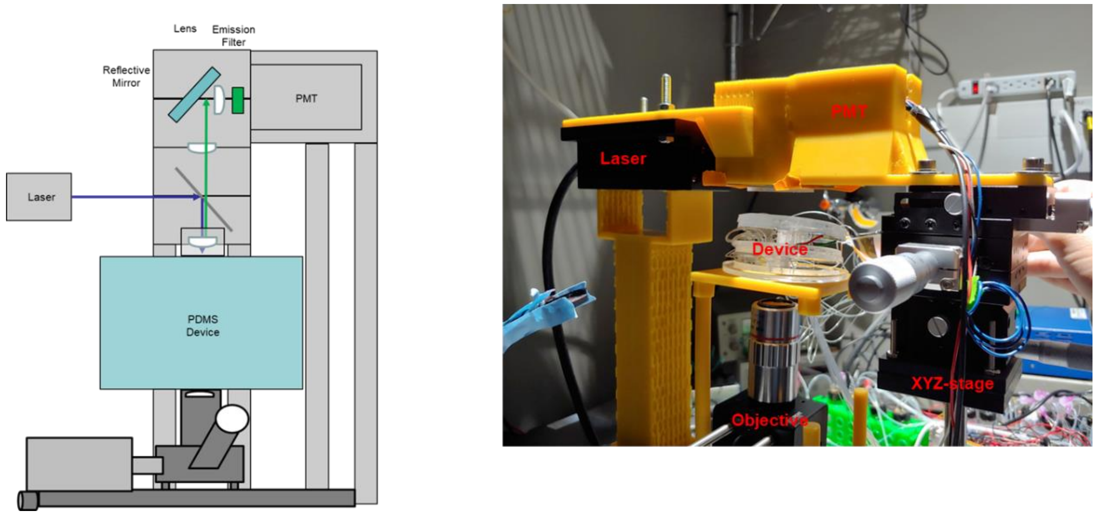

Figure 6.11 Finalized system of XYZ movable stage for laser alignment and highspeed camera observation of the device in real-time.

6.2.6.2. Real-time observation and monitoring of platform

When conducting characterization or operation of the platform, observation of the entire platform (including all layers) at each stage is vital in adequately determining the feasibility of the system. In addition to conducting flow characterization, observation of the device in real-time allows for checking of the device operation during the assay to ensure each of the functionalities are performing as expected. The bottom observation system is comprised of a long-range objective (MY5X-802, Thorlabs, Inc. Newton, NJ, USA), optics, and a highspeed camera (Orca Fusion, C14440-20UP, Hamamatsu, Shizuoka, Japan) capable of focusing through the entire 18-21 layers of the Poly-chip. The objective is coupled to a filter cube (DFM1B/M, Thorlabs, Inc. Newton, NJ, USA) containing a fully reflective mirror (PFR10-P01, Thorlabs, Inc. Newton, NJ, USA), and notch filter (NF488-15, Thorlabs, Inc. Newton, NJ, USA) to protect the camera from the laser line (LRS-0473-PFM-00100-03, Readylaser, Anaheim, CA, USA). Mounting rails (ER8-P4, Thorlabs, Inc. Newton, NJ, USA) are used to couple the filter cube (DFM1T1, Thorlabs, Inc. Newton, NJ, USA) to a lens (AC254-045-A-ML, Thorlabs, Inc. Newton, NJ, USA) and the highspeed camera to perfectly focus the image onto the camera. The camera is mounted (MB1515/M & AP90/M, Thorlabs, Inc. Newton, NJ, USA) to two long-distance XY-stages (TBB1515/M & TBBA1515/M, Thorlabs, Inc. Newton, NJ, USA) and a Z-stage (XR25-YZ/M & XR25-B1/M, Thorlabs, Inc. Newton, NJ, USA) capable of moving the entire bottom objective, optics, and camera system in XYZ-directions for observation of any part of the device. The device is sat on a 3D printed (Perfactory Ultra, LS600 resin, EnvisonTEC Inc., Dearborn, MI, USA) stage with a hollowed center and attachment that is coupled to a an array of mounting post (PH100/M & TR100/M, Thorlabs, Inc. Newton, NJ, USA). Therefore, the device is adjusted to a set height and both the laser and objective systems are capable of moving in the X, Y, and Z directions to allow for ideal adjustment of the laser position and observation of the platform for characterization/validation (Fig. 6.12).

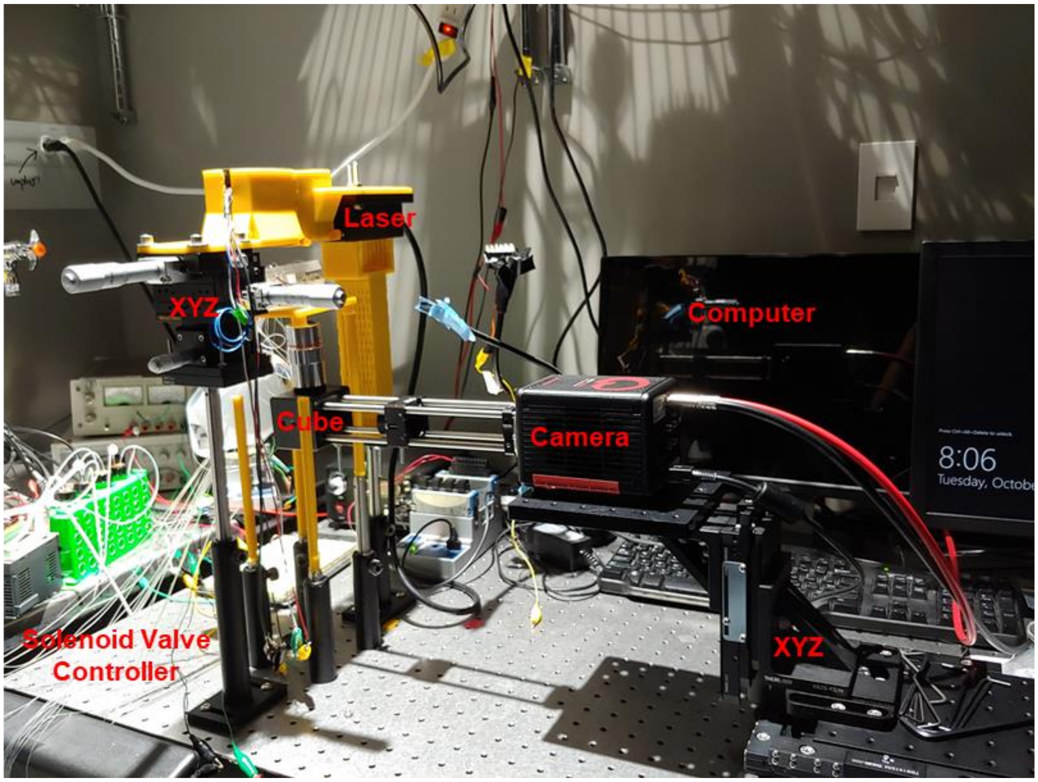

Figure 6.12 Integrated system entailing a microvalve controller system for device operation, laser alignment system, high speed camera observation system, and integrated computer for automated LabView operation.

6.3. LabView controlled graphical user interface for platform

The ability to conduct a complex screening assay with high efficiency and minimal statistical error often requires a standardized operation and protocol that can be conducted in an identical manner repeatedly. Microfluidic lab-on-a-chip platforms have recently gained much interest due to their ability to integrate fluidic control systems or control layers into conventional fluidic devices and allow for maximum controllability of devices in real-time. In addition, with the integration of graphical user interfaces to acquire signals of interest, output desired signals for operation, and control liquid movement in devices, LabView® programs offer the ability to completely control device functionalities in a single executable programing language.

6.3.1. Motivation: LabView GUI

Although most systems have inherent error due to various operations, simple devices usually perform better due to minimal operations and chances of error. Alternatively, complex systems with multiple functionalities and operations often suffer from high error rates that culminate due to series operations compounding errors in previous upstream operations. Considering the integrated Poly-chip system, the complex series functionalities of droplet generation, reflow, spacing, synchronization, merging, cultivation, detection, and sorting integrated into a single chip has an inherent maximum efficiency of 95%. If each of these functionalities are separated into individual chips, the overall efficiency is greatly reduced to less than 80%. Although integration of the functionalities onto one system increases the device performance, human handling of samples being introduced to the system and droplets being collected lead to an increase in the error rate. Therefore, development of an automated fluidic control system, on-the-fly detection interface, on-the-fly sorting system, and on-demand release of “hits” can further reduce the error rate of the platform.

6.3.2. Design: LabView GUI

The graphical interface developed for the droplet microfluidic system entails the control of fluids into and out of the chip using valving structures, acquisition of the fluorescent signal of droplets, thresholding of droplets for sorting, signal generation to initiate an electric field for sorting, and on-demand release of trapped “hits”. The graphic user interface connects through a USB to a microcontroller (DIO-16/16 (USB), Contec®, Osaka, Japan) that controls an array of 16-solenoid valves which control the fluid flow through the chip. All solenoid valves can be independently controlled without interference of other valving operations, allowing for precise control of the microfluidic chip during operation (Fig. 6.13).

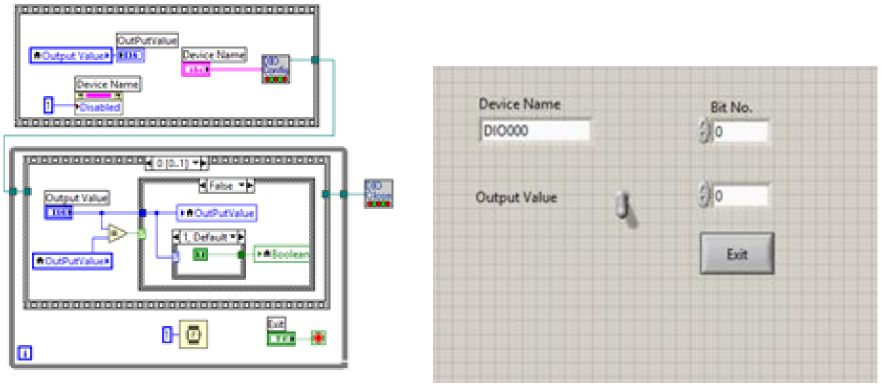

Device Name
DIO000

Bit No.
0

Output Value
0

Figure 6.13 The graphical user interface entails a loop for controlling all valves independently using a LabView system. Subvi provided by Contec®.

6.3.2.1. GUI: Automated device valve operation

The two most common types of control systems require the integration of valving structures that close or open channels on-demand to control the flow of reagents inside microfluidic devices. Normally-open valves are the most common valves where the channel is open at steady state. Vacuum can be incorporated to make sure the valves are fully open, but typically no vacuum is needed as the fluid flow through the channel naturally keeps the valve open. When the desired valve needs to be closed a pressure is typically used to deflect the PDMS membrane between the channel and valve layer and close the microfluidic channel. Although normally-open valves are widely utilized for fluidic control and have much simpler fabrication processes compared to normally-closed valve configurations, fully closing the valve is sometimes difficult leading to leakage of the fluid past the valve. Other rounded channels have previously been reported to help eliminate the issue of leakage, but at high pressures and long device operation leakage is still possible. Alternatively, normally-closed valves have been used to help eliminate leakage inside microfluidic channels, providing more precise control of microfluidic systems. Normally-closed valves are usually comprised of a bottom channel layer with a pillar to physical block the channel from allowing fluid to flow down the corresponding microchannel. Considering that there is a physical break in the channel, a more complex fabrication process is often required for creating normally-closed valving structures. This usually entails a first step of methanol bonding a thin PDMS channel layer to a thick PDMS valve controlling layer using conventional plasma bonding (Plasma cleaner, Harrick Plasma, Ithaca, NY). This allows for precise alignment of the valve and channel layer to ensure the valves actuate the pillar that will physically block the fluidic flow through the device. The resulting two layers must then be treated with oxygen plasma (Plasma cleaner, Harrick Plasma, Ithaca, NY) and actuated during bonding along with post-bonding heat treatment to ensure the blocking pillar does not collapse and seal the channel. Although the fabrication process requires an additional step, the increased integrity of the valve and prevention of leakage provides ideal control of the fluidic system for automated platform operation.

6.3.2.2. GUI: Automated fluorescent detection

Additionally, the graphical user interface entails a real-time waveform display of the fluorescent detected droplet (Fig. 6.14 & 6.15).

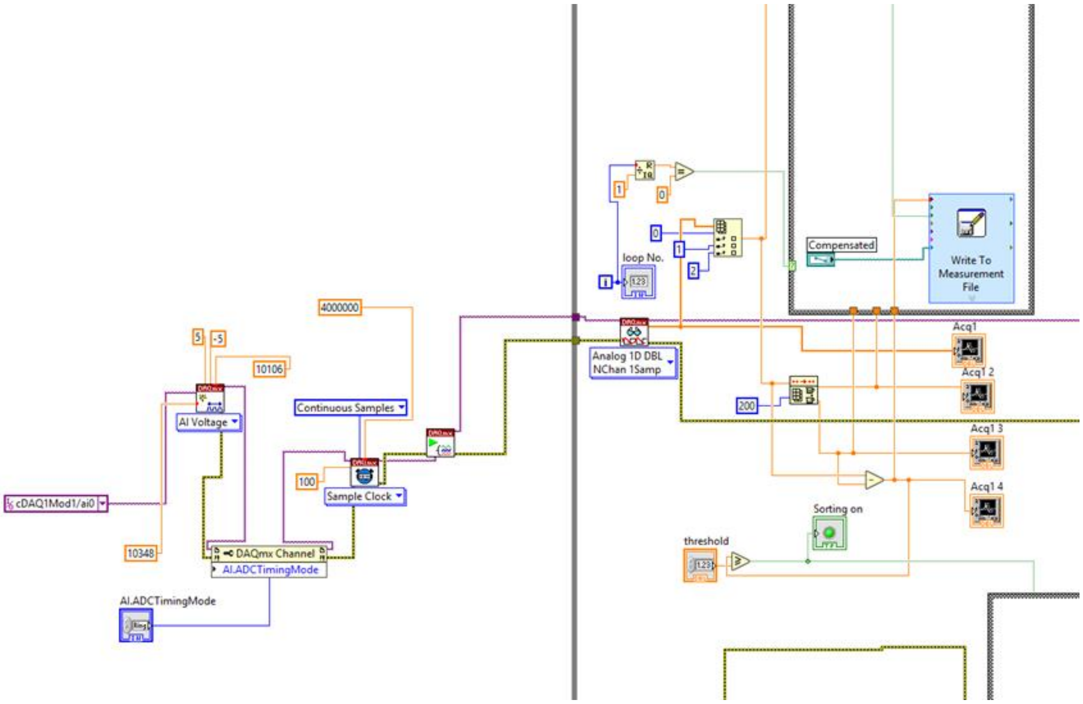

Figure 6.14 A portion of the graphical user interface is used to acquire the PMT output voltage from the detector and plot the resulting peaks in real-time.

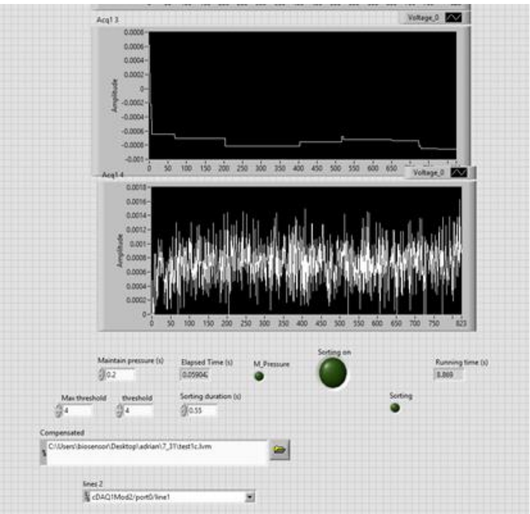

Maintain pressure (s) 0.2

Elapsed Time (s) 0.05904

Running time (s) 0.869

Max threshold 4

threshold 4

Sorting duration (s) 0.55

Compensated C:\Users\biosensor\Desktop\adrian\7_31\test1c.lvm

lines 2 cDAQ1Mod2/port0/line1

Figure 6.15 A portion of the front panel of the graphical user interface.

6.3.2.3. GUI: Automated droplet sorting

This signal is then compared to a set threshold value and when the desired (low fluorescence, or high fluorescence) signal is attained, a case-loop with a sequence-loop inside, with a set delay time generates a signal to be relayed to the high voltage amplifier (Trek 2200, Trek Inc., Lockport, NY, USA) for sorting (Fig. 6.16).

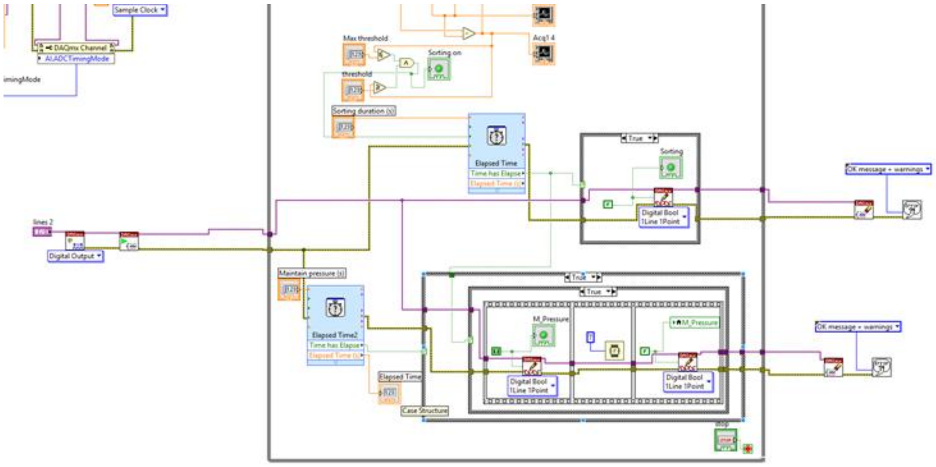

Figure 6.16 A final case-loop is used to generate a signal for droplet sorting.

6.3.3. Operation: LabView GUI

The overall operation and integration of the system is comprised of a network of instruments connected in such a way that real-time detection, monitoring, sorting, and control can be conducted simultaneously without adverse effects on other functionalities. The device fluid control system utilizes 16 (or more) solenoid valves (sy114-6lz, Purvis Industries, Dallas, TX, USA) each powered by the same 12 V DC power supply (237-1301-ND, Digi-Key, Thief River Falls, MN, USA), with the grounded terminal of the power supply connecting to the microcontroller (DIO-16/16 (USB), Contec®, Osaka, Japan). This provides a 0 or 12 V signal to actuate the solenoid valve in an off/on manner allowing for pressure or vacuum, respectively. Each of the solenoid valves are connected to a manifold (SS3Y1-S41-16-M3, Purvis Industries, Dallas, TX, USA) that integrates pressure and vacuum from a single pressure/vacuum pump (UX-79204-20, Cole Palmer, Vernon Hills, IL, USA). The pump output pressure and vacuum are each connected to their own manual regulators (4ZM08 & 30J548, Grainger, Lake Forest, IL, USA) with a gauge through vacuum tubing (63013-763, VWR, Radnor, PA, USA) and connectors (KQ2H07-32A, Purvis Industries, Dallas, TX, USA). The pressure is set to 10 psi while the vacuum is set to 40 mmHg to apply adequate pressure to close the corresponding microfluidic valves. Higher pressures over 20 psi often lead to device issues with the membrane tearing or valves bulging, so for the Poly-chip system 10-15 psi was used. Each of the solenoid valve outputs (sy110-77-1A, Purvis Industries, Dallas, TX, USA) are connected to their respective sealed vials (VSC-2/12, Shandong, China, Amazon, Seattle, WA, USA) using soft silicon tubing (HelixMark®, 32829-180, VWR, Radnor, PA, USA) coupled to FEP tubing (21511-376, VWR, Radnor, PA, USA). The inlet FEP tubing is terminated at the top of the vial while the outlet FEP tubing is terminated at the bottom of the vial. Each of the inlet and outlets are sealed with epoxy glue (4200101, Home Depot, Atlanta, GA, USA) to create a completely closed system that serves as a pressure driven system for controlling the system with water pressurized valves. Filling the valves with water eliminates air bubble formation in the channel which often occurs when using air pressurized valves that leak air through the valve membrane. The outlet FEP tubing of each vial is then connected to a leur-lock to barb connector (P-850x, IDEX Health & Science, LLC Rochester, NY, USA), needle (EA30S-1/2, Techcon™, Cypress, CA, USA), and Tygon® tubing (AAD04091, Saint Gobain, Courbevoie, France) that connects directly to the Poly-chip device. This essentially allows for complete control of the microfluidic flow inside the platform using a comprehensive graphical interface that combines device control, real-time detection, and on-the-fly automated droplet sorting.

6.3.4. Laser-based signal acquisition

The PMT-based detection system uses 2 triple output power supplies (E3030A, Agilent, Santa Clara, CA, USA) to provide adjustable voltage settings for the electronic circuit and PMT. A 5 V DC output is used to power the PMT module and the same 5 V DC output is used to power the amplifier (OPA350PA, National Instruments, Austin, TX, USA) for the amplification circuit. The ground (0 V DC) of the power supply connects to the respective grounding terminal pin for the amplifier and the grounding terminal for the PMT. Lastly, a .6-.9 V DC output is used to control the gain of the PMT and allows for precise tuning of the signal to maximize the possible resolution of the detected fluorescent signal. The amplification circuit also entails a 1 kOhm resistor with one end connected to the input terminal for the PMT signal and the other end connected to the output terminal of the amplifier circuit. The final amplified output signal and corresponding ground are connected to a DAQ module (NI9219 DAQ, National Instruments, Austin, TX, USA) that is USB connected to a desktop computer (Dell Precision 3630 Desktop, Dell, Round Rock, TX, USA) to be interfaced with LabView®.

6.3.5. Real-time monitoring

Integration of the laser-alignment and highspeed camera observation system also allows for the integration of the camera output video directly into LabView®. A set of LabView® based drivers and subvi’s provided by Hamamatsu allow for the integration of the camera video into the desired graphical user interface program. This allows for the capturing of real-time highspeed video of the device and various functionalities, such as droplet detection, so that the performance of the detection and sorting can be confirmed visually during operation. Furthermore, this makes characterization of the system much simpler, as all of the functional manipulation techniques and device performance can be monitored using a single graphical user interface.

6.3.6. Automated droplet sorting

Considering droplet sorting, a 5 V trigger signal is output from a DAQ unit (USB-6341 DAQ, National Instruments, Austin, TX, USA) to a function generator which is set to output a 10 kHz square wave to a high voltage amplifier. The output of the function generator (DG1022Z, Rigol Technologies, Beijing, China) is connected to the input of a high voltage amplifier (Trek 2200, Trek Inc., Lockport, NY, USA) which is then connected to the positive and ground terminals of the device electrodes. This allows for automated generation of an electric field at the precise moment when the desired droplet needs to be deflected to the collection channel. The droplet merging function is conducted in a similar manner but with the electric field being continuously generated (Fig. 6.17).

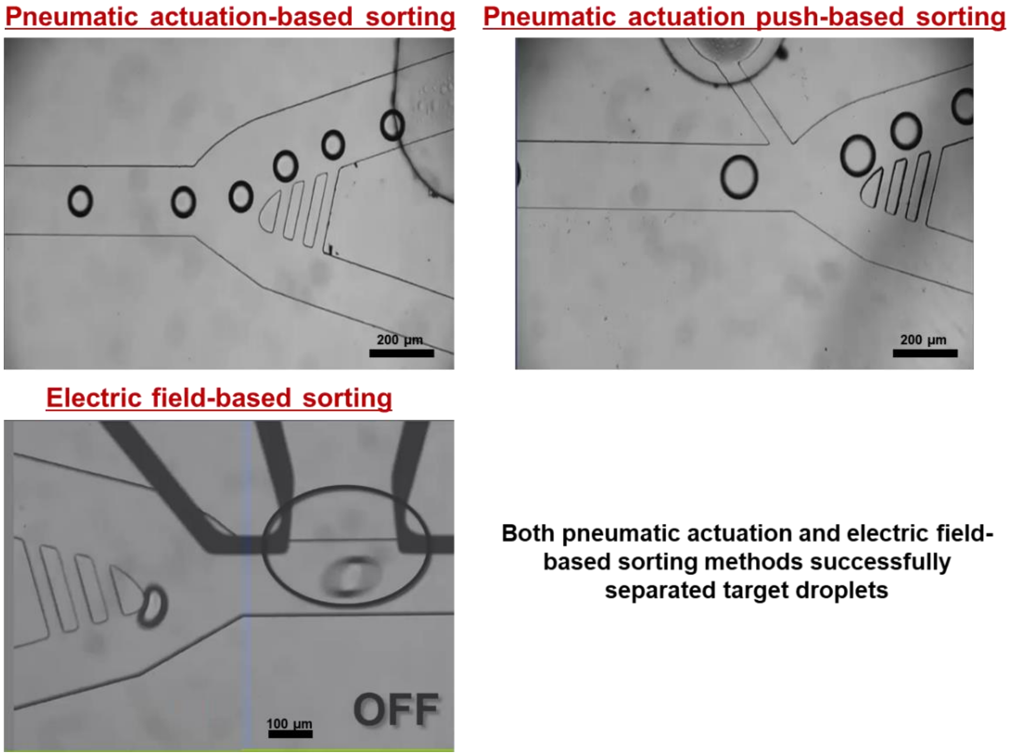

Both pneumatic actuation and electric field-based sorting methods successfully separated target droplets

Figure 6.17 Micrograph images of three different droplet sorting techniques using push valve sorting, oil push sorting, and electric field-based sorting.

6.4. Fully-integrated Poly-chip platform characterization

The finalized fully-integrated Poly-chip platform is characterized by conducting repeated experiments of droplet generation, culture chamber filling, controlled reflow, controlled spacing, secondary droplet generation, synchronization of paired droplets, merging, co-cultivation, secondary reflow, on-the-fly detection, sorting of “hits”, trapping of “hits”, and reflow of “hits” for post-processing.

When conducting the characterization of the fully-integrated Poly-chip system, debris material can have a significant impact on the functionality of the system. A single piece of debris can completely ruin the device operation and therefore we have employed a few steps to minimize the effect of debris and clogging. First, inline fluidic PFTE syringe filters (422, Acrodisc®, Pall Laboratory, Port Washington, NY, USA) are utilized for all of the oil inlets to prevent the introduction of debris into the tubing and device. Second, pillar-based fluidic filters are introduced into each of the oil and aqueous inlets to prevent debris from entering into the small fluidic channels (Fig. 6.18).

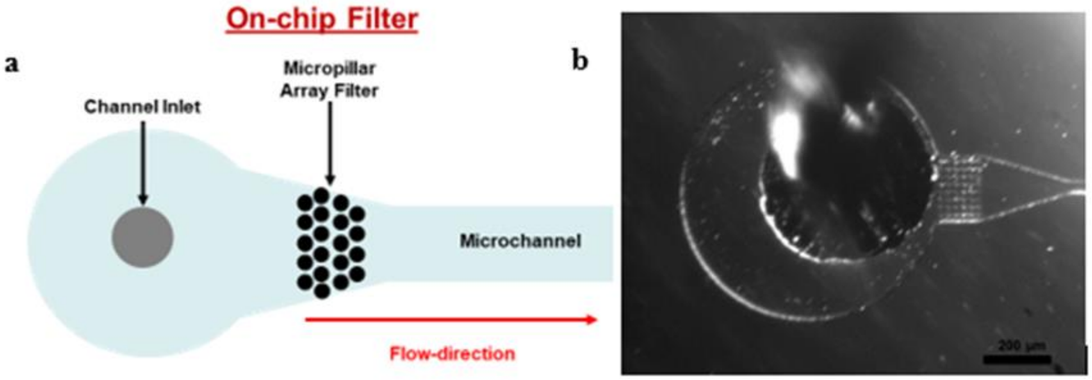

Figure 6.18 (a) Illustration of the design of on-chip pillar-based filters for capturing debris or cell clumps and prevent device clogging. (b) Micrograph image of the on-chip syringe filter.

Finally, a reservoir system is designed to buffer the outlet of droplets/oil exiting the device which rapidly evaporates and clogs the outlet of the device. Each outlet tubing is terminated at the bottom of a sealed centrifuge tube and a secondary tubing starting at the bottom of the tube releases oil. This allows for excess droplets to float to the top of the reservoir and collect while pressurized oil exits from the bottom of the chamber to an adjacent open reservoir (Fig. 6.19).

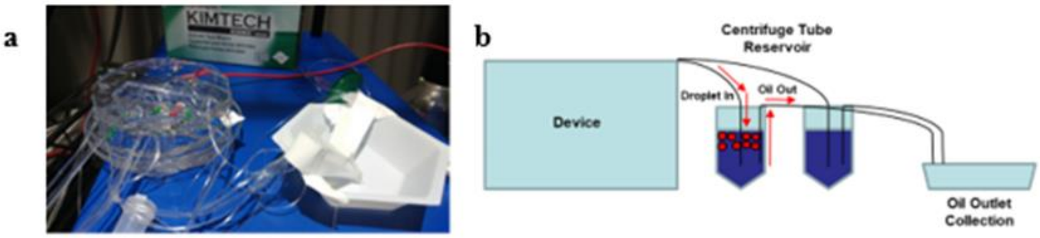

Figure 6.19 (a) Image of actual Poly-chip device and reservoir system, and (b) illustration of the reservoir system and operation to prevent device outlet clogging/evaporation.

With the integration of valves in the system, the first half of the platform can function separately form the second half of the system, allowing the characterization of the front half and back half of the system separately. The front half of the system is first characterized by generating the appropriate size environmental droplets using a flow speed of 20 μL h^{-1} and 70 μL h^{-1} for the water and oil, respectively. This generates droplets at a rate of 10 droplets s^{-1}, which will be the droplet manipulation speed for the entire system to ensure identical culture durations for all samples. After droplets have filled the large-vertical first-in first-out culture chamber, secondary droplets are allowed to generate in the synchronization/merging layer to allow for stabilization of the inlet flows to the second layer (this is also true for the oil spacing inlet of reflowed environmental droplets prior to synchronization). The flow rate of the droplet spacer is 70 μL h^{-1} with a reflow rate of 20 μL h^{-1} for environmental samples from the first culture chamber. Secondary droplets are generated using a flow rate of 20 μL h^{-1} and 73 μL h^{-1} for the water and oil, respectively. Synchronization and merging are characterized using a highspeed camera (Orca Fusion, C14440-20UP, Hamamatsu, Shizuoka, Japan) and frame-by-frame analysis is conducted as described previously. The electric field input voltage is optimized to 200 V which ensures all droplets in the electric field region merge at a high efficiency. After co-cultivation of droplets in the second set of staggered chamber, droplets are then reflowed with a reflow rate of 40 μL h^{-1} and spacing oil flow rate of 140 μL h^{-1} to ensure the flow rate and speed of droplets are identical to previous generation/merging operations of 10 droplets s^{-1}. A set distance of 2 mm separates the detection and sorting region and a corresponding delay time of 200 ms is utilized to account for the delay in droplets traveling from the detection region to the sorting region. A droplet sorting duration of 50 ms is used to sort the droplet of interest but allow for dissipation of the electric field before the next droplet enters the sorting region. The electric field voltage utilized for droplet sorting is optimized to 300 V to ensure all droplets that are expected to be sorted are deflected to the desired collected channel. After automated basket trapping of “hit”, droplets are flowed at a rate of 20 μL h^{-1} with a spacing oil flow rate of 800 μL h^{-1} to ensure all droplets have significant spacing for agar plating and each colony corresponds to one droplet “hit”.

7. FUTURE WORK: MOCK-SCREENING OF ENVIRONMENTAL ISOLATE AND YEAST

7.1. Mock screening using low concentration GFP-yeast

A mock-screening of the entire Poly-chip system is used as a proof-of-concept model to demonstrate the functionality of the system and validate its performance as a fully characterized and integrated system for polymicrobial interaction studies and drug discovery. A basic mock screening will first be conducted using only GFP-yeast that are encapsulated at a low cell number, ensuring most droplets have 0 or 1-2 cells. When conducting the assay, the resulting system should produce droplets with 0 cells or 20-30 cells which can be easily distinguished using the on-the-fly detection system and can be sorted to ascertain the overall platform performance. A corresponding Z-score will be calculated and demonstrate the platforms ability to conduct high efficiency screening assays.

7.2. Mock screening using a known anti-fungal producing cell strain

Additionally, a similar mock-screening will be conducted using a low concentration encapsulation of a known anti-fungal strain (*PK*) resulting in a population of empty or antifungal drug droplets. Environmental droplet will be cultivated for 2 h to accrue toxin, reflowed, synchronized with GFP- yeast droplets containing 5 buds, and merged for co-cultivation. After co-cultivation, droplets will be reflowed through the detection/sorting functions and the resulting sorting efficiency will be calculated to obtain a final Z-score of the system. Three repeats of this experiment will be conducted to ensure the full characterization of the system and flow rates, delay times, and actuation times will be adjusted if necessary.

8. CONCLUSIONS

With the continual emergence of resistant strains of bacteria/fungi and pathogens, combined with the decline of clinically useful antimicrobials/antifungals, the need for a low-cost comprehensive screening system to revitalize the drug discovery industry is paramount. Here we conducted an in-depth study and investigation into various functionalities and methods for conducting droplet generation, droplet incubation, droplet synchronization, droplet merging, droplet detection, and droplet sorting. Utilizing the most ideal method for conducting each of these functionalities with a high efficiency and integrating these functions into a single fully-integrated automate on-chip screening system we have drastically reduced the error rate that has prevented the success of integrated droplet microfluidic systems. In addition, integrating a programmable automated control system has allowed for the precise characterization of the Poly-chip screening platform to be utilized for a variety of screening-based applications. This system marks the first truly fully-integrated automated lab-on-a-chip microfluidic droplet-based screening platform capable of performing all operations at an efficiency of 95% or greater. The development, fabrication, and methods for characterizing the Poly-chip system can be considered a milestone achievement in the development of complex integrated droplet microfluidic screening systems. With this platform we hope to set the groundwork for future more complex assay to be integrated into fully-functional comprehensive lab-on-a-chip systems, paving the way for droplet microfluidics to revolutionize drug discovery, cell-cell interaction studies, and molecule investigations.

REFERENCES

1. A. L. Demain, *Nature Biotechnology*, 2002, **20**, 331.
2. W. Sneader, *Drug Discovery: A History*, John Wiley & Sons, 2005.
3. A. Bryskier, *Antimicrobial Agents: Antibacterials and Antifungals*, ASM press, 2005.
4. A. Coates, Y. Hu, R. Bax and C. Page, *Nature Reviews Drug Discovery*, 2002, **1**, 895.
5. D. J. Payne, M. N. Gwynn, D. J. Holmes and D. L. Pompliano, *Nature Reviews Drug Discovery*, 2007, **6**, 29.
6. A. Banerjee, E. Dubnau, A. Quemard, V. Balasubramanian, K. S. Um, T. Wilson, D. Collins, G. de Lisle and W. R. Jacobs, *Science*, 1994, **263**, 227-230.
7. K. Lewis, *Nature Reviews Drug Discovery*, 2013, **12**, 371.
8. C. A. Lipinski, F. Lombardo, B. W. Dominy and P. J. Feeney, *Advanced Drug Delivery Reviews*, 1997, **23**, 3-25.
9. R. O'Shea and H. E. Moser, *Journal of Medicinal Chemistry*, 2008, **51**, 2871-2878.
10. R. S. Bohacek, C. McMartin and W. C. Guida, *Medicinal Research Reviews*, 1996, **16**, 3-50.
11. W. Y. Edward, G. McDermott, H. I. Zgurskaya, H. Nikaido and D. E. Koshland, *Science*, 2003, **300**, 976-980.
12. J. H. Rex, B. I. Eisenstein, J. Alder, M. Goldberger, R. Meyer, A. Dane, I. Friedland, C. Knirsch, W. R. Sanhai and J. Tomayko, *The Lancet Infectious Diseases*, 2013, **13**, 269-275.
13. R. A. Dixon, *Nature*, 2001, **411**, 843.
14. S. H. Gillespie, *Antimicrobial Agents and Chemotherapy*, 2002, **46**, 267-274.
15. P.-C. Hsieh, S. A. Siegel, B. Rogers, D. Davis and K. Lewis, *Proceedings of the National Academy of Sciences*, 1998, **95**, 6602-6606.
16. C. Walsh, *Antibiotics: Actions, Origins, Resistance*, American Society for Microbiology (ASM), 2003.
17. T. E. Renau, R. Léger, E. M. Flamme, J. Sangalang, M. W. She, R. Yen, C. L. Gannon, D. Griffith, S. Chamberland and O. Lomovskaya, *Journal of Medicinal Chemistry*, 1999, **42**, 4928-4931.
18. I. B. Seiple, Z. Zhang, P. Jakubec, A. Langlois-Mercier, P. M. Wright, D. T. Hog, K. Yabu, S. R. Allu, T. Fukuzaki, P. N. Carlsen, Y. Kitamura, X. Zhou, M. L. Condakes, F. T. Szczypiński, W. D. Green and A. G. Myers, *Nature*, 2016, **533**, 338.
19. J. Wang, S. M. Soisson, K. Young, W. Shoop, S. Kodali, A. Galgoci, R. Painter, G. Parthasarathy, Y. S. Tang and R. Cummings, *Nature*, 2006, **441**, 358.
20. J. Clardy, M. A. Fischbach and C. T. Walsh, *Nature Biotechnology*, 2006, **24**, 1541-1550.
21. F. García-Olmedo, A. Molina, J. M. Alamillo and P. Rodríguez-Palenzuéla, *Peptide Science*, 1998, **47**, 479-491.
22. K. Lewis and F. M. Ausubel, *Nature Biotechnology*, 2006, **24**, 1504-1507.

23. L. L. Silver, *Expert Opinion on Drug Discovery*, 2008, **3**, 487-500.
24. M. N. Alekshun and S. B. Levy, *Cell*, 2007, **128**, 1037-1050.
25. P. E. Almeida Da Silva and J. C. Palomino, *Journal of Antimicrobial Chemotherapy*, 2011, **66**, 1417-1430.
26. H. W. Boucher, G. H. Talbot, J. S. Bradley, J. E. Edwards, D. Gilbert, L. B. Rice, M. Scheld, B. Spellberg and J. Bartlett, *Clinical Infectious Diseases*, 2009, **48**, 1-12.
27. E. R. Choffnes, D. A. Relman and A. Mack, *Antibiotic Resistance: Implications for Global Health and Novel Intervention Strategies. Workshop Summary*, National Academies Press, Washington, 2010.
28. A. G. Fleming, *Canadian Medical Association Journal*, 1929, **20**, 11.
29. A. Schatz, E. Bugle and S. A. Waksman, *Proceedings of the Society for Experimental Biology and Medicine*, 1944, **55**, 66-69.
30. W. D. Bellamy and J. W. Klimek, *Journal of Bacteriology*, 1948, **55**, 153.
31. G. M. Eliopoulos, S. Willey, E. Reiszner, P. Spitzer, G. Caputo and R. Moellering, *Antimicrobial Agents and Chemotherapy*, 1986, **30**, 532-535.
32. N. Q. Balaban, J. Merrin, R. Chait, L. Kowalik and S. Leibler, *Science*, 2004, **305**, 1622-1625.
33. M. A. Fischbach and C. T. Walsh, *Science*, 2009, **325**, 1089-1093.
34. B. R. Levin and D. E. Rozen, *Nature Reviews Microbiology*, 2006, **4**, 556.
35. K. Andries, P. Verhasselt, J. Guillemont, H. W. Göhlmann, J.-M. Neefs, H. Winkler, J. Van Gestel, P. Timmerman, M. Zhu and E. Lee, *Science*, 2005, **307**, 223-227.
36. A. H. Diacon, A. Pym, M. Grobusch, R. Patientia, R. Rustomjee, L. Page-Shipp, C. Pistorius, R. Krause, M. Bogoshi and G. Churchyard, *New England Journal of Medicine*, 2009, **360**, 2397-2405.
37. O. Lomovskaya, M. S. Warren, A. Lee, J. Galazzo, R. Fronko, M. Lee, J. Blais, D. Cho, S. Chamberland and T. Renau, *Antimicrobial Agents and Chemotherapy*, 2001, **45**, 105-116.
38. R. Nakashima, K. Sakurai, S. Yamasaki, K. Nishino and A. Yamaguchi, *Nature*, 2011, **480**, 565-569.
39. M. F. Symmons, E. Bokma, E. Koronakis, C. Hughes and V. Koronakis, *Proceedings of the National Academy of Sciences*, 2009, **106**, 7173-7178.
40. O. Genilloud, *Antonie van Leeuwenhoek*, 2014, **106**, 173-188.
41. H.-G. Sahl and G. Bierbaum, *Annual Reviews in Microbiology*, 1998, **52**, 41-79.
42. S. Gibbons, *Natural Product Reports*, 2004, **21**, 263-277.
43. F. R. Stermitz, P. Lorenz, J. N. Tawara, L. A. Zenewicz and K. Lewis, *Proceedings of the National Academy of Sciences*, 2000, **97**, 1433-1437.
44. M. S. Rappé and S. J. Giovannoni, *Annual Reviews in Microbiology*, 2003, **57**, 369-394.
45. K. Seow, G. Meurer, M. Gerlitz, E. Wendt-Pienkowski, C. R. Hutchinson and J. Davies, *Journal of Bacteriology*, 1997, **179**, 7360-7368.
46. A. D'Onofrio, J. M. Crawford, E. J. Stewart, K. Witt, E. Gavrish, S. Epstein, J. Clardy and K. Lewis, *Chemistry & Biology*, 2010, **17**, 254-264.

47. J. J. Irwin, *Current Protocols in Bioinformatics*, 2008, **22**, 14.16. 11-14.16. 23.
48. M. Elliott, A. W. Farnham, N. F. Janes, D. M. Johnson and D. A. Pulman, *Pesticide Science*, 1987, **18**, 191-201.
49. S. Mirzoeva, A. Sawkar, M. Zasadzki, L. Guo, A. V. Velentza, V. Dunlap, J.-J. Bourguignon, H. Ramstrom, J. Haiech, L. J. Van Eldik and D. M. Watterson, *Journal of Medicinal Chemistry*, 2002, **45**, 563-566.
50. S. L. Schreiber, *Science*, 2000, **287**, 1964-1969.
51. O. E. Beske and S. Goldbard, *Drug Discovery Today,* 2002, **7**, S131-S135.
52. Z. Hua, J. L. Rouse, A. E. Eckhardt, V. Srinivasan, V. K. Pamula, W. A. Schell, J. L. Benton, T. G. Mitchell and M. G. Pollack, *Analytical Chemistry*, 2010, **82**, 2310-2316.
53. U. B. Nielsen and B. H. Geierstanger, *Journal of Immunological Methods*, 2004, **290**, 107-120.
54. D. L. Taylor and K. A. Giuliano, *Drug Discovery Today: Technologies*, 2005, **2**, 149-154.
55. A. S. Basu and Y. B. Gianchandani, *Journal of Micromechanics and Microengineering*, 2008, **18**, 115031.
56. E. Gavrish, A. Bollmann, S. Epstein and K. Lewis, *Journal of Microbiological Methods*, 2008, **72**, 257-262.
57. H. S. Kim, T. P. Devarenne and A. Han, *Lab on a Chip*, 2015, **15**, 2467-2475.
58. H. S. Kim, T. L. Weiss, H. R. Thapa, T. P. Devarenne and A. Han, *Lab on a Chip*, 2014, **14**, 1415-1425.
59. B. L. Wang, A. Ghaderi, H. Zhou, J. Agresti, D. A. Weitz, G. R. Fink and G. Stephanopoulos, *Nature Biotechnology*, 2014, **32**, 473.
60. D. Nichols, N. Cahoon, E. Trakhtenberg, L. Pham, A. Mehta, A. Belanger, T. Kanigan, K. Lewis and S. Epstein, *Applied Environmental Microbiology*, 2010, **76**, 2445-2450.
61. E. Brouzes, M. Medkova, N. Savenelli, D. Marran, M. Twardowski, J. B. Hutchison, J. M. Rothberg, D. R. Link, N. Perrimon and M. L. Samuels, *Proceedings of the National Academy of Sciences*, 2009, **106**, 14195-14200.
62. B. El Debs, R. Utharala, I. V. Balyasnikova, A. D. Griffiths and C. A. Merten, *Proceedings of the National Academy of Sciences*, 2012, **109**, 11570-11575.
63. A. Huebner, M. Srisa-Art, D. Holt, C. Abell, F. Hollfelder and J. Edel, *Chemical Communications*, 2007, 1218-1220.
64. R. M. Schoeman, E. W. Kemna, F. Wolbers and A. van den Berg, *Electrophoresis*, 2014, **35**, 385-392.
65. L. M. Fidalgo, G. Whyte, B. T. Ruotolo, J. L. Benesch, F. Stengel, C. Abell, C. V. Robinson and W. T. Huck, *Angewandte Chemie International Edition*, 2009, **48**, 3665-3668.
66. W.-H. Tan and S. Takeuchi, *Lab on a Chip*, 2006, **6**, 757-763.
67. D. Bardin, M. R. Kendall, P. A. Dayton and A. P. Lee, *Biomicrofluidics*, 2013, **7**, 034112.
68. X. Leng, W. Zhang, C. Wang, L. Cui and C. J. Yang, *Lab on a Chip*, 2010, **10**, 2841-2843.

69. J. Park, A. Kerner, M. A. Burns and X. N. Lin, *PloS One*, 2011, **6**, e17019.
70. J. J. Agresti, E. Antipov, A. R. Abate, K. Ahn, A. C. Rowat, J.-C. Baret, M. Marquez, A. M. Klibanov, A. D. Griffiths and D. A. Weitz, *Proceedings of the National Academy of Sciences*, 2010, DOI: 10.1073/pnas.0910781107.
71. S. Cho, D.-K. Kang, S. Sim, F. Geier, J.-Y. Kim, X. Niu, J. B. Edel, S.-I. Chang, R. C. R. Wootton, K. S. Elvira and A. J. deMello, *Analytical Chemistry*, 2013, **85**, 8866-8872.
72. K. Churski, T. S. Kaminski, S. Jakiela, W. Kamysz, W. Baranska-Rybak, D. B. Weibel and P. Garstecki, *Lab on a Chip*, 2012, **12**, 1629-1637.
73. K. Churski, P. Korczyk and P. Garstecki, *Lab on a Chip*, 2010, **10**, 816-818.
74. J. Clausell-Tormos, D. Lieber, J.-C. Baret, A. El-Harrak, O. J. Miller, L. Frenz, J. Blouwolff, K. J. Humphry, S. Köster and H. Duan, *Chemistry & Biology*, 2008, **15**, 427-437.
75. L. Granieri, J.-C. Baret, A. D. Griffiths and C. A. Merten, *Chemistry & Biology*, 2010, **17**, 229-235.
76. R. Ostafe, R. Prodanovic, W. Lloyd Ung, D. A. Weitz and R. Fischer, *Biomicrofluidics*, 2014, **8**, 041102.
77. T. C. Scanlon, S. M. Dostal and K. E. Griswold, *Biotechnology and Bioengineering*, 2014, **111**, 232-243.
78. Y.-C. Tan, V. Cristini and A. P. Lee, *Sensors and Actuators B: Chemical*, 2006, **114**, 350-356.
79. V. Trivedi, A. Doshi, G. K. Kurup, E. Ereifej, P. J. Vandevord and A. S. Basu, *Lab on a Chip*, 2010, **10**, 2433-2442.
80. S. Xu, Z. Nie, M. Seo, P. Lewis, E. Kumacheva, H. A. Stone, P. Garstecki, D. B. Weibel, I. Gitlin and G. M. Whitesides, *Angewandte Chemie International Edition*, 2005, **44**, 724-728.
81. S. C. C. Shih, N. S. Mufti, M. D. Chamberlain, J. Kim and A. R. Wheeler, *Energy & Environmental Science*, 2014, **7**, 2366-2375.
82. S. L. Sjostrom, Y. Bai, M. Huang, Z. Liu, J. Nielsen, H. N. Joensson and H. Andersson Svahn, *Lab on a Chip*, 2014, **14**, 806-813.
83. C. N. Baroud, F. Gallaire and R. Dangla, *Lab on a Chip*, 2010, **10**, 2032-2045.
84. A. Huebner, S. Sharma, M. Srisa-Art, F. Hollfelder, J. B. Edel and A. J. Demello, *Lab on a Chip*, 2008, **8**, 1244-1254.
85. R. Seemann, M. Brinkmann, T. Pfohl and S. Herminghaus, *Reports on Progress in Physics*, 2011, **75**, 016601.
86. A. R. Abate, T. Hung, P. Mary, J. J. Agresti and D. A. Weitz, *Proceedings of the National Academy of Sciences*, 2010, DOI: 10.1073/pnas.1006888107.
87. K. Ahn, J. Agresti, H. Chong, M. Marquez and D. A. Weitz, *Applied Physics Letters*, 2006, **88**, 264105.
88. M. Chabert, K. D. Dorfman and J. L. Viovy, *Electrophoresis*, 2005, **26**, 3706-3715.
89. C. Priest, S. Herminghaus and R. Seemann, *Applied Physics Letters*, 2006, **89**, 134101.
90. M. Zagnoni and J. M. Cooper, *Lab on a Chip*, 2009, **9**, 2652-2658.

91. M. Zagnoni, G. Le Lain and J. M. Cooper, *Langmuir*, 2010, **26**, 14443-14449.
92. J.-C. Baret, O. J. Miller, V. Taly, M. Ryckelynck, A. El-Harrak, L. Frenz, C. Rick, M. L. Samuels, J. B. Hutchison and J. J. Agresti, *Lab on a Chip*, 2009, **9**, 1850-1858.
93. Z. Cao, F. Chen, N. Bao, H. He, P. Xu, S. Jana, S. Jung, H. Lian and C. Lu, *Lab on a Chip*, 2013, **13**, 171-178.
94. M. T. Guo, A. Rotem, J. A. Heyman and D. A. Weitz, *Lab on a Chip*, 2012, **12**, 2146-2155.
95. L. Mazutis, J.-C. Baret, P. Treacy, Y. Skhiri, A. F. Araghi, M. Ryckelynck, V. Taly and A. D. Griffiths, *Lab on a Chip*, 2009, **9**, 2902-2908.
96. R. Ostafe, R. Prodanovic, W. L. Ung, D. A. Weitz and R. Fischer, *Biomicrofluidics*, 2014, **8**, 041102.
97. S.-Y. Teh, R. Lin, L.-H. Hung and A. P. Lee, *Lab on a Chip*, 2008, **8**, 198-220.
98. N. Bremond, H. Doméjean and J. Bibette, *Physical Review Letters*, 2011, **106**, 214502.
99. N. Bremond, A. R. Thiam and J. Bibette, *Physical Review Letters*, 2008, **100**, 024501.
100. G. F. Christopher, J. Bergstein, N. B. End, M. Poon, C. Nguyen and S. L. Anna, *Lab on a Chip*, 2009, **9**, 1102-1109.
101. M. Mohammadi, S. Shahhosseini and M. Bayat, *Chemical Engineering & Technology*, 2014, **37**, 27-35.
102. A. Lai, N. Bremond and H. A. Stone, *Journal of Fluid Mechanics*, 2009, **632**, 97-107.
103. Y.-C. Tan, Y. L. Ho and A. P. Lee, *Microfluidics and Nanofluidics*, 2007, **3**, 495-499.
104. A. R. Guzman, H. S. Kim, P. de Figueiredo and A. Han, *Biomedical Microdevices*, 2015, **17**, 35.
105. A. Guzman, *The Development of a High-throughput Microdroplet Bioreactor Device for Microbial Studies*, Texas A&M University Libraries, 2012, 87.
106. O. Pulz and W. Gross, *Applied Microbiology and Biotechnology*, 2004, **65**, 635-648.
107. P. Spolaore, C. Joannis-Cassan, E. Duran and A. Isambert, *Journal of Bioscience and Bioengineering*, 2006, **101**, 87-96.
108. S.-F. Han, W.-B. Jin, R.-J. Tu and W.-M. Wu, *Critical Reviews in Biotechnology*, 2015, **35**, 255-268.
109. T. M. Mata, A. A. Martins and N. S. Caetano, *Renewable and Sustainable Energy Reviews*, 2010, **14**, 217-232.
110. A. Ghosh, S. Khanra, M. Mondal, G. Halder, O. Tiwari, S. Saini, T. K. Bhowmick and K. Gayen, *Energy Conversion and Management*, 2016, **113**, 104-118.
111. M. Hlavova, Z. Turoczy and K. Bisova, *Biotechnology Advances*, 2015, **33**, 1194-1203.
112. A. Dewan, J. Kim, R. H. McLean, S. A. Vanapalli and M. N. Karim, *Biotechnology and Bioengineering*, 2012, **109**, 2987-2996.

113. H. S. Kim, S. C. Hsu, S. I. Han, H. R. Thapa, A. R. Guzman, D. R. Browne, M. Tatli, T. P. Devarenne, D. B. Stern and A. Han, *Plant Direct*, 2017, **1**, e00011.
114. H. S. Kim, A. R. Guzman, H. R. Thapa, T. P. Devarenne and A. Han, *Biotechnology and bioengineering*, 2016, **113**, 1691-1701.
115. B. Ahn, K. Lee, H. Lee, R. Panchapakesan and K. W. Oh, *Lab on a Chip*, 2011, **11**, 3956-3962.
116. L. Mazutis, J. Gilbert, W. L. Ung, D. A. Weitz, A. D. Griffiths and J. A. Heyman, *Nature Protocols*, 2013, **8**, 870.
117. M. Najah, R. Calbrix, I P. Mahendra-Wijaya, T. Beneyton, Andrew D. Griffiths and A. Drevelle, *Chemistry & Biology*, 2014, **21**, 1722-1732.
118. M. Ryckelynck, S. Baudrey, C. Rick, A. Marin, F. Coldren, E. Westhof and A. D. Griffiths, *RNA*, 2015, **21**, 458-469.
119. M. Seo, C. Paquet, Z. Nie, S. Xu and E. Kumacheva, *Soft Matter*, 2007, **3**, 986-992.
120. W. Shi, J. Qin, N. Ye and B. Lin, *Lab on a Chip*, 2008, **8**, 1432-1435.
121. H. C. Shum, A. R. Abate, D. Lee, A. R. Studart, B. Wang, C. H. Chen, J. Thiele, R. K. Shah, A. Krummel and D. A. Weitz, *Macromolecular Rapid Communications*, 2010, **31**, 108-118.
122. J. Dai, H. S. Kim, A. R. Guzman, W.-B. Shim and A. Han, *RSC Advances*, 2016, **6**, 20516-20519.

APPENDIX A

SUPPLEMENTARY MICROALGAE SCREENING DATA

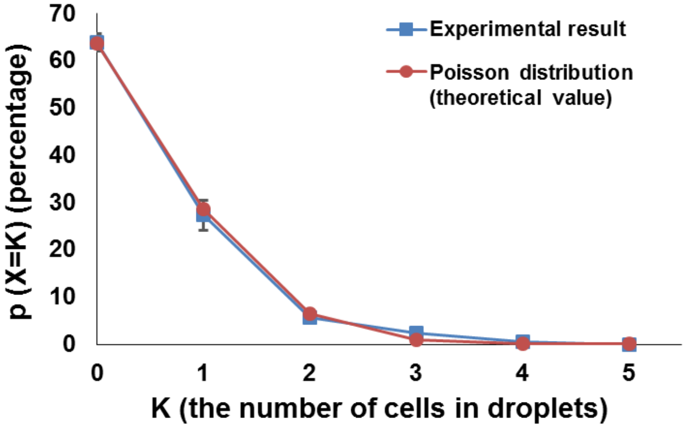

Figure 8.1 Figure showing the cell encapsulation distribution for microalgae droplets (*n=3*). Encapsulation closely matches the expected Poisson's distribution. Reprinted with permission from Wiley Periodicals, Inc. [114]

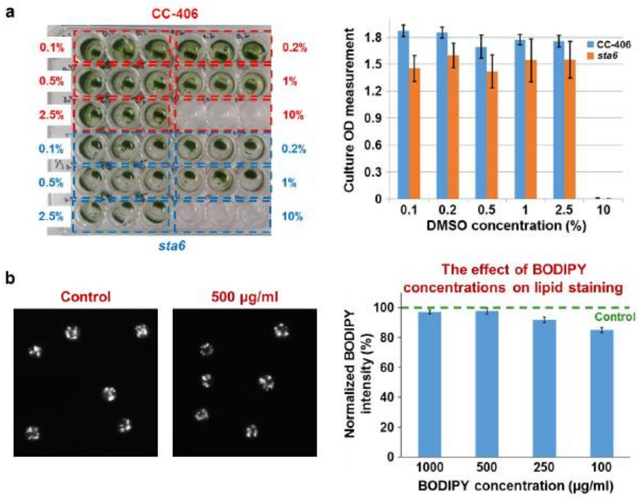

Figure 8.2 (a) Characterization of on-chip BODIPY staining and viability of cells after cultivation (*n=3*). (b) Fluorescent analysis characterization of BODIPY at different concentrations (*n=24*). BODIPY concentrations higher than 500 μg mL^{-1} showed more than 95% staining similarity compared to the control. All data shown are mean ± standard error. Reprinted with permission from Plant Direct. [113]

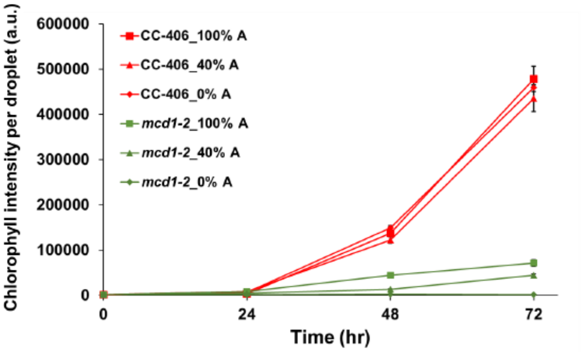

Figure 8.3 Growth comparison of *C. reinhardtii CC-406* and *mcd1-2* with varying acetate (A) concentrations (*n=17*). All data shown are mean ± standard error. Reprinted with permission from Plant Direct. [113]

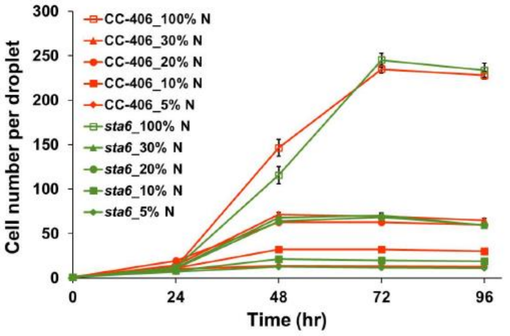

Figure 8.4 Growth comparison analysis of *C. reinhardtii CC-406* and *sta6* under varying nitrogen concentrations (*n=20*). Data shown are mean ± standard error. Reprinted with permission from Plant Direct. [113]

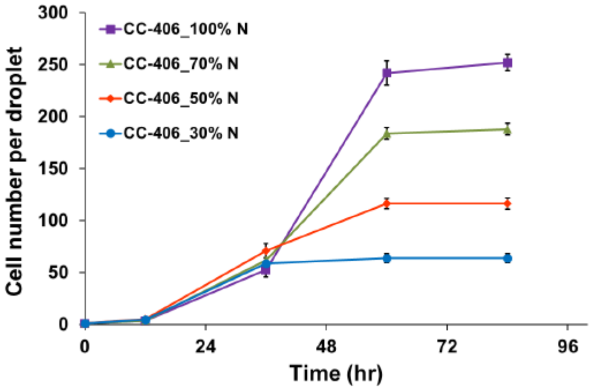

Figure 8.5 Growth comparison analysis of *C. reinhardtii CC-406* with at varying nitrogen concentrations (*n=14*). All data shown are mean ± standard error. Reprinted with permission from Plant Direct. [113]

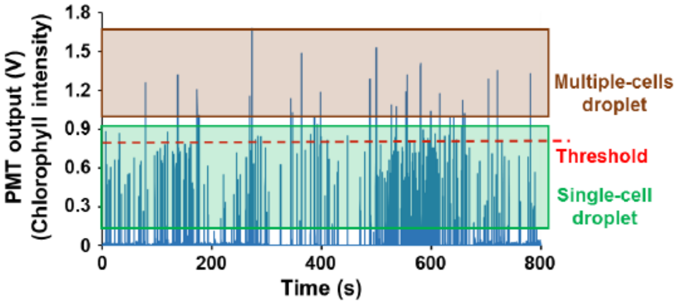

Figure 8.6 **Fluorescent detection of *C. reinhardtii CC-406* autofluorescence after 36 h culture. Green box indicates single cell encapsulated droplets and the red line indicates the threshold of 0.8V set to collect EMS-mutated cells. Reprinted with permission from Plant Direct.** [113]

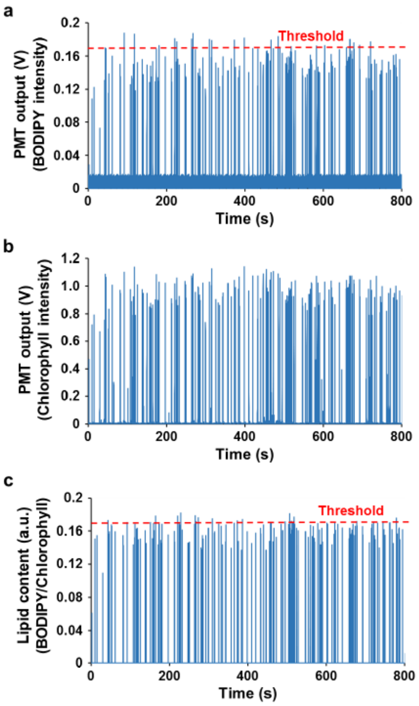

Figure 8.7 **(a) Detection of lipid content for fluorescent detection characterization. (b) growth characterization of *C. reinhardtii CC-406* after 4 days of culture. (c) Normalizing of BODIPY to chlorophyll autofluorescence for final detection characterization analysis. Reprinted with permission from Plant Direct.** [113]

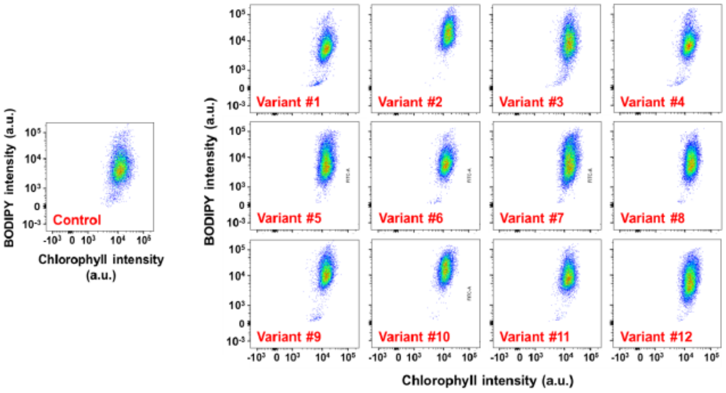

Figure 8.8 Characterization of lipid content in 12 selected variants through the flow cytometry measurement. Reprinted with permission from Plant Direct. [113]

APPENDIX B

SUPPLEMENTARY POLY-CHIP SCREENING DATA

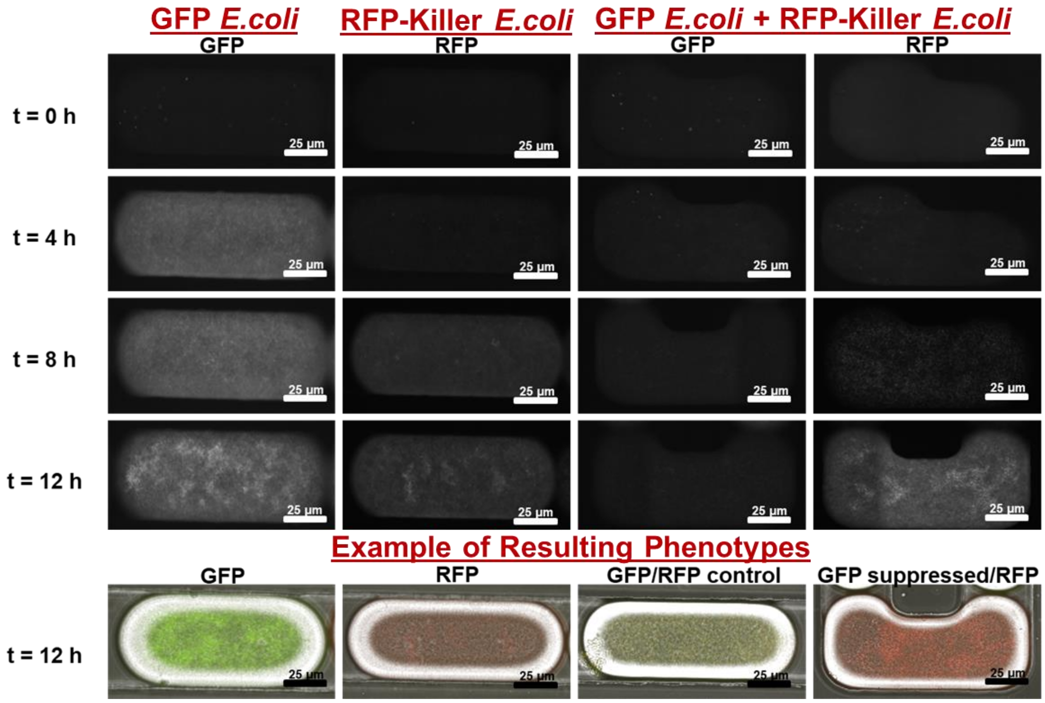

Figure 8.9 In-droplet growth characterization analysis assay of GFP-*E. coli*, RFP-Killer *E. coli*, and GFP-*E. coli* with RFP-killer *E. coli*.

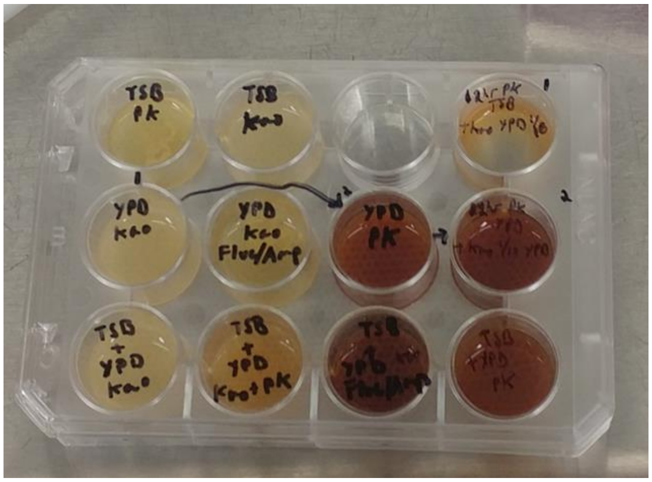

Figure 8.10 Multi well plate growth characterization analysis of yeast, yeast with *PK* (antifungal), yeast with *E. coli*, and yeast with Fluconazole/Amphotericin B (control) in both YPD and TSB media. Cultured for 12 h.

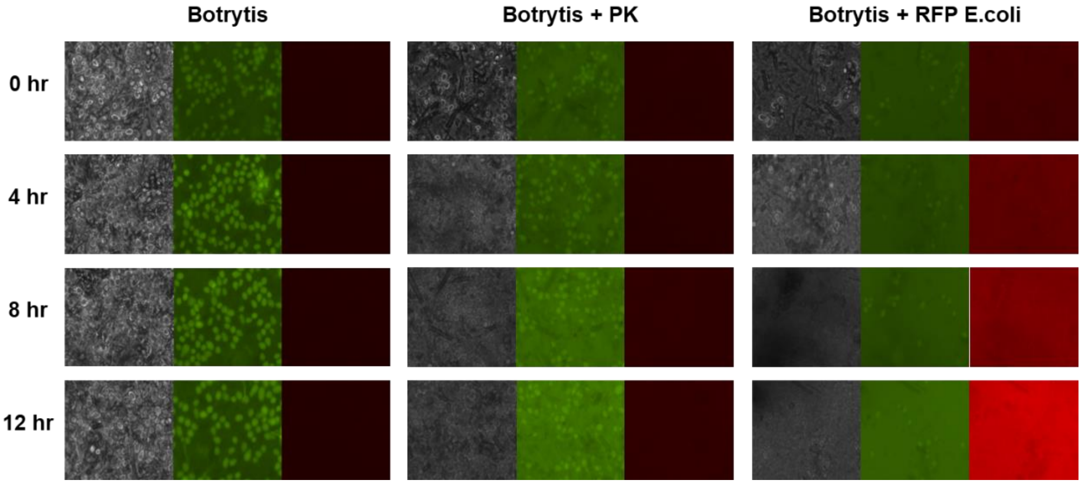

Figure 8.11 Growth comparison of *B. cinerea*, *B. cinerea* with *PK* (antifungal), and *B. cinerea* with *E. coli*. Cultured for 12 h.

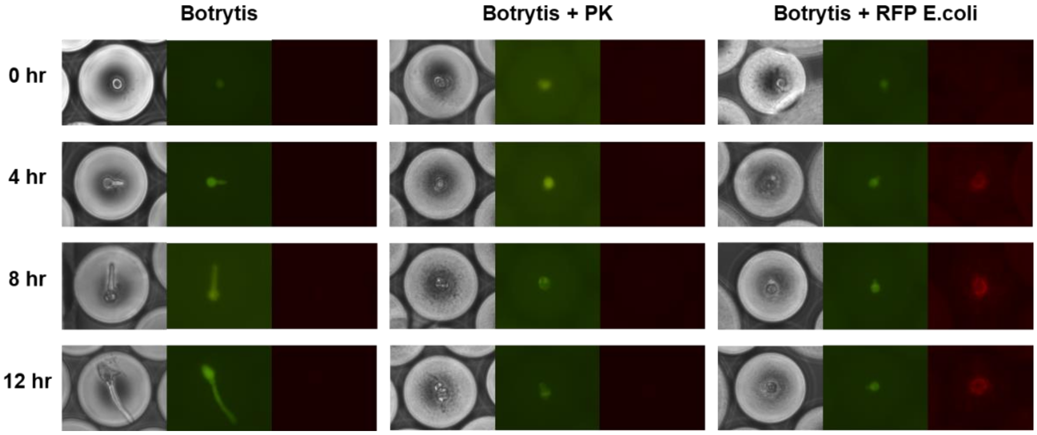

Figure 8.12 In-droplet growth characterization analysis of *B. cinerea*, *B. cinerea* with *PK* (antifungal), and *B. cinerea* with *E. coli*.

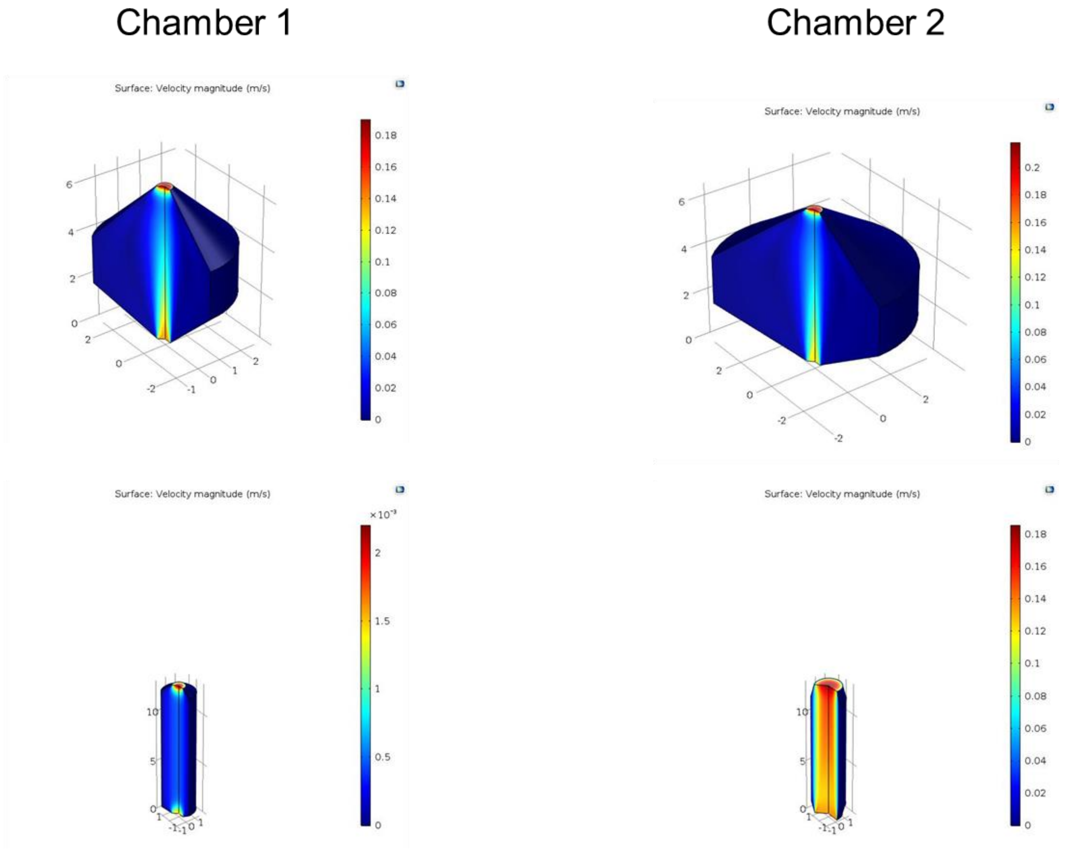

Figure 8.13 Comsol simulation of vertical droplet culture chamber for first and second chamber in Poly-chip system. Optimization of chamber design is conducted to reduce dead volume and maintain first-in first-out flow.

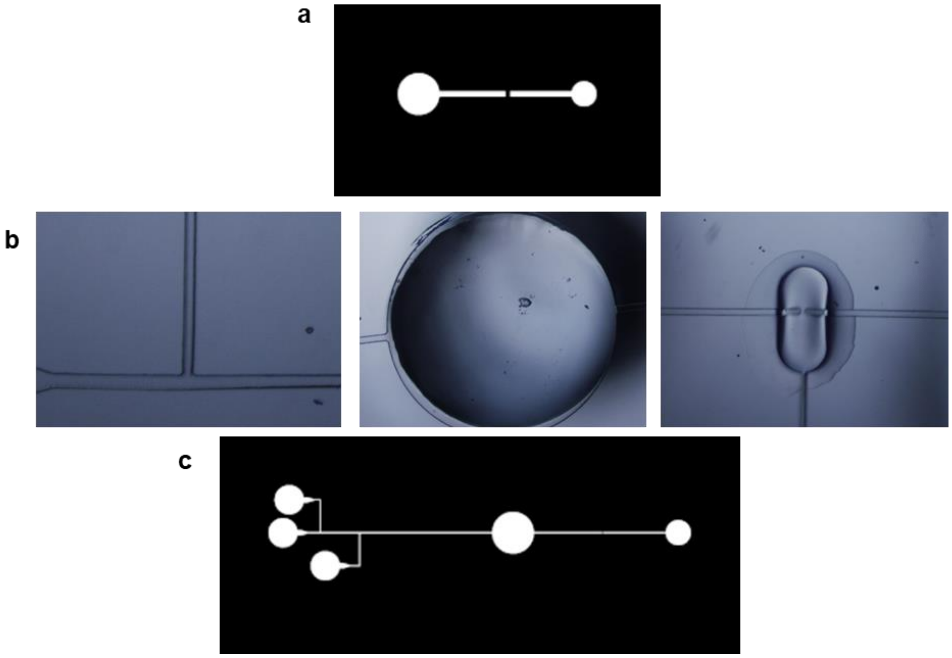

Figure 8.14 Configuration of bottom-up chamber design for validation. (a) Mask design of top layer where valve releases droplets from the chamber. (b) Micrograph images of droplet generator, bottom-up chamber, and valves. (c) Mask design of bottom layer entailing droplet generator, bottom of chamber, and outlet valve for excess oil to escape.

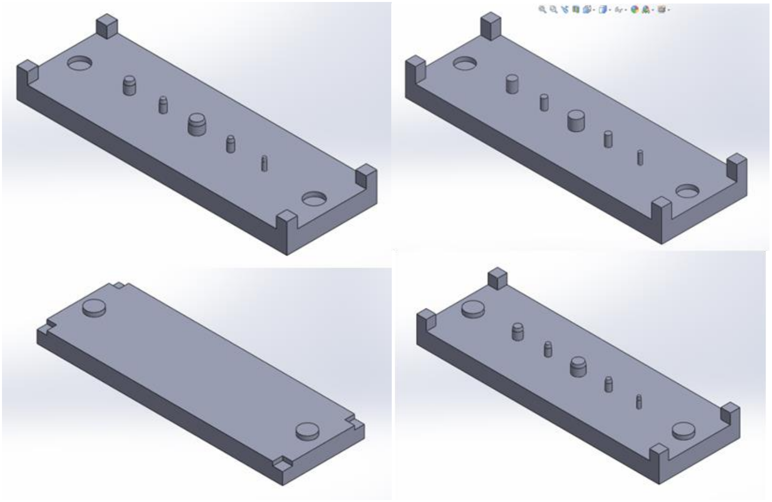

Figure 8.15 3D printed molds for droplet cultivation chamber layers.

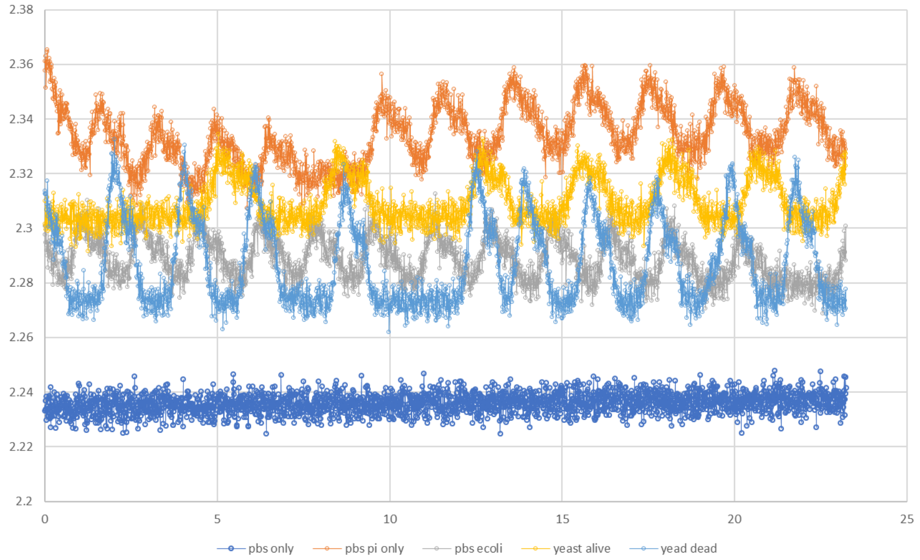

Figure 8.16 Droplet flow through fluorescent comparison of PBS, PBS with PI, PBS with *E. coli*, PBS with live yeast and PI, and PBS with dead yeast and PI. Background dye staining makes fluorescent detection difficult without a rinsing step or dye concentration optimization.

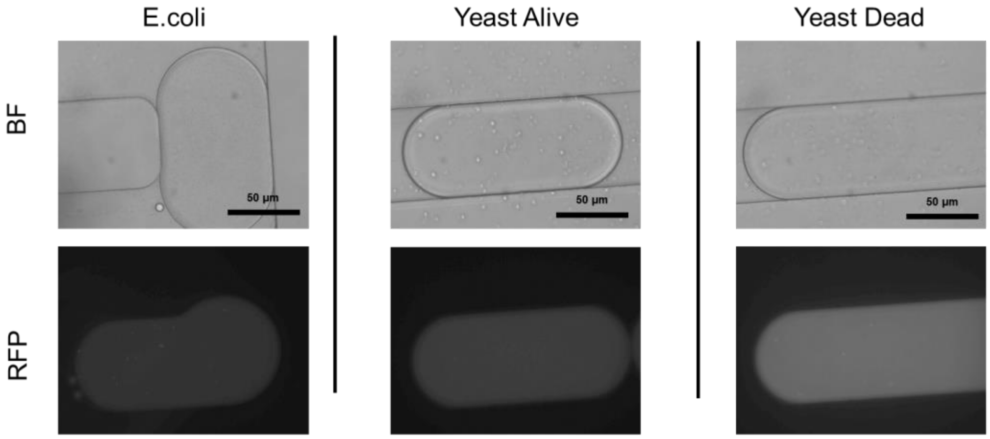

Figure 8.17 Micrograph images showing high background fluorescence in droplets containing stained yeast cells.

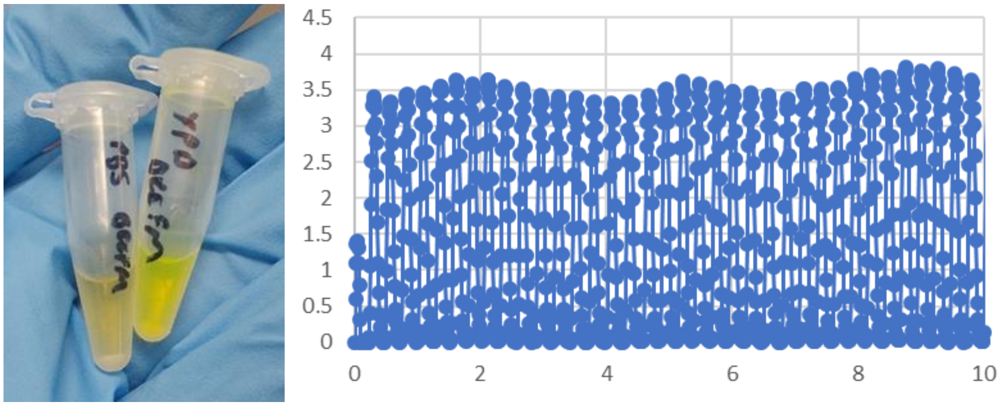

Figure 8.18 Dye staining comparison of PBS and YPD media with yeast, showing significant change in media color leading to high background noise. Fluorescent detection using PMT-based system cannot distinguish cell fluorescent intensity.

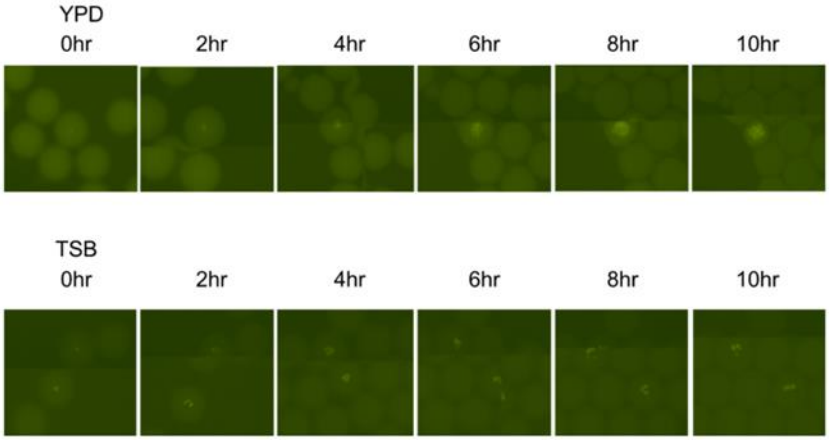

Figure 8.19 Fluorescent micrograph images of yeast encapsulated in YPD and TSB over a 10 h culture. YPD shows a higher background fluorescence when compared to TSB media.

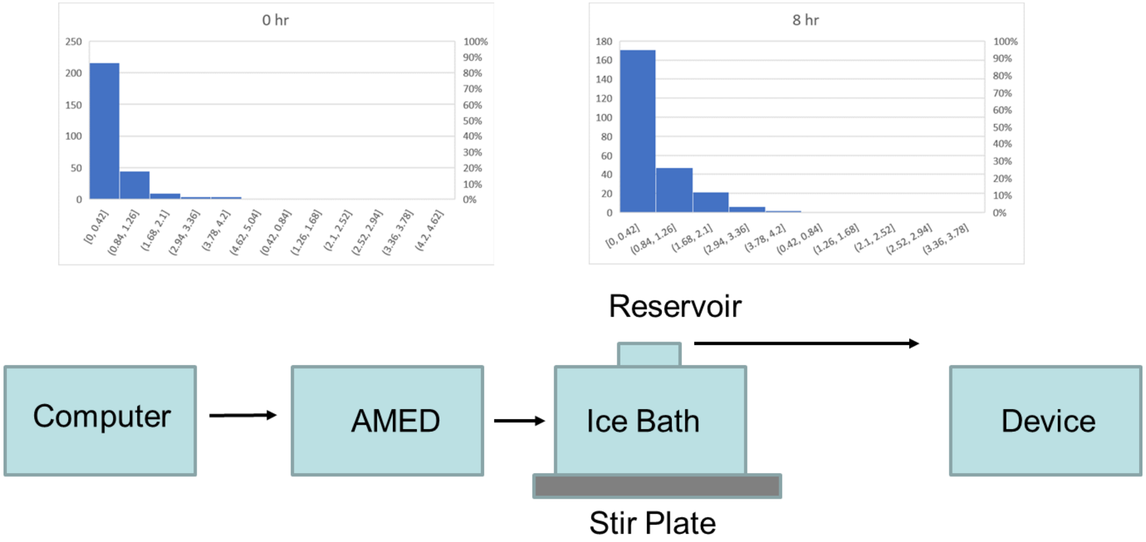

Figure 8.20 Long-term droplet generation system to maintain cell encapsulation number and distribution. Cells can be kept in a vial inside an ice bath that sits on a magnetic stir plate. Droplets are generated using a pressure driven pump to push liquid into the device. Distribution shows only a marginal increase in cell number after 8 h or continuous encapsulation.

APPENDIX C

SUPPLEMENTARY MASK DESIGNS

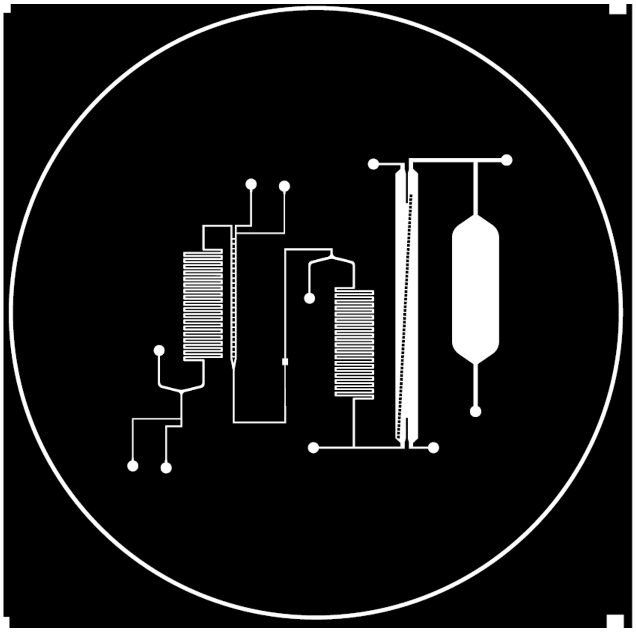

Figure 8.21 Mask design of microalgae droplet rinsing platform.

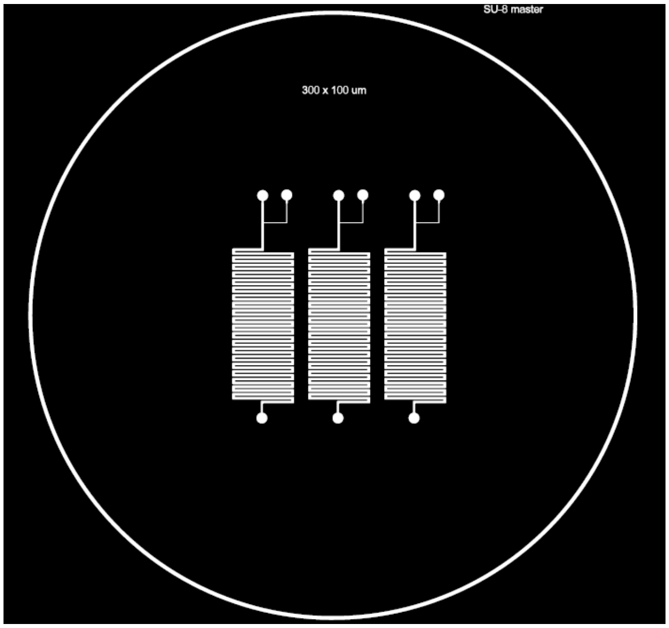

Figure 8.22 Mask design of droplet generator and serpentine culture chamber.

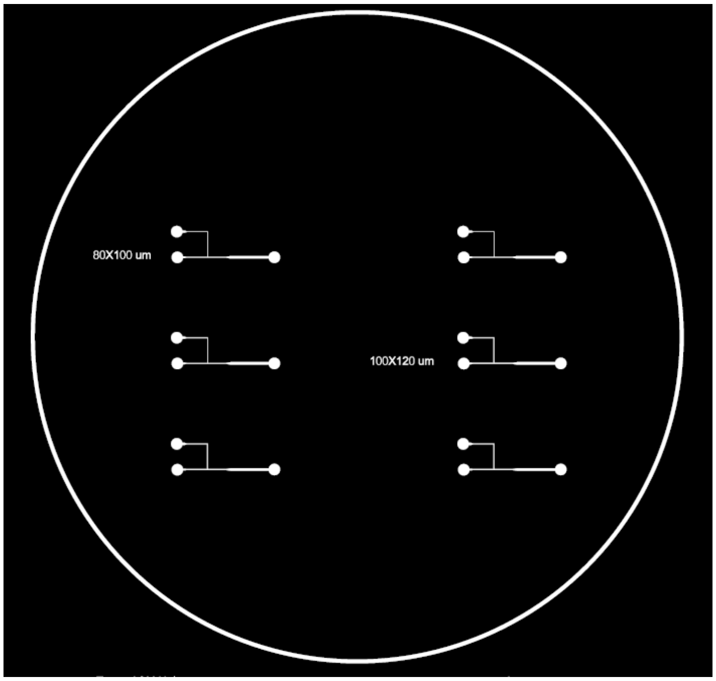

Figure 8.23 Mask design of droplet generators.

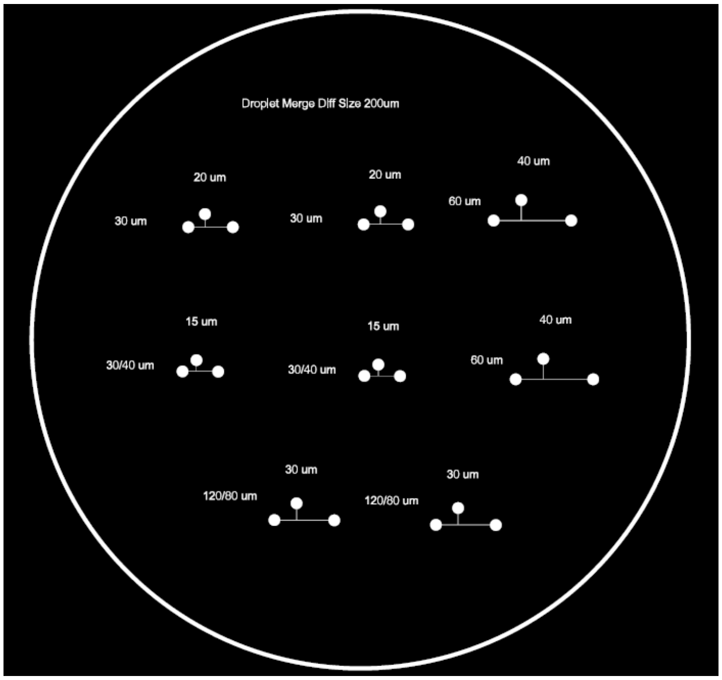

Figure 8.24 Mask design of droplet generators.

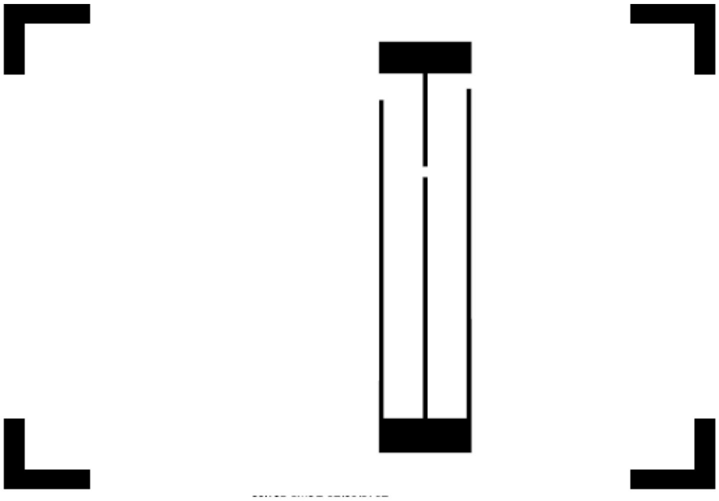

Figure 8.25 Mask design of planar electrode for microalgae/merging chips.

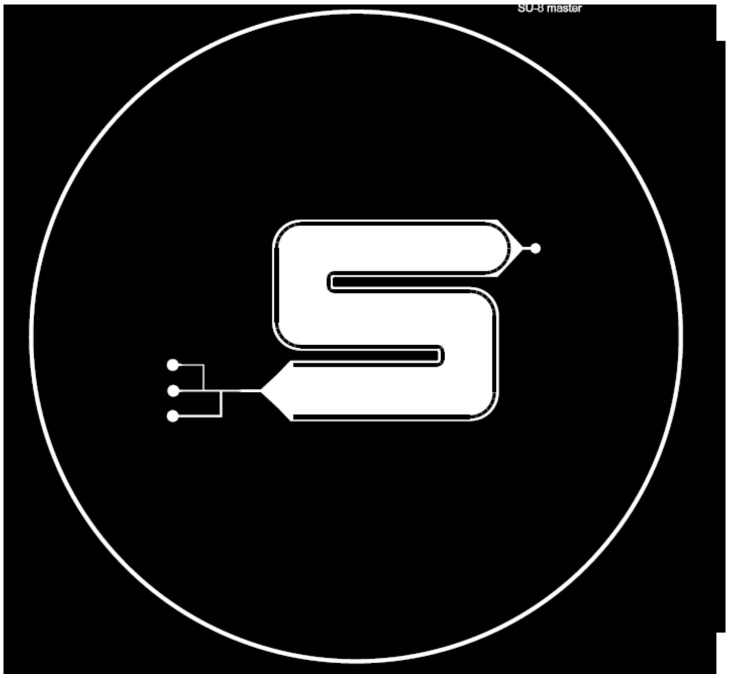

Figure 8.26 Mask design of large culture chamber for microalgae/A. baumannii.

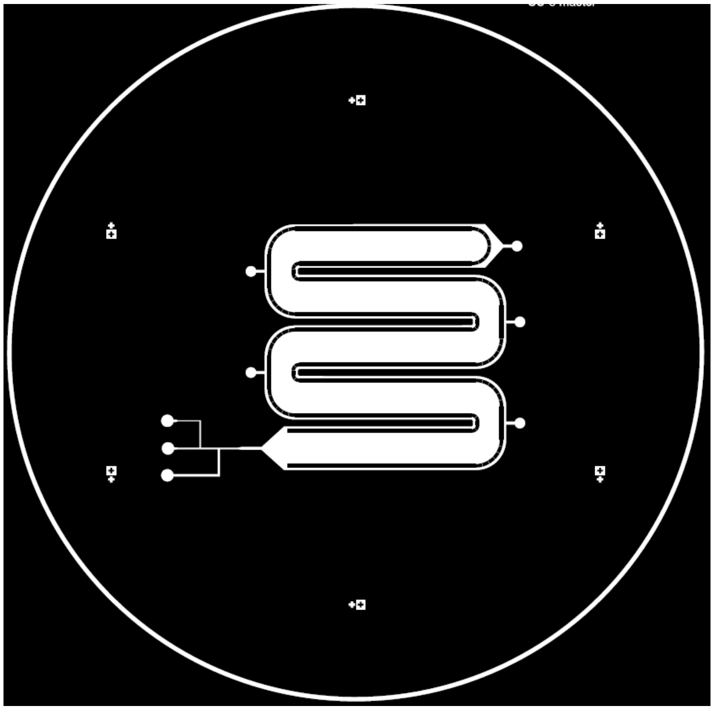

Figure 8.27 Mask design of large culture chamber for microalgae/*A. baumannii*.

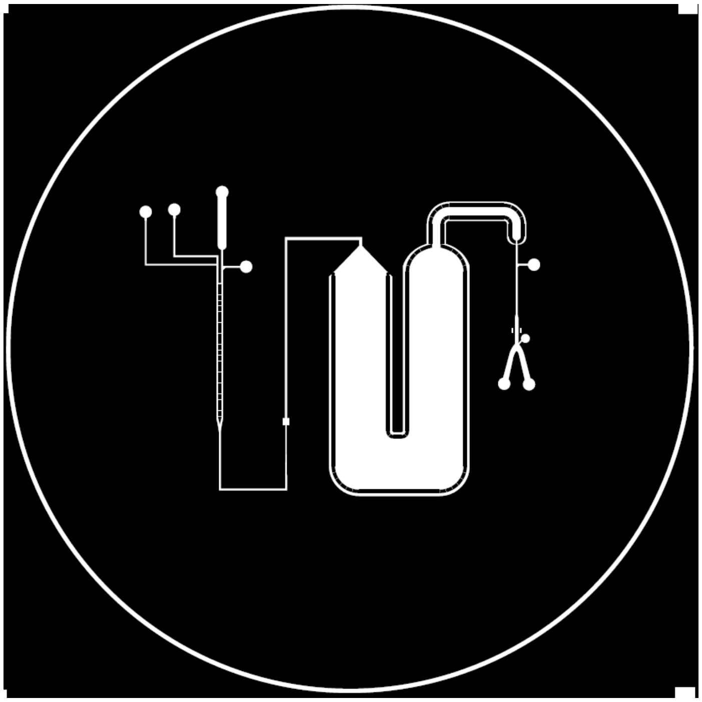

Figure 8.28 Mask design of droplet merging chip for microalgae/*A. baumannii*.

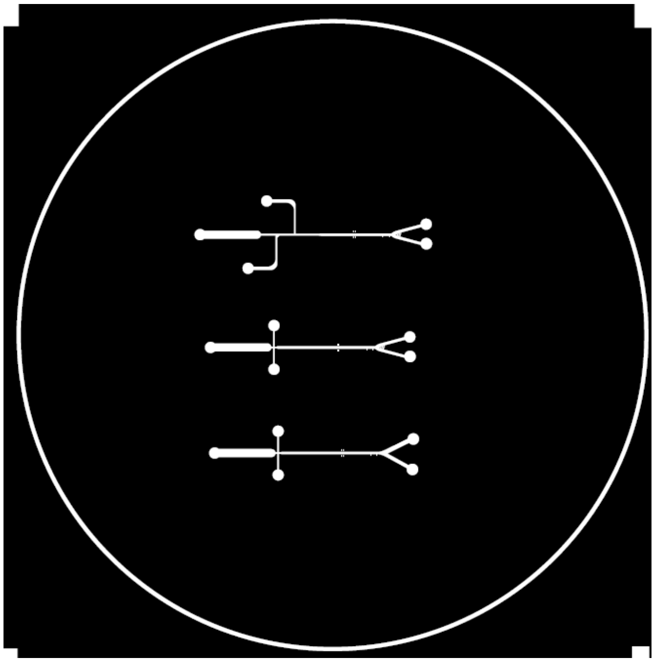

Figure 8.29 Mask design of detection/sorting chip for *A. baumannii* screen.

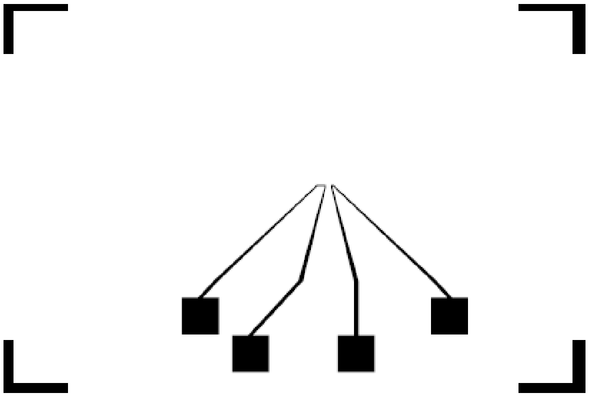

Figure 8.30 Mask design of planar electrode for sorting chip.

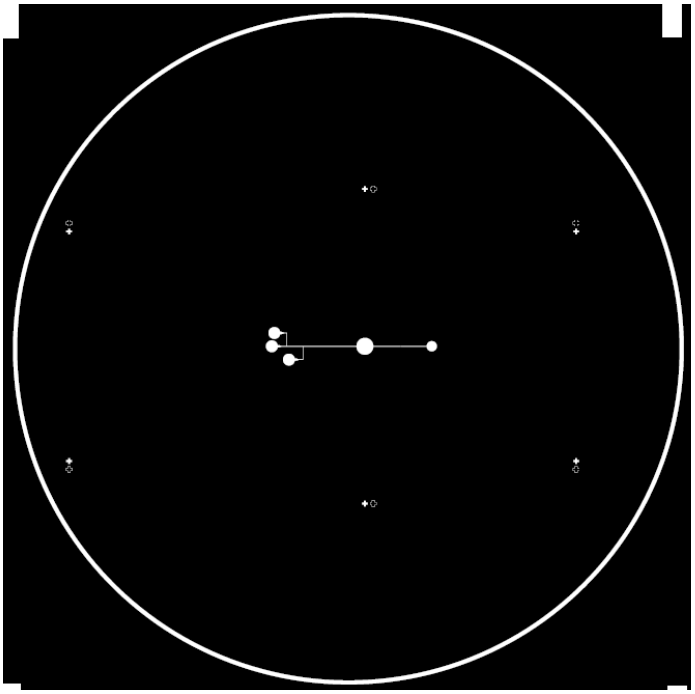

Figure 8.31 Mask design of bottom droplet generator for bottom-up culture chamber.

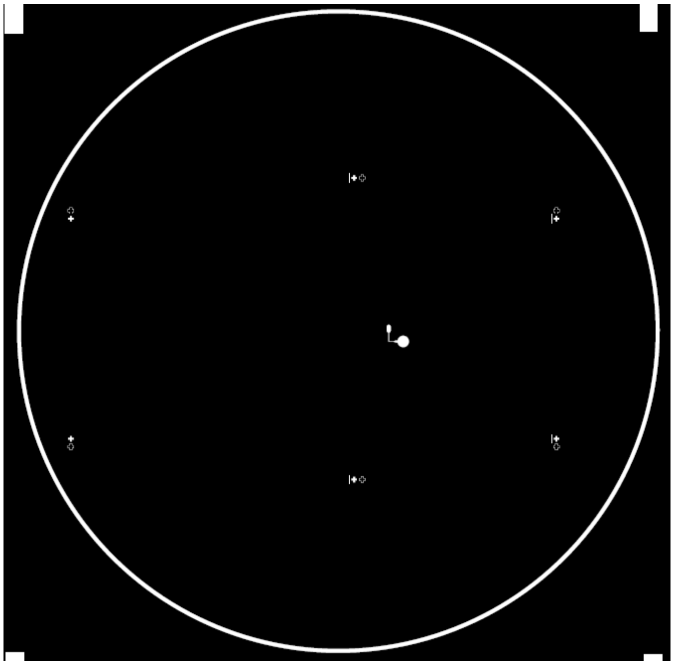

Figure 8.32 Mask design of bottom valve layer for bottom-up culture chamber.

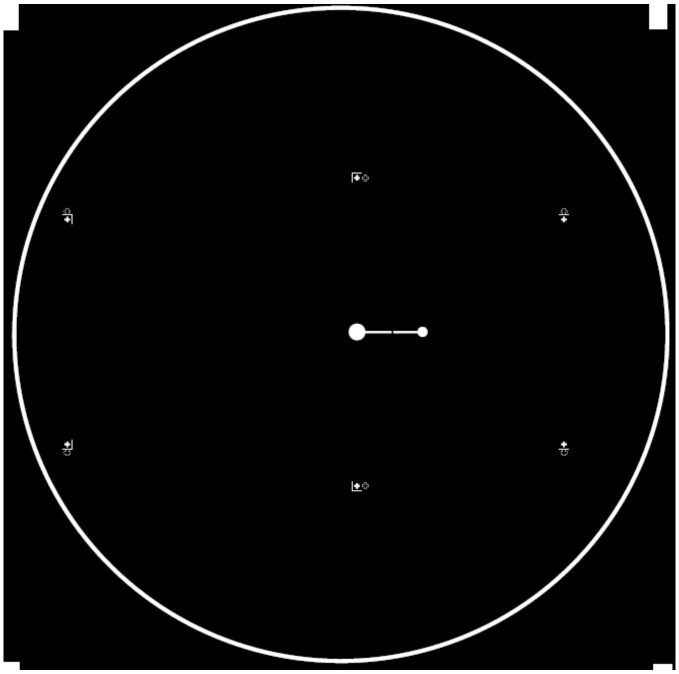

Figure 8.33 Mask design of top channel for bottom-up culture chamber.

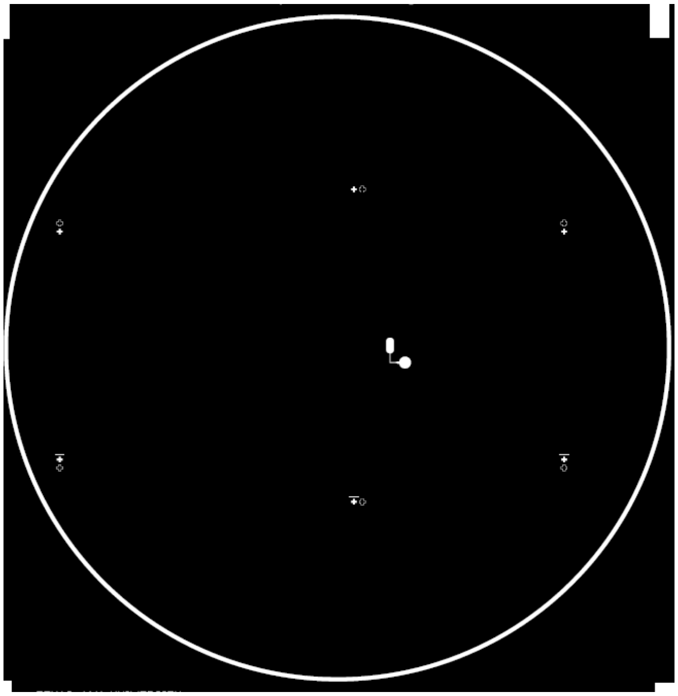

Figure 8.34 Mask design of top valve layer for bottom-up culture chamber.

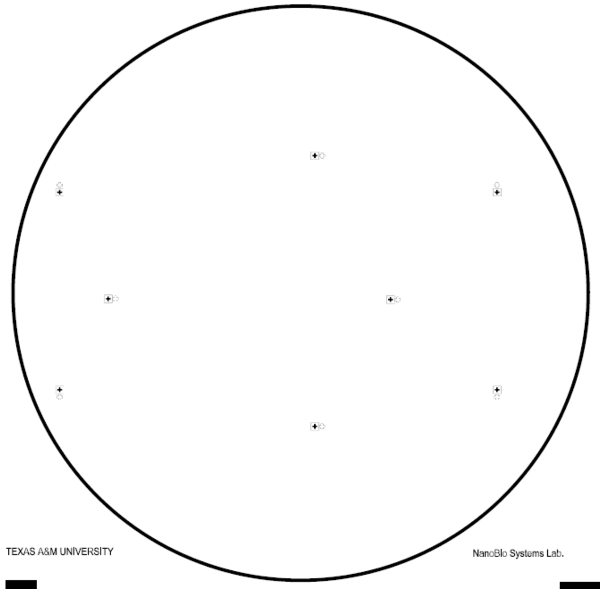

Figure 8.35 Mask design of alignment marks for Poly-chip stacking.

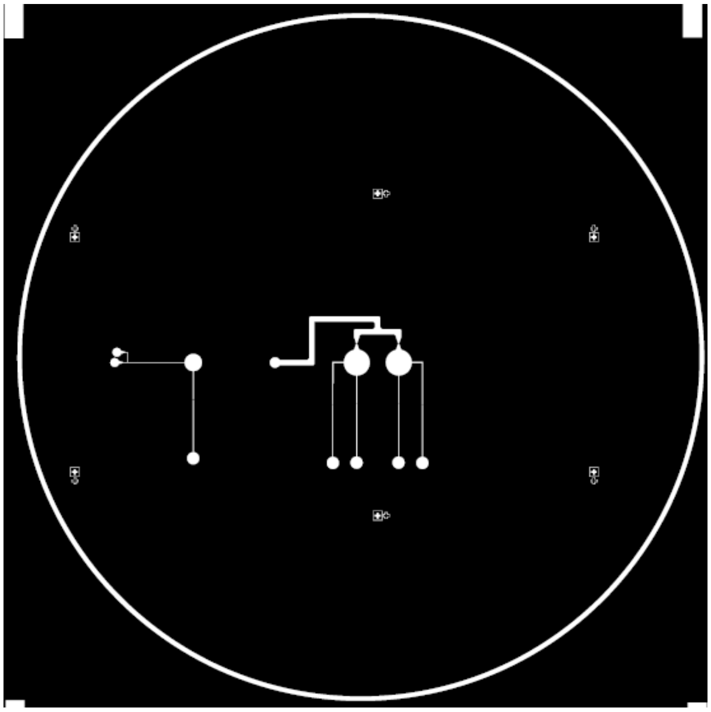

Figure 8.36 Mask design of Poly-chip sandwich bottom layer.

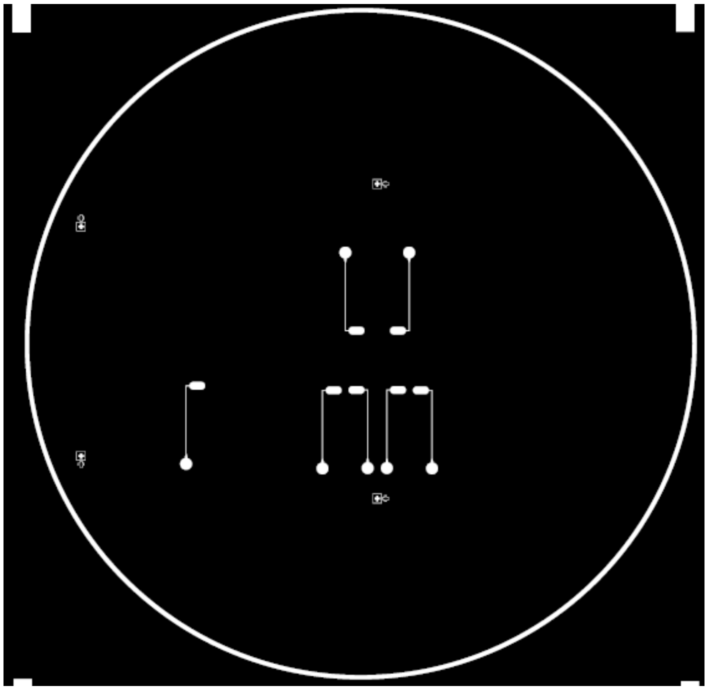

Figure 8.37 Mask design of Poly-chip sandwich bottom valve layer.

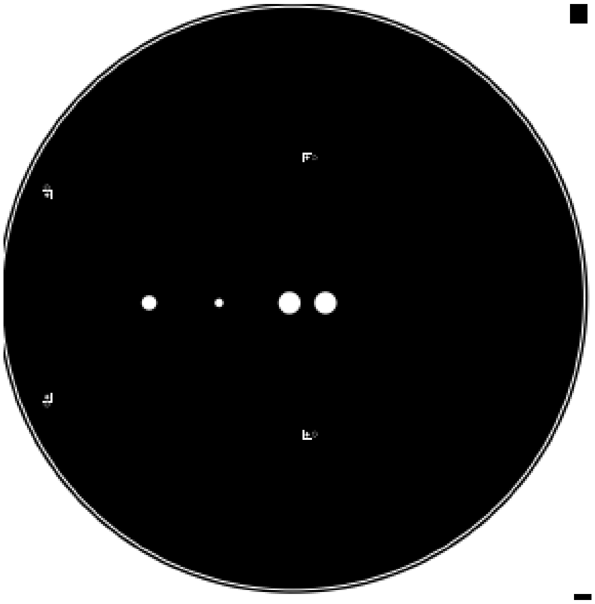

Figure 8.38 Mask design of Poly-chip sandwich top base layer.

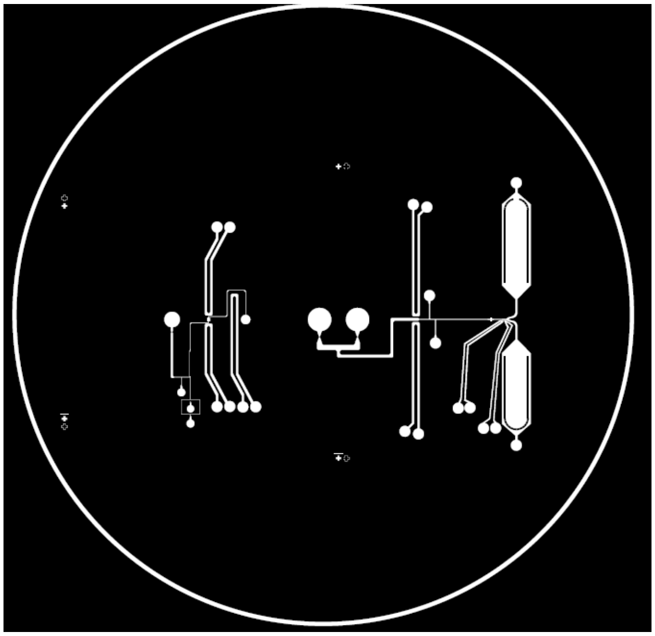

Figure 8.39 Mask design of Poly-chip sandwich top layer.

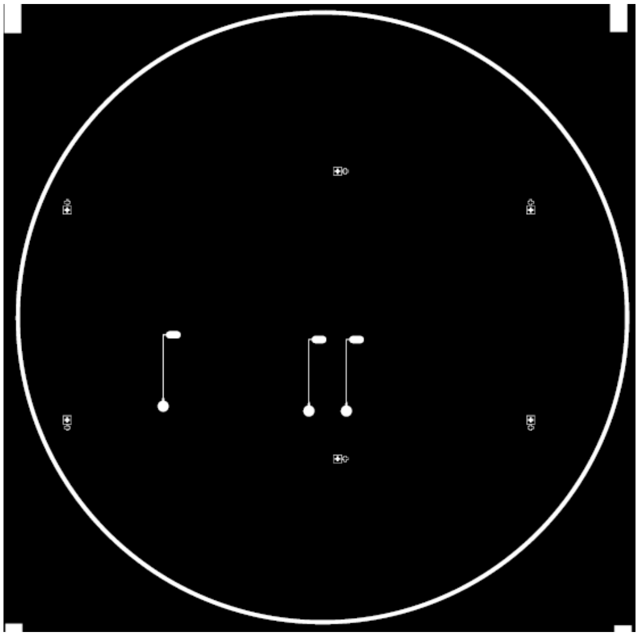

Figure 8.40 Mask design of Poly-chip sandwich top valve layer.

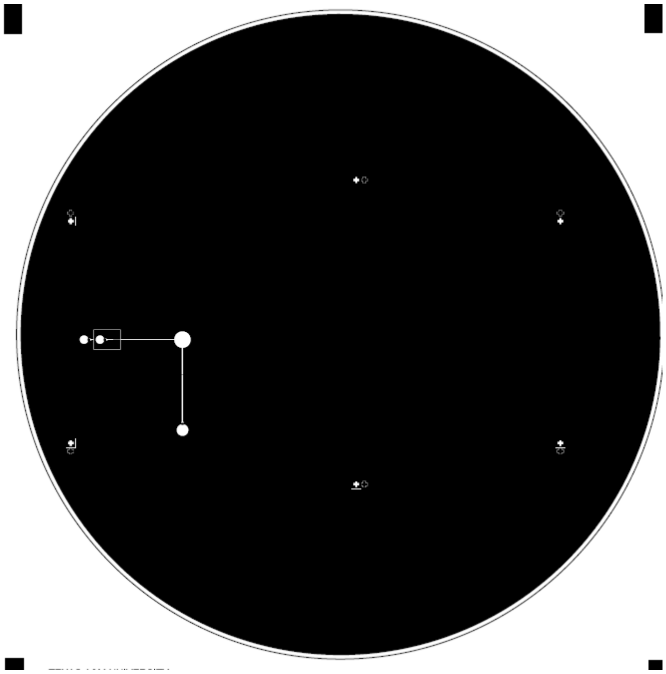

Figure 8.41 Mask design of Poly-chip stacked bottom layer.

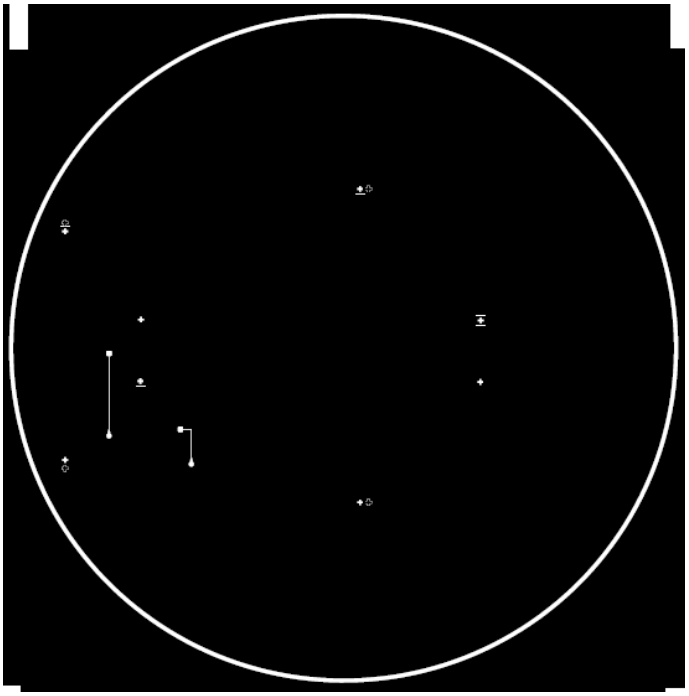

Figure 8.42 Mask design of Poly-chip stacked bottom valve layer.

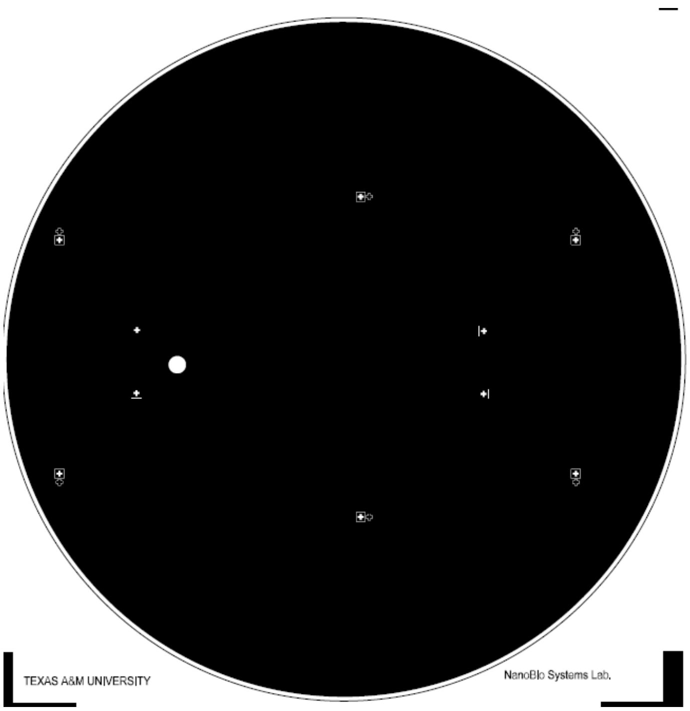

Figure 8.43 Mask design of Poly-chip stacked middle base layer.

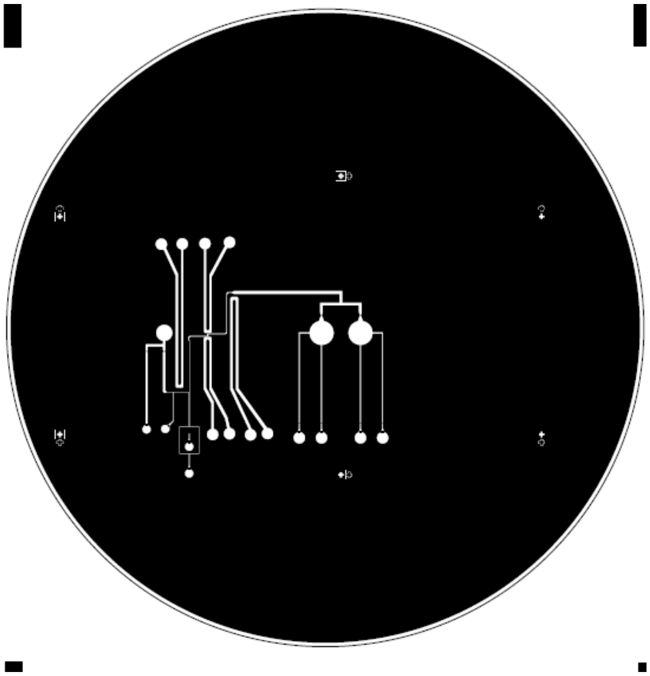

Figure 8.44 Mask design of Poly-chip stacked middle layer.

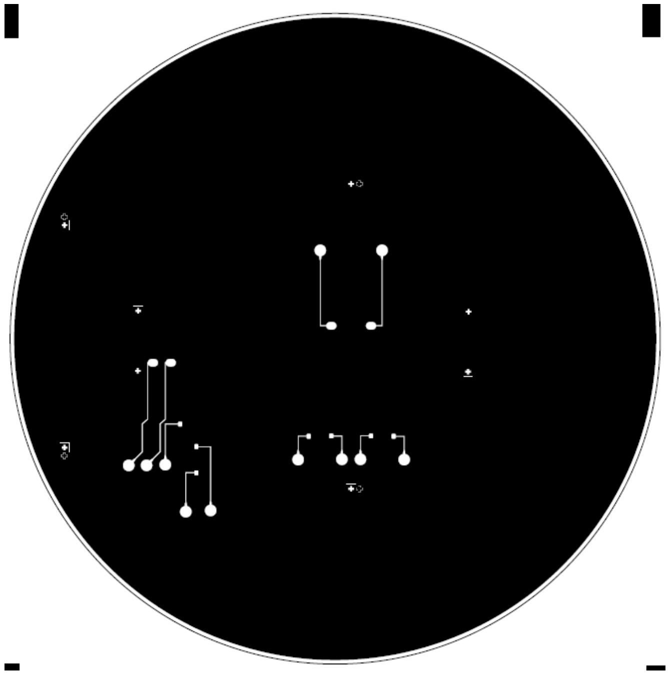

Figure 8.45 Mask design of Poly-chip stacked middle valve layer.

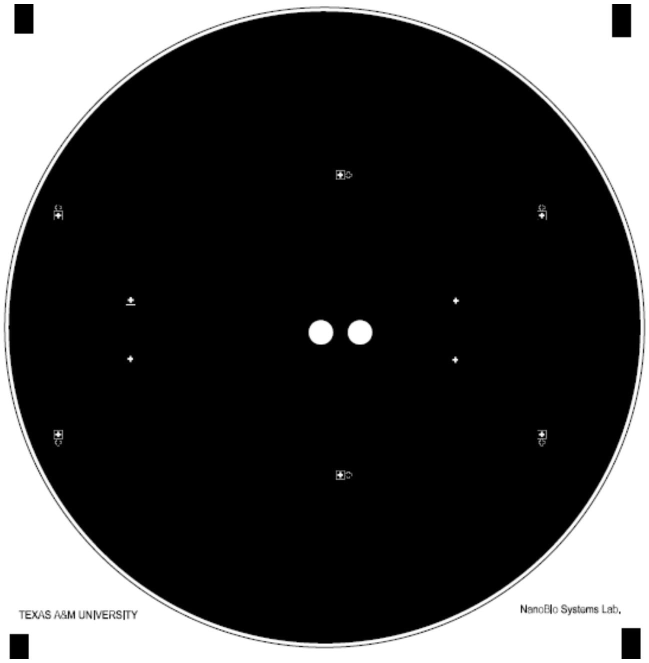

Figure 8.46 Mask design of Poly-chip stacked top base layer.

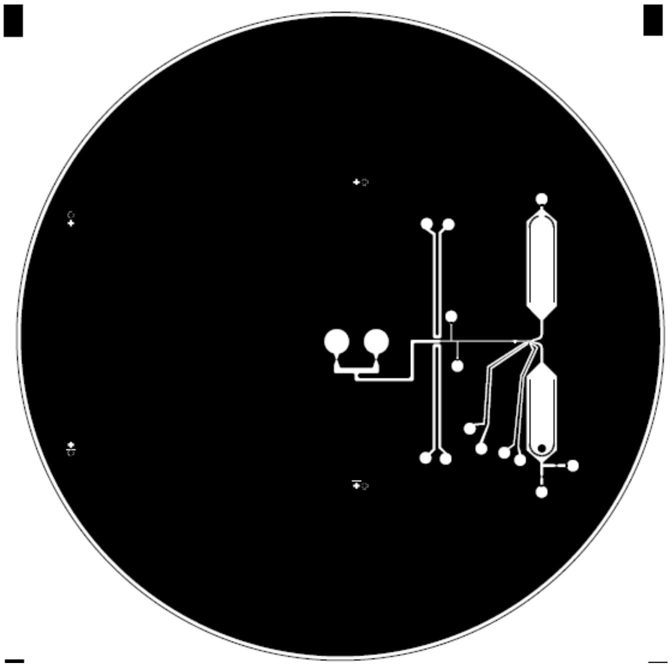

Figure 8.47 Mask design of Poly-chip stacked top layer.

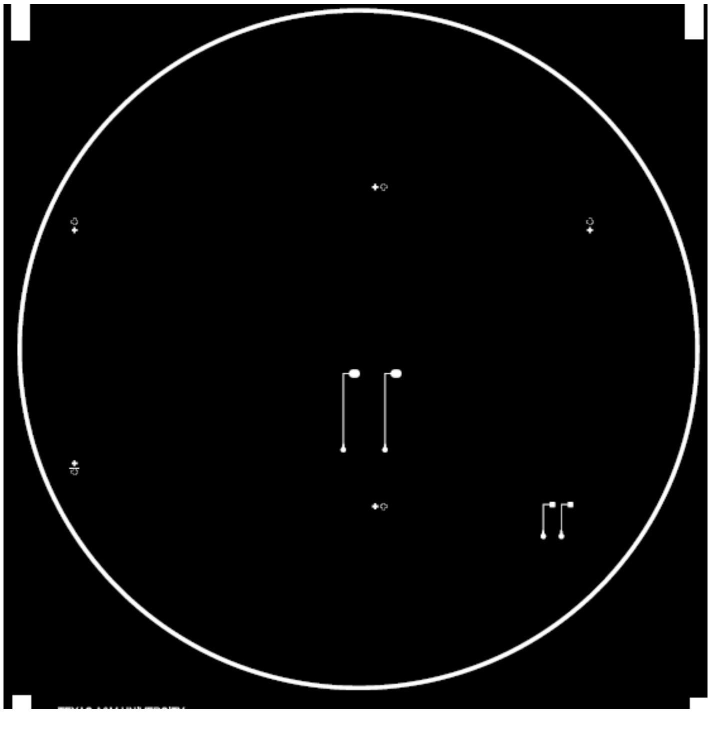

Figure 8.48 Mask design of Poly-chip stacked top valve layer.

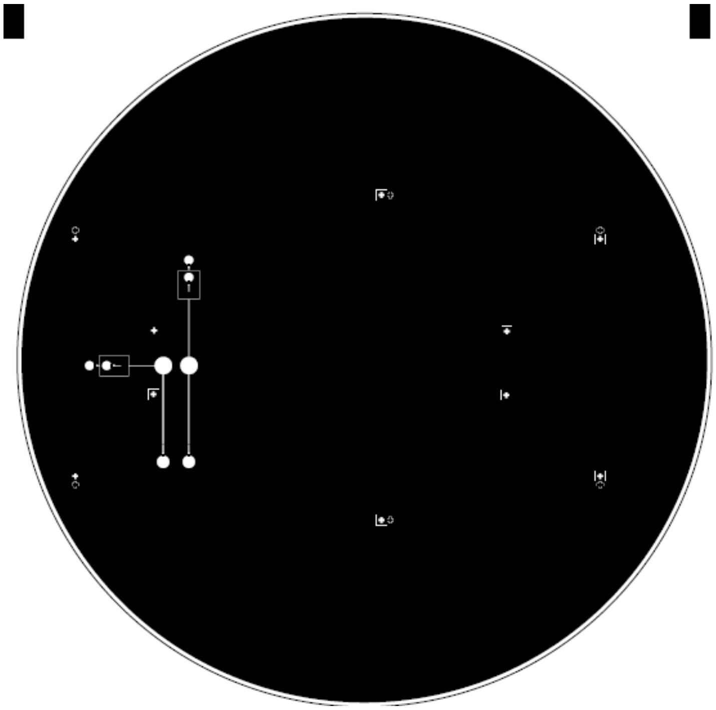

Figure 8.49 Mask design of Poly-chip stacked dual reflow bottom layer.

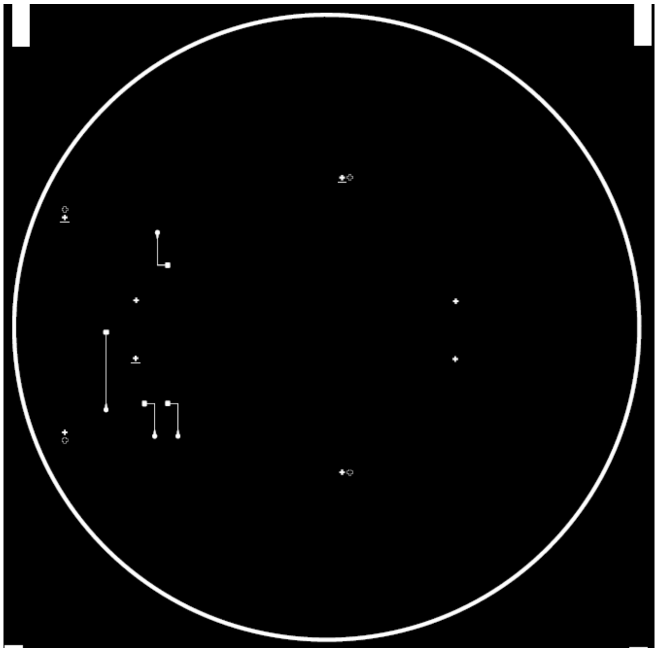

Figure 8.50 Mask design of Poly-chip stacked dual reflow bottom valve layer.

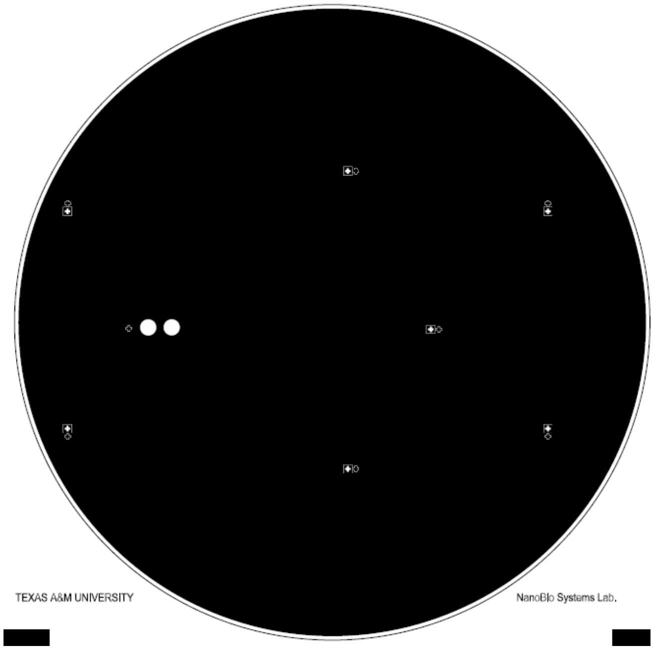

Figure 8.51 Mask design of Poly-chip stacked dual reflow middle base layer.

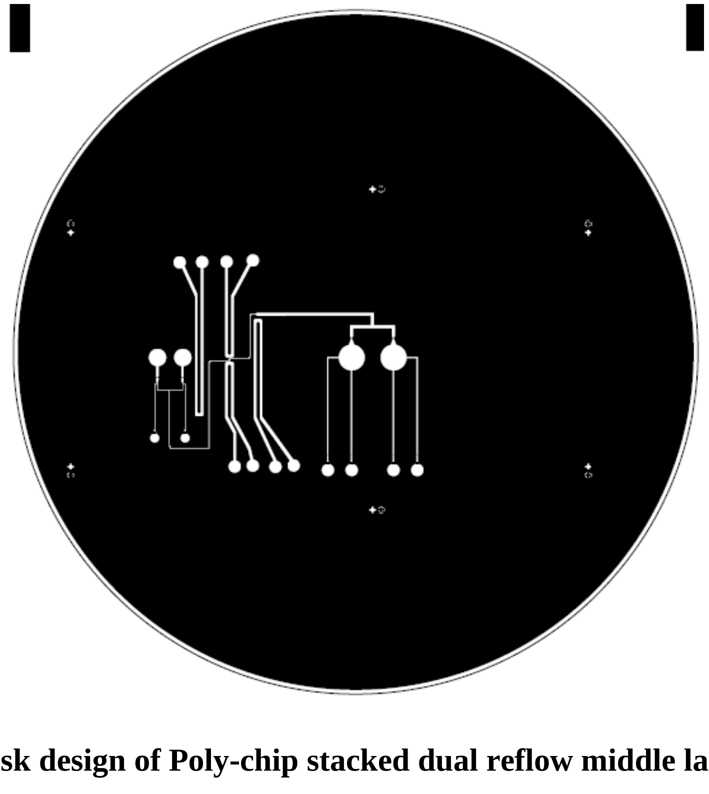

Figure 8.52 Mask design of Poly-chip stacked dual reflow middle layer.

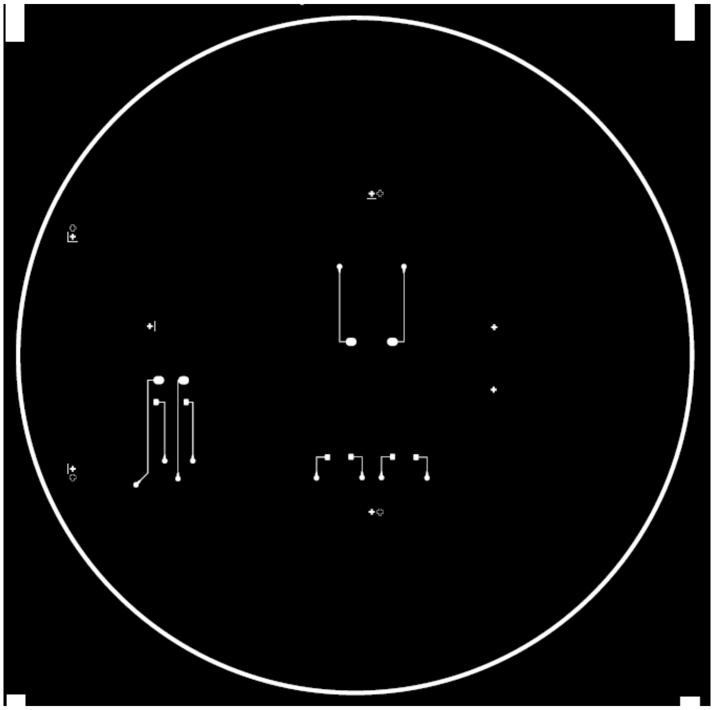

Figure 8.53 Mask design of Poly-chip stacked dual reflow middle valve layer.

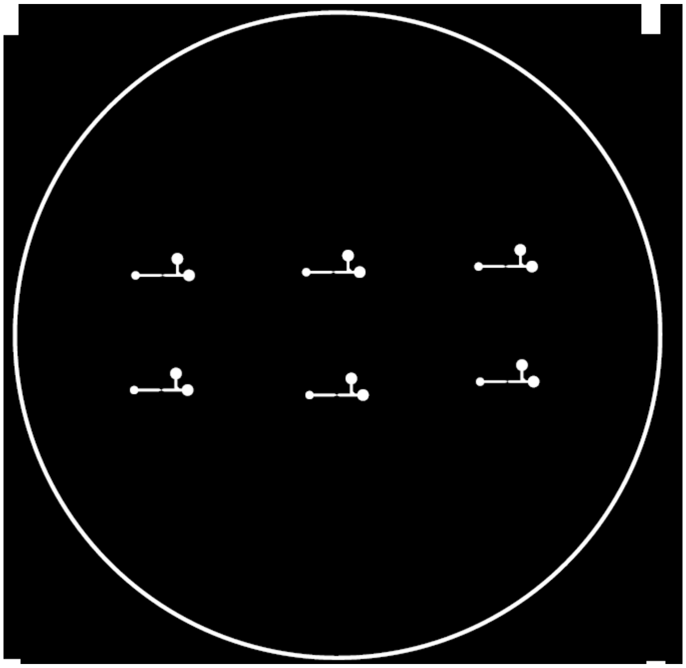

Figure 8.54 Mask design of Poly-chip stacked fourth channel layer (automated release of hits).

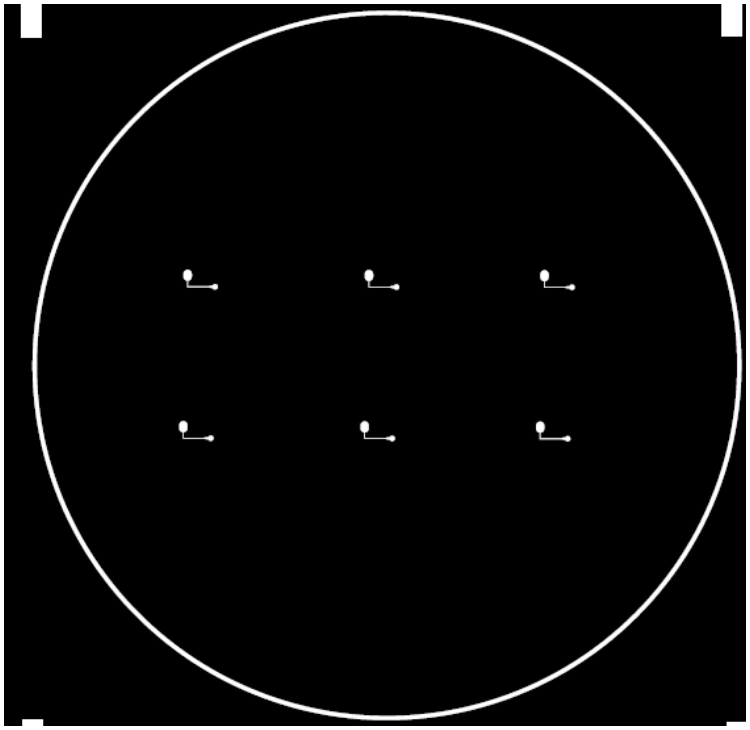

Figure 8.55 Mask design of Poly-chip stacked fourth valve layer (automated release of hits).

Figure 8.56 Solidworks model of the 3 inch x 3 inch 3D printed device holder for the Poly-chip system.

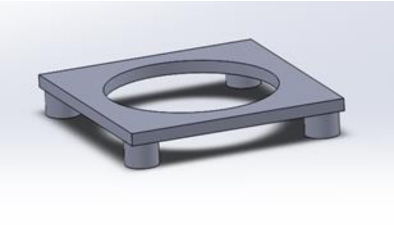

Figure 8.57 Solidworks model of the 5 inch x 5 inch 3D printed top for device holder for the Poly-chip system.

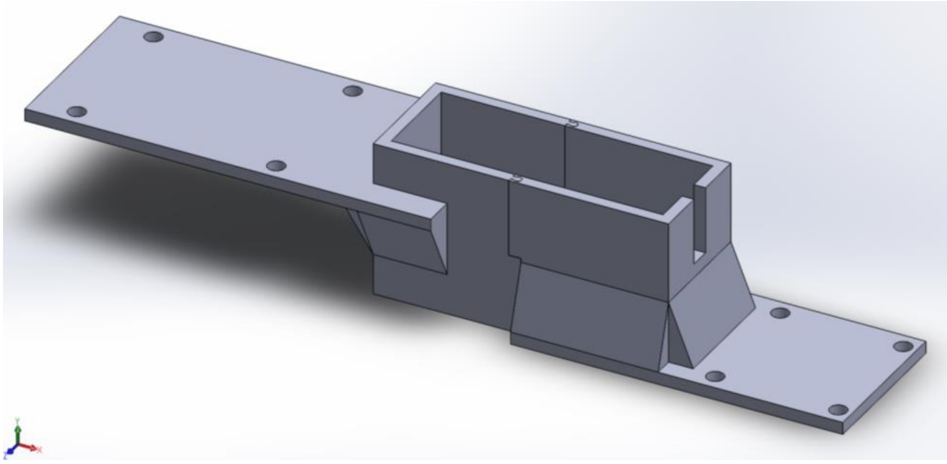

Figure 8.58 Solidworks model of the 3D printed laser alignment system.

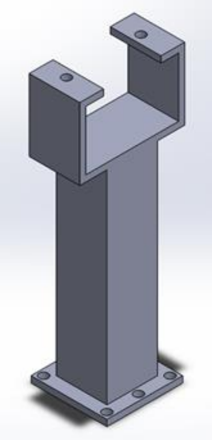

Figure 8.59 Solidworks model of the 3D printed laser support for alignment system.